MODULAR DYNAMIC MODELING AND DEVELOPMENT OF MICRO AUTONOMOUS UNDERWATER VEHICLE: LANCELET

CHAO SHUZHE

NATIONAL UNIVERSITY OF SINGAPORE

2013

MODULAR DYNAMIC MODELING AND DEVELOPMENT OF MICRO AUTONOMOUS UNDERWATER VEHICLE: LANCELET

CHAO SHUZHE

(*M. Eng., Xi'an Jiaotong University*)

A THESIS SUBMITTED

FOR THE DEGREE OF DOCTOR OF PHILOSOPHY

DEPARTMENT OF MECHANICAL ENGINEERING

NATIONAL UNIVERSITY OF SINGAPORE

2013

DECLARATION

I hereby declare that the thesis is my original work and it has been written by me in its entirety. I have duly acknowledged all the sources of information which have been used in the thesis.

This thesis has also not been submitted for any degree in any university previously.

Chao Shuzhe

1 August 2013

Acknowledgements

I want to express my most sincere gratitude to my supervisors, Associate Professor Hong Geok Soon. I want to thank him for his motivation, support, and critique about the work. His depth of knowledge, insight and untiring work ethic has been and will continue to be a source of inspiration to me.

I would like to thank National University of Singapore for offering me the research scholarship, the research facilities and the valuable courses. I also would like to thank the wonderful and caring faculty and staff in the department of Mechanical Engineering.

I would like to thank Eng You Hong from Acoustic Research Laboratory, Tropical Marine Science Institute for sharing the valuable experiment data and giving me plenty of help during this research.

I would like to thank my colleagues and friends in the laboratory of Control and Mechatronics, Dr. Guan Guofeng, Dr. Chen Ruifeng, Dr. Cao Yongxin, Dr. Chanaka Dilhan Senanayake, Dr. Lin Yuheng, Dr. Zhang Ming, Feng Xiaobing, Wu Ning and Li Renjun.

I own my deepest thanks to my family for the unconditional and selfless support. I would like to give my special thanks to my dear wife Shi Yujing for her love, patience and understanding.

Table of Contents

Summary

Modular design methods are widely used in the development of autonomous underwater vehicles (AUVs), in the sense that the vehicle has a highly reconfigurable modular construction, which allows for a simple integration of different payloads and independent subsystem development. Therefore, the method to construct the dynamic models and to design controllers for these modular designed AUVs needs to be flexible for reconfiguration. In this research, a finless torpedo shaped micro AUV named Lancelet is developed, and then we focus on the modular dynamic modeling of this micro AUV.

The Lancelet has no appendages such as rudders, elevators and other external propellers, which might get tangled in the underwater environment. The control electronics including the main control board, the sensing system and the motor driver unit is developed. A novel multi-jet drive propulsion and control system is designed and implemented. This propulsion mechanism is robust and compact and extremely suitable for torpedo shaped micro underwater vehicles, and can provide the Lancelet with high maneuverable capabilities such as turn in place (i.e. zero turning radius) and pitch in place. The performance of the propulsion system is studied and free swimming trials are carried out to explore the Lancelet's dynamic characteristic and special maneuverability.

A nonlinear dynamic model for torpedo shaped AUVs for modular modeling and parameter identification is established. In this model, a vector based algorithm to calculate the damping forces and moments directly from the hydrodynamic coefficients for the decomposed components of the vehicle is derived. Both of the empirical method and the parameter identification method are adopted to estimate the hydrodynamic coefficients of the vehicle. It is concluded that the best way of obtaining the hydrodynamic coefficients of an AUV is combining the empirical method and the identification method together to avoid the coupling of the coefficients and at the same time to improve the estimation accuracy. This technique is particularly suitable for the torpedo shaped AUV with non-streamlined appendages on the hull, but the control surfaces of which are streamlined.

The core issue of modular modeling of the AUV is the modularization of the hydrodynamic coefficients of its hull. These hydrodynamic coefficients are transformed from the lift axis system into the normal-force axis system, where they satisfy the superposition property. Then, the standard reference model method is proposed to calculate these hydrodynamic coefficients from the parameters of modular sections. The hydrodynamic coefficients estimated with both empirical and identification methods are used to verify the proposed method. It is concluded from the results that the standard reference model method could give good estimation of the values of the hydrodynamic coefficients of the hull by the offsets from the reference model in the normal-force axis system.

List of Tables

List of Figures

List of Symbols

m	mass of the AUV
g	acceleration of gravity
ρ	fluid density
V	volume of fluid displaced by the vehicle
W	weight of the AUV
B	buoyancy force of the AUV
I_0	inertia tensor referred in the body-fixed frame
$\boldsymbol{r}_G$	vector of center of gravity
$\boldsymbol{r}_B$	vector of center of buoyancy
X, Y, Z	forces in x, y, z direction of the body-fixed frame
K, M, N	torques around x, y, z direction of the body-fixed frame
u, v, w	linear velocities in the body-fixed frame
p, q, r	angular velocities in the body-fixed frame
x, y, z	position coordinates in the earth fixe frame
ϕ, θ, ψ	Euler angles in the earth fixe frame
η	position and orientation vector in the earth-fixed frame
η_1	position vector in the earth-fixed frame
η_2	orientation vector in the earth-fixed frame
υ	linear and angular velocity in the body-fixed frame
υ_1	linear velocity vector in the body-fixed frame
υ_2	angular velocity vector in the body-fixed frame

M_{RB}	rigid-body inertia matrix
τ	forces and moments acting on the AUV
τ_1	forces acting on the AUV
τ_2	moments acting on the AUV
τ_{RB}	external forces and moments acting on rigid-body
τ_R	radiation-induced forces and moments
τ_E	environmental forces and moments
τ_D	hydrodynamic damping forces and moments
M_A	added inertia matrix
λ_{ij}	elements of added inertia matrix
λ_{ij0}	elements of added mass of planar contour
V_B	total body volume
S_B	maximum body section area
d	maximum body diameter
l_B	length of the body
S_o	body cross-sectional area where the flow is potential
x_m	distance from the vertex to the center of rotation
α	angle of attack in radians
d_b	base diameter
x_c	distance from the vertex to the center of the volume
V_∞	relative free stream velocity
C_m	hydrodynamic moment coefficient

C_L	hydrodynamic lift coefficient
C_D	hydrodynamic drag coefficient
C_{D_0}	hydrodynamic zero-lift drag coefficient
C_f	turbulent skin-friction coefficient
C_{D_b}	base-drag coefficient
$\left(C_{D_f}\right)_b$	zero-lift drag of the body exclusive of the base drag
c_{L_α}	hydrodynamic body lift-curve slope
c_{m_α}	hydrodynamic moment curve slope
c_{L_q}	hydrodynamic lift pitching coefficient
c_{m_q}	hydrodynamic moment pitching coefficient
C_{L_α}	simplified hydrodynamic lift curve slope
C_{m_α}	simplified hydrodynamic moment curve slope
C_{L_q}	simplified hydrodynamic lift pitching coefficient
C_{m_q}	simplified hydrodynamic moment pitching coefficient
C_{N_α}	hydrodynamic normal-force curve slope
C_{N_q}	hydrodynamic normal-force pitching coefficient
C_{D_c}	cross flow drag coefficient of control fin
$C_{L_{\alpha 1}}$	first order hydrodynamic lift coefficient of fin
$C_{L_{\alpha 2}}$	second order hydrodynamic lift coefficient of fin

C_{D_L}	hydrodynamic lift to drag coefficient of fin
$\bar{y}$	effective rotation axis
ω	effective pitching angular velocity
$\boldsymbol{L}$	hydrodynamic lift force vector
$\boldsymbol{D}$	hydrodynamic lift force vector
$\boldsymbol{M}$	hydrodynamic moment vector
$\boldsymbol{r}_{FIN}$	vector of center of fin in the body-fixed frame
δ_H	deflection angle of the horizontal fin
δ_V	deflection angle of the vertical fin
β	jet drive angle with respect to the main axis
a	distance from the outlet of the nozzle to the main axis
l	distance from outlet of nozzle to the vehicle center
h	arm of the torque of the thruster force
T	thruster force in the main axis direction
T_{i}	thruster forces of each jet drive
M_{i}	thruster torques of each jet drive
K_{i}	reaction torques of each jet drive
$\boldsymbol{q}$	orientation quaternion
$\boldsymbol{q}_{gyo}$	orientation quaternion integrated from the gyroscope
$\boldsymbol{q}_{acc,mag}$	accelerometer and magnetometer orientation quaternion

Chapter 1 Introduction

1.1 Background

Autonomous underwater vehicles (AUVs) are unmanned tether-free robotic devices that are controlled by onboard computers with preprogrammed underwater missions. As a new generation of underwater robot, AUV possesses a self-contained power supply and control system, and operates independently of the ship without any external cables or data transmission. It can navigate intelligently and automatically underwater through preset programs. Because of its great commercial significance and large technological challenges, AUV attracts more and more attentions from scientists and technicians.

The oil and gas industry uses AUVs to make detailed maps of the seafloor before they start building subsea infrastructure, and pipelines and subsea completions can be installed in the most cost effective manner with minimum disruption to the environment[1, 2]. The AUV allows survey companies to conduct precise surveys in areas where traditional bathymetric surveys would be less effective or too costly. Also, post-lay pipe surveys are now possible. A typical military mission for an AUV is to map an area to determine if there are any mines, or to monitor a protected area (such as a harbor) for new unidentified objects. AUVs are also employed in anti-submarine warfare, to aid in the detection of manned submarines. Scientists use AUVs to study lakes, the ocean, and the ocean floor. A variety of sensors can be affixed to AUVs to measure the concentration of various elements or compounds, the absorption or reflection of light, and the presence of microscopic life[3].

The first AUV SPURV (Special Purpose Underwater Research Vehicle) was developed in the Applied Physic Laboratory at the University of Washington in 1957, by Stan Murph, Bob Francois and later improved by Terry Ewart to study diffusion, acoustic transmission, and submarine wakes[4]. AUV development in the early period reflects some research and military needs. With the advancement of technologies of AUV, the cost of AUV has declined to affordable levels. Some large marine survey companies began to cooperate

with AUV research agencies and marine survey equipment suppliers to provide the technical methods for marine survey to adapt to more efficient and high quality survey requirements. The major companies include Kongsberg Maritime in Norway, Hydroid in the United States., Bluefin Robotics Corporation in the United States. and Hafmynd Company in Iceland etc.

Kongsberg Maritime from Norway began to develop AUV system in 1980s. It customized Hugin (High Precision Untethered Geosurvey and Inspection System) 3000 AUV that possesses 3000 m working depth for C&C Corporation, a marine commercial survey company in the United States[5]. HUGIN 3000 AUV is 5 m in length, 1 m diameter and weighted 1450 kg. It integrated with Edgetech 120/410 kHz dual-frequency digital side scan sonar, Edgetech 2-10 kHz bottom profiler, precision bathymetric machine, forward-looking sonar and other equipment. The designed aluminum oxide fuel cells allowed the vehicle constantly navigate underwater for 48 hours [6, 7].

Hydroid in the United States was founded in 2001. Separated from Woods Hole Oceanographic Institution, Hydroid took charge of specific maintenance and development on a whole range of REMUS AUVs including REMUS 100, 600, 3000 and 6000. It grew rapidly from light type such as one-man-portable to deep heavy AUV and gains a large number of orders from the military[8, 9]. In December, 2007 Hydroid was purchased by Kongsberg Maritime.

Bluefin Robotics Corporation in the United States was built in 1997, separated from the AUV laboratory in MIT. The modular designed product Bluefin-21 AUV can work underwater at a depth of 4500 m. The basic configuration is 4.9 m in length, 0.5 m in diameter and 750 kg in weight. Usually it is equipped with multi-beam side scan sonar and shallow bottom profiler.

Hafmynd Corporation in Iceland manufactured a kind of portable lightweight Gavia AUV which also adopts modular design. The basic configuration is 2.7 m at length, 0.2 m at diameter and 80 kg at weight. Shallow and deep models possess the same shape, but different materials for pressure resistant. The new model is equipped with GeoSwath interferometer sonar, side scan sonar, shallow bottom profiler and camera[10].

The appearance of many AUV manufacture corporations indicates that development of various AUV technologies has already been popularized. Many international institutions are still making efforts to make AUV more long-range, precise and intelligent. AUV market segments have emerged nowadays. Low-end portable AUV has already appeared in the present product line of manufacturing industry. Some high-end engineering products such as AUV-ROV integrated with the function of ROV (Remotely Operated Vehicle) will take place of current ROV with cables as an effective tool for the marine engineering construction.

1.2 Literature Review

1.2.1 AUV Systems and Components

Depending on the applications, the mechanical and electrical configurations of an underwater vehicle are different. But a basic AUV should at least have a hull to place the onboard components, a propulsion mechanism, a sensor system, a control system and a power system[11], which are reviewed as follows.

The hull shape is mostly dependant on the desired missions. Hulls can be classified as open or closed. Open frame hulls are flexible and modular allowing external sensors and thrusters to be added or moved around the frame. On the other hand, closed frame hulls are compact and provide better hydrodynamics, but are hard to modify[12]. If the vehicle needs high speed motion in the water then a streamline body is required. In this research we only concerned about the close frame streamlined AUVs, which always take the torpedo shape like the REMUS and the Bluefin AUVs.

The propulsion mechanism is used to drive the AUV through water by moving water at some velocity. Propellers, pod propulsions, and jets are the most widely used the propulsion methods in underwater applications[12]. Selecting the appropriate mechanism depends on factors such as the size, cost, power consumption and produced thrust.

An AUV always contains a large number of sensors, which can be divided into two major groups[13]: navigation devices and exploration devices .The first

group includes sensors such as Global Positioning System (GPS) Receiver, Doppler Velocity Log (DVL), one or more sonar modules, depth sensor, compass and gyroscope[14]. The GPS receiver is used to determine the vehicle's position while it is on the surface, while the DVL is used to approximate the vehicle's position when it is submerged. The depth sensor is used to measure the vehicle's depth under the sea. Compasses as well as gyroscopes are used to determine the orientation of the vehicle. Finally, the sonar modules are used to detect obstacles along the vehicle's path. The second group is composed of sensors that allow the AUV to register and log data related to the underwater environment. These devices can vary from one AUV to another. As the AUV technology becomes more reliable, more sensors are added in order to observe more data regarding the oceans[15].

The control system of the AUV is always composed of two architectural levels: the low-level attitude control and the high-level mission control. The attitude control system is one of the most critical parts of an AUV. It is in charge of regulating the depth, speed and orientation of the vehicle. Several challenges need to be taken into consideration when designing the attitude controller, such as the non-linear nature of the vehicle dynamics and the disturbances generated by the water currents in the ocean[16]. Most AUVs are underactuated meaning that they have more degrees of freedom (DOF) to be controlled than the number of independent control inputs. Torpedo shaped AUVs do not usually have independent sway or heave actuators. If classical motion control systems designed for fully or overactuated vehicles are directly used on underactuated AUVs, the resulting performance of controlled systems is poor or control objectives cannot be achieved[17]. Another reason is that underactuated ocean vehicles cannot be stabilized by any time-invariant continuous state feedback controllers although they are open loop controllable. This fact resulted from a direct application of the Brockett necessary condition to feedback stabilization of underactuated ocean vehicles[18]. As a consequence, the classical smooth control theory cannot be applied. This motivates researchers to seek other approaches which can be roughly classified into discontinuous feedback[19-22] and time-varying feedback[17, 18, 23-26]. The discontinuous feedback approach often adopts a switching

control strategy which results in a fast transient response with the drawback of discontinuity in the control input. On the other hand, the time-varying feedback approach provides a smooth controller, however the price is slow convergence. The motion control of underactuated AUVs has opened a new territory in applied nonlinear control, and attracted special attention from both marine technology and control engineering communities not only because it poses many challenging questions in applied nonlinear control theory, but also because of its practical importance.

AUVs should have their own intelligent system or high level-controller, in order to perform a series of missions without human intervention. Therefore, the system should be able to handle unanticipated situations, support real-time reasoning and control the vehicle[27]. A high-level controller allows the definition and planning the desired missions[28, 29]. Additionally, a fault tolerant system is required in order to handle possible failures that may arise during a mission execution[16].

The initial AUV prototypes were powered by conventional lead acid batteries but eventually more advanced AUVs were developed using lithium batteries. Nowadays, some advanced vehicles adopt semi fuel cells (Aluminum-Oxygen) and fuel cells (Hydrogen-Oxygen). Lithium batteries are now commonly used in most modern AUVs since they are easy to use, relatively safe and their energy density is high. Rechargeable lithium batteries can last between 16 and 30 hours when used on a generic AUV with a volume of 1.2 m^3. Primary lithium batteries can last between 40 and 60 hours when installed on the same generic AUV. Fuel cells are mainly used in deep-water operations on large AUVs. Their energy density is very high, but the system is rather complex and there are some safety issues regarding the handling of chemicals[30]. And an emerging trend is to combine different battery and power systems with supercapacitors.

1.2.2 Current Research on Micro AUVs

Hundreds of different AUVs which range in size from man portable lightweight AUVs to large diameter vehicles of over 10 m length have been designed over the past 50 or so years, but only a few companies sell these

vehicles[31, 32]. Large vehicles have advantages in terms of endurance and sensor payload capacity, but they are always equipped with complicated mechanical and electrical systems, which makes them too expensive for many tasks which may actually need them. And large vehicles are more difficult and more costly to transport, launch and recover. In smaller areas that need exploring, such as in wrecks and subterranean rivers, or amongst coral reefs, where it is important for the vehicle to be able to navigate in small spaces, the large AUVs are extremely inefficient.

Micro AUVs benefit significantly from lower logistics (for example: support vessel footprint, launch and recovery systems) and are small enough that many of these problems can be resolved. These vehicles would be able to reach where current AUVs fail, and will be much affordable and won't be a financial problem if they are lost or damaged.

It has been widely accepted by commercial organizations that to achieve the ranges and endurances required to optimize the efficiencies of operating AUVs a larger vehicle is required. Along with the advance of the technology of underwater vehicles, micro AUVs with the advantages of smaller body, lower resistance, better flexibility, high effectiveness/cost and being equipped more conveniently will be able to carry out many missions that the normal size AUVs cannot and expand the application of underwater vehicles. Current research on micro AUVs are reviewed as follows.

A micro AUV MONSUN II has been designed for application in a robotic swarm in University of Lübeck[33]. Following the definition and the requirements of swarm robots, MONSUN is equipped with sensors that allow mainly limited range sensing like the camera or the lateral avoidance sensor. This results in an inexpensive vehicle since costly sensors are not required. The small size makes it even applicable in environments that are difficult to access. Preliminary experiments have shown that MONSUN is capable of maneuvering and diving even in case of malfunction of a vertical thruster. The built-in camera can detect other swarm members and allows them to work as a group.

Nekton Research has developed a new series of micro AUVs called Ranger that house commercial, multi-parameter water sensor arrays[34]. Teams of these 90 mm diameter AUVs work together to allow multi-agent, distributed sensing of inshore and near shore water down to 100 m depth. Swimming in schools of 4 to 12 members, these vehicles will work together to characterize phenomena as diverse as chemical plume geometry, small scale mixing, and 3D flow dynamics. While useful as single vehicles, the real strength of Rangers is their ability to work as a coordinated team.

The Serafina project at the Australian National University is focused on the potentials of multiple, small, fully autonomous, but organized underwater vehicles too[35, 36]. A school of these underwater vehicles offers possibilities far beyond any individual submersible for fault-tolerant, scalable coverage of ocean spaces[37, 38].

The monitoring of liquid-based industrial processes is a technically complex task with few viable solutions for medium to large scale plants[39-41]. Mobile Underwater Sensor Networks (MUSNs) are an attractive solution to this problem for processes that can tolerate the inclusion of foreign objects; examples include nuclear storage ponds and wastewater treatment facilities. Most underwater vehicles are aimed at oceanographic applications and are too large to be used in relatively small space. Micro AUVs can form the basis of MUSNs for monitoring underwater environments. A micro AUV with a 150 mm diameter sphere hull has been developed in the University of Manchester to monitor the radioactive waste in the nuclear storage ponds[42-46].

It can be concluded from the literature review above that micro AUVs usually have quite a limited payload capacity, and the researchers hope they can work as a team to provide the ability of carrying out the specified missions effectively.

1.2.3 Current Research on Modular Designed AUVs

With the increasingly expansion of the field of ocean development, it demands a higher overall performance and operation capacity of the underwater vehicle in different environment, different tasks and different objectives, so a stronger adaptability of the underwater vehicle will be required. An underwater vehicle

system which consists of the basic modules for basic functions and specific modules for different specific tasks provides a practical way for different experimental researches and practical applications[47].

Modular design methods have become a hot research area in the development of AUVs in the sense that the vehicle has a highly reconfigurable modular construction, which allows for a simple integration of different payloads (swapping or adding sensors, for example) and independent subsystem development. Modularity of the system in the overall design can not only reduce the size and weight of the vehicle but also minimize the development and operational costs[48-50], and at the same time reduce the size and weight of the vehicle and the necessary mission support equipment. Furthermore, the modularity of the system allows the integration of other thrusters, to enhance the control of vehicle[51].

The adoption of modular architectures has been exploited in mature manufacturing processes for a long time, with the realization that such approach yields great benefits in terms of adaptation to new demands from customers and also in terms of product variety, i.e., the diversity of solutions that can be manufactured from the same basic components[52]. Such variety should be methodically considered during the design phase, by a proper analysis of module characteristics and how they affect overall system performance[53].

In terms of AUV design, a good example of modularity is the Gavia AUV, with continuous developments to accommodate new systems[54]. Another example of modularity of relatively large vehicles with high performance sensors is the Bluefin AUV[55]. There are some other modular designed torpedo shaped AUVs, such as the REMUS series developed by Hydroid, the United States, the MARES developed by the University of Porto[48, 51, 56], and the Starfish AUV designed by the Acoustic Research Laboratory of the National University of Singapore[49]. They are typical representatives of torpedo shaped modular underwater vehicles, but also reflect the research level of the modular underwater vehicle technology nowadays.

The theory foundation of the modular design method for underwater vehicle is discussed in[47]. The purpose of modular design for underwater vehicle is to seek the best feasible design. This modular design method translates the traditional design process based on experience into a mathematical model based on scientific principle and rules, and uses mathematical language to describe the product design process, which provides a basic method for modular mechanism design and reconfiguration of underwater vehicles.

1.2.4 Review on the Modeling of AUVs

The development of an AUV is an expensive and time consuming task. The more the design and testing process relies on the prototype, the more serious this situation will become. And the risk of damaging or even losing of the prototype in the field testing due to design flaws or control errors is high in the design iteration stage. As a result, computer modeling of the vehicle becomes one of the most powerful tools to AUV designers, particularly in the initial phases of vehicle development[57]. The dynamic model of AUV representing the vehicle's interaction with the surrounding fluid is the core of creating such a computer simulation environment. Such a dynamic model of the AUV provides the designer a tool for understanding the inherent motion characteristics of a proposed vehicle before prototyping.

Establishment of the vehicle's dynamic model can be broken down into three sub-tasks[58]: the derivation of the mathematical equations which govern the motion of the vehicle[59], the determination of the hydrodynamic characteristics for a given vehicle[60, 61], and the computational solution of the system of equations, for a known set of control inputs, to obtain the ensuing motion. The hydrodynamic characteristics of AUV quantified by hydrodynamic coefficients are the main sources of the uncertainty of the dynamic model and usually introduce the greatest error to the final simulation results.

The hydrodynamic coefficients are coefficients in the mathematical model which quantify the forces and moments acting on the vehicle as a function of its attitude and motion. Actually there are at least two sets of hydrodynamic coefficients being widely used in the research field of AUVs. One set makes

use of lift, drag and pitching moment coefficients (like C_L, C_D, C_m) which relates the forces and moments to the relative fluid speed and attack angle of the AUV. The other set are derivatives of the hydrodynamic forces and moments directly to the translational and angular velocities of the AUV in the body-fixed frame (like X_{uu}, Y_{vv}, N_{rr}). We note the former set as hydrodynamic coefficients and the latter set as hydrodynamic derivatives separately in this thesis.

A number of methods have been proposed for the determination of hydrodynamic coefficients and[60] gives an overview of some of these. They can be broadly grouped into predictive methods and testing methods. The predictive methods require only vehicle design data and can predict these parameters before the prototype is built. The test-based methods include direct experimental determination based on wind-tunnel or tow-tank model tests, and trials of full-size captive vehicles[62]. The main disadvantage of the test-based methods is the need of a vehicle and the testing facilities which are often not available, either for reasons of cost or because the vehicle is still under design.

The most basic of the predictive methods are purely analytical which are least likely to yield realistic results. Empirical methods are the most widespread of the predictive methods and have been shown to yield reasonable results when applied to streamlined vehicles[63-65]. Luckily, many AUVs fall into this category, and only the torpedo shaped AUVs are studied in this research.

Torpedo shaped AUVs are always composed of simple shaped components such as a hull which is always a slender body of revolution and several control surfaces (rudders and elevators), whose hydrodynamic behaviors are well known. And the hydrodynamic coefficients of these simple shaped components can be derived from well-known empirical relations which only require the specification of the vehicle's geometry[58]. The hydrodynamic damping forces and moments acting on each of these components can be calculated directly from the relations that govern the flow around simple shapes. By translating these forces and moments into the body-fixed frame and summing them together, the forces and moments acting on the whole vehicle can be reached. Because the model is not linearized, it retains the vehicle's

fundamental nonlinear behaviors. The drawback of this kind of method is the very rudimentary manner in which interference effects are taken into account[66].

But some of these hydrodynamic coefficients may not be estimated by the empirical methods accurately like the pitching and moment related parameter, for they are all related to the pressure center of vehicle at angle of attack which is not easy to be estimated especially for AUVs with non-streamlined appendages mounted on the hull. As a result, to estimate the hydrodynamic coefficients with pure empirical methods in the design stage is attractive but not accurate enough for already constructed specified AUV without perfect streamlined shapes. System identification techniques are a more efficient and flexible test-based method and can be applied to free-swimming model or full-size vehicle tests without complicated laboratory testing facilities.

For a given AUV, the hydrodynamic damping calculated by the method, which makes use of hydrodynamic coefficients, are nonlinear and coupling function of the velocities and the control fin reflection angles of the AUV. The results can be used directly to the simulation of the AUV, but it is not easy to use these results to the controller design of the AUV[67]. The hydrodynamic derivatives can be reached by first order or second order Taylor's expansion with respect to the velocities of the AUV and the control fin reflection angles. Then, the control law can be designed based on the dynamic model of the vehicle with the hydrodynamic damping calculated by these hydrodynamic derivatives.

1.3 Motivation

Most of the labs and companies researching and working in the field of AUVs are concerned with big size vehicles nowadays. But with the development of more advanced processing capabilities and high yield power supplies and micro sensing systems, micro AUVs will definitely be the next generation of underwater vehicles.

The literature of the simulation and control of the AUV is vast, but most of these algorithms require a quite precise dynamics model of the vehicle in order to obtain a reasonable simulation result or to generate the proper thrust and

possibly fin angle commands and hence create smooth and precise trajectories. Modular design methods are widely used in the development of AUVs. Therefore, the method to construct the dynamic models for these modular designed AUVs needs to be flexible for reconfiguration. However, based on the analysis of existing literature, it seems that the technology of modular design of underwater vehicle is structural and primarily focused on the application. And there is still no easy way of obtaining the dynamic model of reconfigured modular designed AUV.

For an AUV reconfigured with modular sections, rebuilding the dynamic model will be quite an effort and time consuming job, especially when some of the hydrodynamic parameters can only be obtained accurately through field testing and parameter identification[68]. The goal of modular dynamic modeling should be to establish a 'parameter list' for each modular section which is determined by either predictive or test-based methods. Then the dynamic model of any newly reconfigured AUV can be constructed readily and precisely by computing the related parameter lists together and transforming these parameters into its body-fixed frame.

1.4 Research Objective and Scopes

Based on the motivations above, the objective of this research is to develop a finless torpedo shaped micro AUV, and to study the modular dynamic modeling of AUV based on this platform. The scopes of this research will cover the following issues:

1. Establish a dynamic model of AUV suitable for parameter estimation and modular dynamic modeling, summarize the empirical methods for the hydrodynamic coefficients and added mass estimation, and find the relationship between hydrodynamic coefficients and hydrodynamic derivatives.

2. Develop a finless torpedo shaped micro AUV named Lancelet with a novel multi-jet drive propulsion system, study the performance of the designed propulsion system, and explore the Lancelet's special maneuverability by open loop free swimming trials.

3. Combine the empirical and parameter identification methods for accurate estimation of the hydrodynamic coefficients of torpedo shaped AUVs based on the experimental data of both the Starfish AUV and the micro AUV Lancelet.

4. Verify the proposed standard reference model method for the modular dynamic modeling of the torpedo shaped AUV with both empirical and experimental methods.

1.5 Thesis Organization

The dynamic model of AUV is summarized in Chapter 2 with relevant literature reviews. The estimation of added mass and the hydrodynamic coefficients with empirical methods, and the relationship between hydrodynamic coefficients and hydrodynamic derivatives are included in this chapter too. The development and the field tests of the finless torpedo shaped micro AUV named Lancelet are presented in Chapter 3. The parameter identification methods are combined with the empirical methods to estimate both the hydrodynamic coefficients and hydrodynamic derivatives of the Starfish AUV and the Lancelet micro AUV in Chapter 4. The key problem of modular dynamic modeling of the AUV, which is the modularization of the hydrodynamic characteristic of the AUV, is discussed in Chapter 5. This chapter also proposed the standard reference model method to address the modular modeling issues with empirical and experimental verification. In Chapter 6, the contributions of this research are summarized and some directions of further work are suggested.

Chapter 2 AUV Dynamic Model and Parameters Estimation

The dynamic model of AUV and the estimation of hydrodynamic parameters with empirical methods are reviewed in this chapter. The kinematic and dynamic models of AUV and the related notation are summarized from Fossen's book[69]. And the empirical methods for the hydrodynamic coefficients and added mass estimation are reviewed. Based on these summaries, a vector based damping forces and moments model for torpedo shaped AUV is established and the relationship between the hydrodynamic coefficients and the hydrodynamic derivatives is presented.

2.1 Kinematics

Two coordinate frames are defined to describe the motion of AUVs in 6 DOF as shown in Figure 2.1, the body-fixed reference frame ($x_b y_b z_b$), and the earth-fixed frame ($x_e y_e z_e$). The body-fixed frame coincide with the principal axes of inertia of the vehicle with the longitudinal axis x_b from aft to fore, the transverse axis y_b from starboard to port, and the normal axis z_b from bottom to top. The origin of the body-fixed frame is coincident with the center of buoyancy of the vehicle in this thesis. The earth-fixed frame are defined according to the east north up notation.

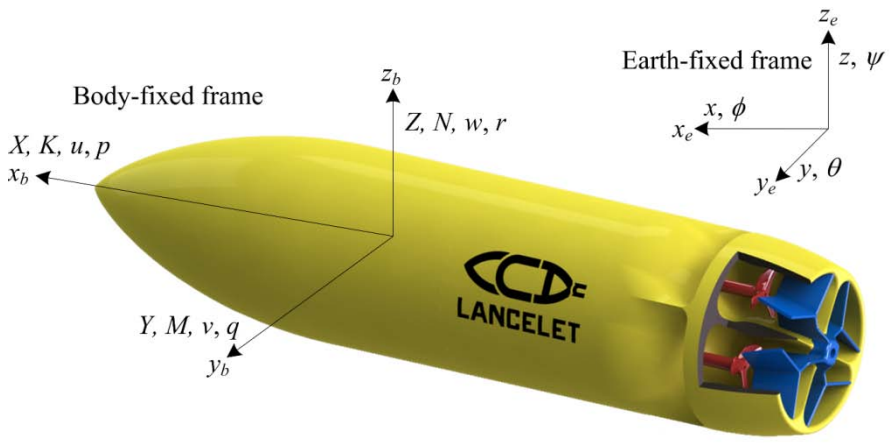

Figure 2.1 Body-fixed and earth-fixed reference frames

The position and orientation of the vehicle are described relative to the earth-fixed reference frame while the linear and angular velocities of the vehicle are expressed in the body-fixed coordinate system, shown in Table 2.1 [69].

Table 2.1 Notation used for underwater vehicles

6 motion components	forces and moments	linear and angular velocities	positions and Euler angles
surge (motions in the *x*-direction)	X	u	x
sway (motions in the *y*-direction)	Y	v	y
heave (motions in the *z*-direction)	Z	w	z
roll (rotation about the *x*-axis)	K	p	ϕ
pitch (rotation about the *y*-axis)	M	q	θ
yaw (rotation about the z-axis)	N	r	ψ

Based on this notation, the general motion of a underwater vehicle in 6 DOF can be described by the following vectors[69].

$$\eta = \left[\boldsymbol{\eta}_1^T, \boldsymbol{\eta}_2^T\right]^T; \quad \boldsymbol{\eta}_1 = \left[x, y, z\right]^T; \quad \boldsymbol{\eta}_2 = \left[\phi, \theta, \psi\right]^T$$

$$\upsilon = \left[\boldsymbol{\upsilon}_1^T, \boldsymbol{\upsilon}_2^T\right]^T; \quad \boldsymbol{\upsilon}_1 = \left[u, v, w\right]^T; \quad \boldsymbol{\upsilon}_2 = \left[p, q, r\right]^T$$

$$\tau = \left[\boldsymbol{\tau}_1^T, \boldsymbol{\tau}_2^T\right]^T; \quad \boldsymbol{\tau}_1 = \left[X, Y, Z\right]^T; \quad \boldsymbol{\tau}_2 = \left[K, M, N\right]^T$$

Here, η denotes the position and orientation vector with coordinates in the earth-fixed frame, υ denotes the linear and angular velocity vector with coordinates in the body-fixed frame and τ is used to describe the forces and moments acting on the vehicle in the body-fixed frame. The Euler angular transformation in equation (2.1) relates η and υ, which gives the kinematics transformation between the body-fixed frame and the earth-fixed frame,

$$\dot{\eta} = J(\eta)\upsilon = \begin{bmatrix} J_1(\boldsymbol{\eta}_2) & 0 \\ 0 & J_2(\boldsymbol{\eta}_2) \end{bmatrix} \upsilon \tag{2.1}$$

where,

$$J_1(\boldsymbol{\eta}_2) = \begin{pmatrix} \mathrm{c}\psi\mathrm{c}\theta & -\mathrm{s}\psi\mathrm{c}\phi + \mathrm{c}\psi\mathrm{s}\theta\mathrm{s}\phi & \mathrm{s}\psi\mathrm{s}\phi + \mathrm{c}\psi\mathrm{c}\phi\mathrm{s}\theta \\ \mathrm{s}\psi\mathrm{c}\theta & \mathrm{c}\psi\mathrm{c}\phi + \mathrm{s}\phi\mathrm{s}\theta\mathrm{s}\psi & -\mathrm{c}\psi\mathrm{s}\phi + \mathrm{s}\theta\mathrm{s}\psi\mathrm{c}\phi \\ -\mathrm{s}\theta & \mathrm{c}\theta\mathrm{s}\phi & \mathrm{c}\theta\mathrm{c}\phi \end{pmatrix} \tag{2.2}$$

$$J_2(\boldsymbol{\eta}_2) = \begin{pmatrix} 1 & \mathrm{s}\phi\mathrm{t}\theta & \mathrm{c}\phi\mathrm{t}\theta \\ 0 & \mathrm{c}\phi & -\mathrm{s}\phi \\ 0 & \mathrm{s}\phi/\mathrm{c}\theta & \mathrm{c}\phi/\mathrm{c}\theta \end{pmatrix} \tag{2.3}$$

where s denotes sin, c denotes cos and t denotes tan.

2.2 Dynamics

General 6 DOFs rigid body dynamic equations are as follows[69],

$$m\left[\frac{\partial \boldsymbol{\upsilon}_1}{\partial t}+\boldsymbol{\upsilon}_2\times\boldsymbol{\upsilon}_1+\frac{d\boldsymbol{\upsilon}_2}{dt}\times\mathbf{r}_G+\boldsymbol{\upsilon}_2\times\left(\boldsymbol{\upsilon}_2\times\mathbf{r}_G\right)\right]=\boldsymbol{\tau}_1 \tag{2.4}$$

$$I_0\frac{d\boldsymbol{\upsilon}_2}{dt}+\boldsymbol{\upsilon}_2\times\left(I_0\boldsymbol{\upsilon}_2\right)+m\mathbf{r}_G\times\left(\frac{\partial \boldsymbol{\upsilon}_1}{\partial t}+\boldsymbol{\upsilon}_2\times\boldsymbol{\upsilon}_1\right)=\boldsymbol{\tau}_2 \tag{2.5}$$

where, $\mathbf{r}_G=\left[x_G,y_G,z_G\right]^T$ is the center of gravity in the body-fixed frame, and I_0 is the inertia tensor referred to the body-fixed frame. These two equations can be expressed in a more compact form as

$$M_{RB}\dot{\upsilon}+C_{RB}(\upsilon)\upsilon=\tau_{RB} \tag{2.6}$$

The rigid-body inertia matrix M_{RB} is,

$$M_{RB}=\begin{bmatrix} mI_{3\times3} & -mS\left(\mathbf{r}_G\right) \\ mS\left(\mathbf{r}_G\right) & I_0 \end{bmatrix} \tag{2.7}$$

The Coriolis and Centripetal matrix is,

$$C_{RB}\left(\upsilon\right)=\begin{bmatrix} 0_{3\times3} & -mS\left(\boldsymbol{\upsilon}_1\right)-mS\left(\boldsymbol{\upsilon}_2\right)S\left(\mathbf{r}_G\right) \\ -mS\left(\boldsymbol{\upsilon}_1\right)+mS\left(\mathbf{r}_G\right)S\left(\boldsymbol{\upsilon}_2\right) & -S(I_0\boldsymbol{\upsilon}_2) \end{bmatrix} \tag{2.8}$$

where *S* is the skew-symmetric matrix function defined in[69].

$\tau_{RB}=\left[X,Y,Z,K,M,N\right]^T$ is the generalized vector of external forces and moments.

2.3 External Forces and Moments

The external forces and moments acting on the AUV can be classified according to[69] as the following expression,

$$\tau_{RB}=\tau_R+\tau_E+\tau \tag{2.9}$$

τ_R is the radiation-induced forces (forces and moments). τ_E is the environmental forces acting on the vehicle due to ocean currents, waves, and the wind. τ denotes the thruster forces. The environmental forces are mainly related to floating objects[70]. For AUVs operated underwater the environmental forces can be neglected or can be treated as disturbance if needed. The thruster forces are the inputs to the AUV, and can be treated

separately. The radiation-induced forces are composed of the restoring forces (weight and buoyancy), and the hydrodynamic forces which include the added mass and the hydrodynamic damping forces. The radiation-induced forces are always denoted by expression (2.10) [69], the terms of which will be discussed in more detail.

$$\tau_R = \underbrace{-g(\eta)}_{\text{restoring forces}} \underbrace{-M_A\dot{\upsilon} - C_A(\upsilon)\upsilon}_{\text{added mass}} \underbrace{-D(\upsilon)\upsilon}_{\text{damping}} \tag{2.10}$$

2.3.1 Restoring Forces and Moments

Let *m* be the mass of the AUV, *V* the volume of fluid displaced by the vehicle, *g* the acceleration of gravity and ρ the fluid density. The weight of the AUV is defined as: $W=mg$, while the buoyancy force is defined as: $B=\rho Vg$. According to the east north up notation, the weight and buoyancy force can be transformed to the body-fixed coordinate system by,

$$f_G(\boldsymbol{\eta}_2) = J_1^{-1}(\boldsymbol{\eta}_2)\begin{bmatrix} 0 \\ 0 \\ -W \end{bmatrix}, f_B(\boldsymbol{\eta}_2) = J_1^{-1}(\boldsymbol{\eta}_2)\begin{bmatrix} 0 \\ 0 \\ B \end{bmatrix} \tag{2.11}$$

According to equation (2.10), the sign of the restoring forces and moments $g(\eta)$ must be changed since this term is included on the left-hand side of Newton's 2nd law. Consequently, the restoring force and moment vector in the body-fixed coordinate system is,

$$g(\eta) = -\begin{bmatrix} f_G + f_B \\ \boldsymbol{r}_G \times f_G + \boldsymbol{r}_B \times f_B \end{bmatrix} \tag{2.12}$$

where, $\boldsymbol{r}_B = [x_B, y_B, z_B]^T$ is the center of buoyancy in the body-fixed frame Expanding this expression yields,

$$g(\eta) = \begin{bmatrix} -(W-B)s\theta \\ (W-B)c\theta s\phi \\ (W-B)c\theta c\phi \\ (y_G W - y_B B)c\theta c\phi - (z_G W - z_B B)c\theta s\phi \\ -(z_G W - z_B B)s\theta - (x_G W - x_B B)c\theta c\phi \\ (x_G W - x_B B)c\theta s\phi + (y_G W - y_B B)s\theta \end{bmatrix} \tag{2.13}$$

2.3.2 Hydrodynamic Forces and Moments

The hydrodynamic forces and moments acting on a body moving in real incompressible fluid are determined by inertial and viscous properties of the fluid. In certain approximations one can distinguish the forces and moments of inertial nature which can be computed assuming that the fluid is ideal (non-viscous), and the forces and moments which are related to viscosity.

The forces and moments of the inertial nature can be expressed in terms of the added mass of the body. It is especially important to take the added mass (or added moments of inertia) into account if they are comparable with the mass (or moments of inertia) of the body. The methods for added mass estimation will be discussed in details in the later subsections.

The forces and moments due to the viscosity of the fluid are noted as hydrodynamic damping. Hydrodynamic damping for ocean vehicles are mainly caused by potential damping, wave drift damping, skin friction and vortex shedding[69]. In general, the damping of an AUV moving with 6 DOFs will be highly nonlinear and coupled. It is impossible to calculate each of these damping effects separately. The empirical method of calculating damping forces and moments based on hydrodynamic coefficients will be discussed in the later subsections.

The modeling of the hydrodynamic forces including added mass and damping forces is the main problem of constructing the dynamic model of the AUV. The specific method to estimate and simplify the hydrodynamic forces acting on the AUV distinguishes one dynamic model from those of other modeling methods.

2.4 Added Mass Estimation

Added mass is used to describe the hydrodynamic forces and moments acting on the accelerating or decelerating body due to the inertial property of the fluid. Added mass should be understood as pressure induced forces and moments which are proportional to the acceleration of the body. Added mass can be described with an added inertia matrix M_A and a matrix of hydrodynamic Coriolis and centripetal terms denoted $C_A(\upsilon)$ as follows[71].

$$M_A = \begin{bmatrix} A_{11} & A_{12} \\ A_{21} & A_{22} \end{bmatrix} = -\begin{bmatrix} X_{\dot{u}} & X_{\dot{v}} & X_{\dot{w}} & X_{\dot{p}} & X_{\dot{q}} & X_{\dot{r}} \\ Y_{\dot{u}} & Y_{\dot{v}} & Y_{\dot{w}} & Y_{\dot{p}} & Y_{\dot{q}} & Y_{\dot{r}} \\ Z_{\dot{u}} & Z_{\dot{v}} & Z_{\dot{w}} & Z_{\dot{p}} & Z_{\dot{q}} & Z_{\dot{r}} \\ K_{\dot{u}} & K_{\dot{v}} & K_{\dot{w}} & K_{\dot{p}} & K_{\dot{q}} & K_{\dot{r}} \\ M_{\dot{u}} & M_{\dot{v}} & M_{\dot{w}} & M_{\dot{p}} & M_{\dot{q}} & M_{\dot{r}} \\ N_{\dot{u}} & N_{\dot{v}} & N_{\dot{w}} & N_{\dot{p}} & N_{\dot{q}} & N_{\dot{r}} \end{bmatrix} \tag{2.14}$$

$$C_A(\upsilon) = \begin{bmatrix} 0_{3\times 3} & -S(A_{11}\upsilon_1 + A_{12}\upsilon_2) \\ -S(A_{11}\upsilon_1 + A_{12}\upsilon_2) & -S(A_{21}\upsilon_1 + A_{22}\upsilon_2) \end{bmatrix} \tag{2.15}$$

2.4.1 Properties of Added Mass

1) Properties of added inertia matrix

First: The values for the M_A do not depend on the kinematics of the motion of the fluid; these values are determined only by the shape of the body, chosen coordinate system and fluid density ρ.

Second: For a rigid-body at rest ($\upsilon \approx 0$) under the assumption of an ideal fluid, no incident waves, no sea currents and frequency independence the added inertia matrix is symmetrical and positive definite.

$$M_A = M_A{}^T > 0$$

The diagonal of the added inertia matrix will all be positive for most applications. In some textbooks the notation $\lambda_{ij} = \{M_A\}_{ij}$ is used instead which implies that $\lambda_{21} = -Y_{\dot{u}}$.

2) Transformation of added mass under a change of coordinate system

Transformation laws for the added mass under a change of the coordinate system can be derived from invariance of quadratic form under a change of coordinate systems[69]. Let λ_{ij} (i, j =1, 2, 3, 4, 5, 6) be the added mass of the body computed in the coordinate system *xyz*. Let us find the added mass λ'_{ij} (i, j =1, 2, 3, 4, 5, 6) of the same body in the new coordinate system $x_1y_1z_1$. We denote the coordinates of the origin of the new coordinate system in the coordinate system *xyz* by ξ_1, ξ_2, ξ_3. Let us consider the matrix of cosines of the angles between the axis of the coordinate systems *xyz* and $x_1y_1z_1$,

	x	y	z
x_1	α_{11}	α_{12}	α_{13}
y_1	α_{21}	α_{22}	α_{23}
z_1	α_{31}	α_{32}	α_{33}

The elements of this matrix satisfy the standard orthogonally relations,

$$\sum_{i=1}^{3} \alpha_{pi}\alpha_{iq} = \delta_{pq} \tag{2.16}$$

where p, q=1, 2, 3, and δ_{pq} is the Kronecker symbol: $\delta_{pq} = 0$ if $p \neq q$ and δ_{pq}=1 if $p = q$.

Then, the added mass in the coordinate system $x_1 y_1 z_1$ is as following,

$$\lambda'_{kr} = \sum_{i=1}^{3}\sum_{j=1}^{3} \lambda_{ij}\alpha_{ki}\alpha_{rj}, \ (k, r = 1, 2, 3) \tag{2.17}$$

For $k = 1, 2, 3$ and $r = 4, 5, 6$

$$\lambda'_{kr} = \sum_{i=1}^{3}\sum_{j=4}^{6} \lambda_{ij}\alpha_{ki}\alpha_{rj} + \sum_{i=1}^{3}\sum_{j=1}^{3} \lambda_{ij}\alpha_{ki}\left(\alpha_{r,j+2}\xi_{j+1} - \alpha_{r,j+1}\xi_{j+2}\right) \tag{2.18}$$

For $k, r = 4, 5, 6$

$$\begin{aligned}\lambda'_{kr} = &\sum_{i=4}^{6}\sum_{j=4}^{6} \lambda_{ij}\alpha_{ki}\alpha_{rj} + \sum_{i=1}^{3}\sum_{j=4}^{6} \lambda_{ij}\alpha_{kj}\left(\alpha_{r,i+2}\xi_{i+1} - \alpha_{r,i+1}\xi_{i+2}\right) \\ &+\sum_{i=1}^{3}\sum_{j=4}^{6} \lambda_{ij}\alpha_{rj}\left(\alpha_{k,i+2}\xi_{i+1} - \alpha_{k,i+1}\xi_{i+2}\right) \\ &+\sum_{i=1}^{3}\sum_{j=1}^{3} \lambda_{ij}\left(\alpha_{k,i+2}\xi_{i+1} - \alpha_{k,i+1}\xi_{i+2}\right)\left(\alpha_{r,j+2}\xi_{j+1} - \alpha_{r,j+1}\xi_{j+2}\right)\end{aligned} \tag{2.19}$$

In these three formulas above it is assumed that,

$$\begin{aligned} &\alpha_{i4} = \alpha_{i1}, \quad \alpha_{i5} = \alpha_{i2}, \quad \alpha_{i6} = \alpha_{i3}; \\ &\alpha_{4i} = \alpha_{1i}, \quad \alpha_{5i} = \alpha_{i2}, \quad \alpha_{6i} = \alpha_{3i}; \\ &\xi_4 = \xi_1, \quad \xi_5 = \xi_2, \quad \xi_6 = \xi_3. \end{aligned}$$

2.4.2 Simplification of Added Inertia Matrix for Symmetrical AUVs

1) *xz*-plane (port-starboard) symmetry

For the AUV with *xz*-plane symmetry, *u*, *w*, *q* and *X*, *Z*, *M* are symmetrical parameters, *v*, *p*, *r* and *Y*, *K*, *N* are asymmetrical parameters. For there is no

relationship between *u*, *w*, *q* and *Y*, *K*, *N*, and the added inertia matrix is symmetrical. As a result, the added inertia matrix can be simplified to the following form.

$$M_A = -\begin{bmatrix} X_{\dot{u}} & 0 & X_{\dot{w}} & 0 & X_{\dot{q}} & 0 \\ 0 & Y_{\dot{v}} & 0 & Y_{\dot{p}} & 0 & Y_{\dot{r}} \\ Z_{\dot{u}} & 0 & Z_{\dot{w}} & 0 & Z_{\dot{q}} & 0 \\ 0 & K_{\dot{v}} & 0 & K_{\dot{p}} & 0 & K_{\dot{r}} \\ M_{\dot{u}} & 0 & M_{\dot{w}} & 0 & M_{\dot{q}} & 0 \\ 0 & N_{\dot{v}} & 0 & N_{\dot{p}} & 0 & N_{\dot{r}} \end{bmatrix} \tag{2.20}$$

2) *xy*-plane (bottom-top) symmetry

Similar to the *xz*-plane symmetry, the added inertia matrix can be simplified as,

$$M_A = -\begin{bmatrix} X_{\dot{u}} & X_{\dot{v}} & 0 & 0 & 0 & X_{\dot{r}} \\ Y_{\dot{u}} & Y_{\dot{v}} & 0 & 0 & 0 & Y_{\dot{r}} \\ 0 & 0 & Z_{\dot{w}} & Z_{\dot{p}} & Z_{\dot{q}} & 0 \\ 0 & 0 & K_{\dot{w}} & K_{\dot{p}} & K_{\dot{q}} & 0 \\ 0 & 0 & M_{\dot{w}} & M_{\dot{p}} & M_{\dot{q}} & 0 \\ N_{\dot{u}} & N_{\dot{v}} & 0 & 0 & 0 & N_{\dot{r}} \end{bmatrix} \tag{2.21}$$

3) *yz*-plane (fore-aft) symmetry

Similar to the *xz*-plane symmetry, the added inertia matrix can be simplified as,

$$M_A = -\begin{bmatrix} X_{\dot{u}} & 0 & 0 & 0 & X_{\dot{q}} & X_{\dot{r}} \\ 0 & Y_{\dot{v}} & Y_{\dot{w}} & Y_{\dot{p}} & 0 & 0 \\ 0 & Z_{\dot{v}} & Z_{\dot{w}} & Z_{\dot{p}} & 0 & 0 \\ 0 & K_{\dot{v}} & K_{\dot{w}} & K_{\dot{p}} & 0 & 0 \\ M_{\dot{u}} & 0 & 0 & 0 & M_{\dot{q}} & M_{\dot{r}} \\ N_{\dot{u}} & 0 & 0 & 0 & N_{\dot{q}} & N_{\dot{r}} \end{bmatrix} \tag{2.22}$$

4) *xz*-plane and *yz*-plane symmetry

Summarizing the above results, the added inertia matrix can be simplified as,

$$M_A = -\begin{bmatrix} X_{\dot{u}} & 0 & 0 & 0 & 0 & 0 \\ 0 & Y_{\dot{v}} & 0 & 0 & 0 & Y_{\dot{r}} \\ 0 & 0 & Z_{\dot{w}} & 0 & Z_{\dot{q}} & 0 \\ 0 & 0 & 0 & K_{\dot{p}} & 0 & 0 \\ 0 & 0 & M_{\dot{w}} & 0 & 0 & 0 \\ 0 & N_{\dot{v}} & 0 & 0 & 0 & N_{\dot{r}} \end{bmatrix} \tag{2.23}$$

5) *xz*-plane, *xy*-plane and *yz*-plane symmetry

Summarizing the above results, the added inertia matrix can be simplified as,

$$M_A = -\begin{bmatrix} X_{\dot{u}} & 0 & 0 & 0 & 0 & 0 \\ 0 & Y_{\dot{v}} & 0 & 0 & 0 & 0 \\ 0 & 0 & Z_{\dot{w}} & 0 & 0 & 0 \\ 0 & 0 & 0 & K_{\dot{p}} & 0 & 0 \\ 0 & 0 & 0 & 0 & M_{\dot{q}} & 0 \\ 0 & 0 & 0 & 0 & 0 & N_{\dot{r}} \end{bmatrix} \tag{2.24}$$

2.4.3 Approximate Methods for Added Mass Calculation

For most real AUV structures it is impossible to compute the added mass explicitly and one needs to make use of various approximate methods.

1) Method of plane sections

If a body is elongated along one of its axes (typically this axis is assumed to coincide with the *x*-axis) the added mass in orthogonal directions (i.e., along *y* and *z* axes) can be computed by the method of plane sections (Strip theory).

$$\begin{aligned}
\lambda_{22} &= \mu(\lambda)\int_{L_1}^{L_2} \lambda_{220}(x)\,dx \\
\lambda_{33} &= \mu(\lambda)\int_{L_1}^{L_2} \lambda_{330}(x)\,dx \\
\lambda_{24} &= \mu(\lambda)\int_{L_1}^{L_2} \lambda_{240}(x)\,dx \\
\lambda_{34} &= \mu(\lambda)\int_{L_1}^{L_2} \lambda_{340}(x)\,dx \\
\lambda_{44} &= \mu(\lambda)\int_{L_1}^{L_2} \lambda_{440}(x)\,dx \\
\lambda_{26} &= \mu_1(\lambda)\int_{L_1}^{L_2} \lambda_{220}(x)\,x dx \\
\lambda_{35} &= -\mu_1(\lambda)\int_{L_1}^{L_2} \lambda_{330}(x)\,x dx \\
\lambda_{55} &= \mu_1(\lambda)\int_{L_1}^{L_2} \lambda_{330}(x)\,x^2 dx \\
\lambda_{66} &= \mu_1(\lambda)\int_{L_1}^{L_2} \lambda_{220}(x)\,x^2 dx
\end{aligned} \tag{2.25}$$

The idea of this method is that one computes the added mass of all plane sections orthogonal to the *x*-axis and then integrates them along *x*. It is assumed that the motion of fluid in the *x* direction is negligible if the body moves in any direction orthogonal to the *x* axis. This assumption is well

satisfied for prolate bodies, when the ratio of the length of the body (L) to its diameter (B) is large enough. The formulas for added mass computed via the method of plane sections can be written as equations (2.25), where λ_{ij0} is the added mass of the related planar contours[72]. The smaller the elongation of the body, the less precise is the method of plane sections. To decrease the arising error one introduces the correction coefficients μ and μ_1 related to flow of fluid along the body. The most well-known experimental correction is the Pabst correction derived from experiments as follows,

$$\begin{aligned} \mu(\lambda) &= \frac{\lambda}{\sqrt{1+\lambda^2}}\left(1-0.425\frac{\lambda}{1+\lambda^2}\right) \\ \mu_1(\lambda) &= 1-e^{-0.4\lambda} \end{aligned} \tag{2.26}$$

where $\lambda = L/B$ is the elongation of the body.

2) Method of components composition

A torpedo shaped AUV can be disassembled into simple shaped components such as a hull and several other appendages such as rudders and elevators. Each of these components can be treated as a simple geometric body with its added mass calculated with the empirical methods. The hull can be simplified into an ellipsoid or a slender body of revolution, and the rudders and elevators can be treated as plates. Calculating the added mass of each simple geometric body and summing them together, the added mass of the whole vehicle will be reached.

$$\lambda_{ij} = \left(\lambda_{ij}\right)_{hull} + \sum\left(\lambda_{ij}\right)_{app} \qquad \left(i, j = 1,2,3,4,5,6\right) \tag{2.27}$$

2.4.4 Added Mass of Planar Contours

Application of the approximate methods to calculate added mass requires the knowledge of the added mass of corresponding cross sections in a planar flow. The formulas to calculate added mass of two most common contours moving in an infinite two-dimensional fluid are listed as follows. And the formulas to calculate the added mass of some other contours are list in[72] too.

1) Elliptic contour

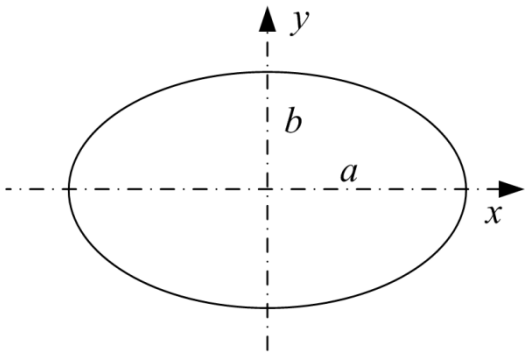

Figure 2.2 Elliptic Contour

$$\begin{aligned}
\lambda_{110} &= \rho\pi b^2 \\
\lambda_{220} &= \rho\pi a^2 \\
\lambda_{660} &= \frac{\rho\pi}{8}\left(a^2 - b^2\right)^2 \\
\lambda_{120} &= \lambda_{160} = \lambda_{260} = 0
\end{aligned} \tag{2.28}$$

2) Elliptic contour with two symmetric ribs

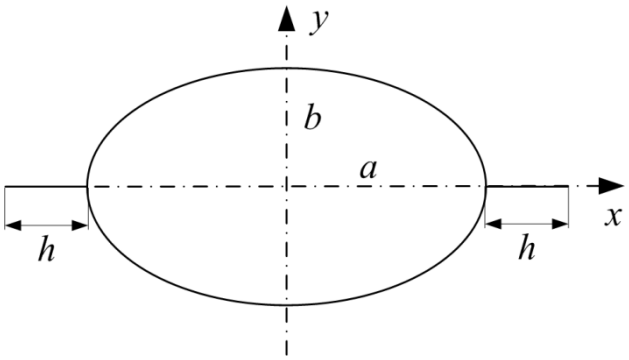

Figure 2.3 Elliptic Contour with two symmetric ribs

$$\begin{aligned}
\lambda_{110} &= \rho\pi b^2 \\
\lambda_{220} &= \rho\pi a^2\left[m^2\left(1+\frac{b}{a}\right)^2 - 2\frac{b}{a} - \frac{b^2}{a^2}\right] \\
\lambda_{660} &= \frac{\rho\pi}{8}\left(a+b\right)^2\left[\left(a+b\right)^2\left(m^4-1\right) + \left(a-b\right)^2\right] \\
\lambda_{120} &= \lambda_{160} = \lambda_{260} = 0
\end{aligned} \tag{2.29}$$

where, $m = \dfrac{a+h}{a+b} + \dfrac{b}{a+h+\sqrt{b^2+h^2+2ah}}$.

2.5 Hydrodynamic Coefficients Estimation

The modeling of the damping forces is the main uncertainty of the dynamic model of the AUV. For torpedo shaped AUVs, they are always composed of simple shaped components such as a hull and several control fins, whose hydrodynamic behaviors are well known. The hydrodynamic damping forces and moments acting on each of these components can be calculated directly with empirical methods. By translating these forces and moments into the body fixed frame and summing them together, the forces and moments acting on the vehicle can be reached. In this section, the empirical methods of determining the hydrodynamic coefficients of the hull and the fins are summarized, and the functions to calculate the hydrodynamic damping forces and moments acting on the AUV with 3D underwater motion are derived.

2.5.1 Hull Hydrodynamic Coefficients

2.5.1.1 Moment, lift and drag coefficients

An empirical method for calculating the forces and moments for bodies of revolution inclined at moderate angles of attack at low speed is presented by[73]. In this method the transverse forces on a forward portion of the body are calculated from potential flow considerations. The transverse forces on the remaining portion of the body are estimated by relating the local transverse force for the inclined body to the drag force for a circular cylinder. The moment, lift and drag coefficients can be expressed in equation form as follows which are also the equations used by the DATCOM methods[74],

$$
\begin{aligned}
C_m &= \frac{(k_2-k_1)2\alpha}{V_B}\int_0^{x_o}\frac{dS_x}{dx}(x_m-x)\,dx+\frac{2\alpha^2}{V_B}\int_{x_o}^{l_B}\xi rc_{d_C}(x_m-x)\,dx \\
C_L &= \frac{(k_2-k_1)2\alpha}{V_B^{2/3}}\int_0^{x_o}\frac{dS_x}{dx}\,dx+\frac{2\alpha^2}{V_B^{2/3}}\int_{x_o}^{l_B}\xi rc_{d_C}\,dx \\
C_D &= C_{D_0}\frac{S_B}{V_B^{2/3}}+\frac{(k_2-k_1)2\alpha^2}{V_B^{2/3}}\int_0^{x_o}\frac{dS_x}{dx}\,dx+\frac{2\alpha^3}{V_B^{2/3}}\int_{x_o}^{l_B}\xi rc_{d_C}\,dx
\end{aligned}
\tag{2.30}
$$

where, C_m is the moment coefficient based on V_B, C_L is the lift coefficient based on $V_B^{2/3}$, C_D is the drag coefficient based on $V_B^{2/3}$, C_{D_0} is the zero-lift drag coefficient based on S_B, V_B is the total body volume, S_B is the maximum body section area, l_B is the length of the body, S_o is the body cross-sectional

area at x_o, x is the longitudinal distance from the vertex to the intended body section, x_m is the longitudinal distance from the vertex to the center of the damping moment, S_x is the body cross-sectional area at position x, α is the body angle of attack in radians, (k_2 - k_1) is the apparent mass factor developed by Munk[73], ξ is the ratio of the drag on a finite cylinder to the drag on an infinite cylinder, c_{d_C} is the experimental cross-flow drag coefficient of a circular cylinder of infinite length. x_o is the body station where the flow ceases to be potential, which is a function of x_1 as equation (2.31). x_1 is the body station where the parameter dS_x/dx first reaches its maximum negative value.

$$x_o = 0.378 l_B + 0.527 x_1 \tag{2.31}$$

2.5.1.2 Zero-lift drag coefficient

At low speeds the zero-lift drag of streamlined bodies is primarily skin friction, since theatrically the pressure drag of a closed body is zero in inviscid fluid. Actually the displacement of the boundary layer causes an incomplete pressure recovery at the end of the body which produces the pressure drag. For non closed body, there exists the base drag too. The zero-lift drag of a revolution body based on the maximum body section area is given as follows[74],

$$C_{D_0} = C_f \left[1 + \frac{60}{\left(l_B / d \right)^3} + 0.0025 \left(\frac{l_B}{d} \right) \right] \frac{S_S}{S_B} + C_{D_b} \tag{2.32}$$

where, d is the maximum body diameter, C_f is the turbulent skin-friction coefficient, as a function of the Reynolds number Re based on the length of the body. It can be expressed as

$$C_f = \frac{0.075}{\left(\log \mathrm{Re} - 2 \right)^2} + 0.00025 \tag{2.33}$$

C_{D_b} is the base-drag coefficient. It can be expressed as

$$C_{D_b} = 0.029 \left(\frac{d_b}{d} \right)^3 \Big/ \sqrt{\left(C_{D_f} \right)_b} \tag{2.34}$$

where, d_b is the base diameter, $\left(C_{D_f}\right)_b$ is the zero-lift drag of the body exclusive of the base drag (i.e. the first term of the right side of equation (2.32)), S_S is the wetted area or surface area of the body excluding the base area.

2.5.1.3 Hull pitching coefficients

The pitching coefficients are measures of the damping lift and moment produced by rotational motion of the body about a spanwise axis.

1) Lift pitching coefficient

The lift pitching coefficient based on maximum section area and body length is derived by DATCOM methods as follows[74],

$$c_{L_q} = 2c_{L_\alpha}\left(1-\frac{x_m}{l_B}\right)\frac{V_B^{2/3}}{S_B} \tag{2.35}$$

where, c_{L_α} is the body lift curve slope from equation (2.30), x_m is the longitudinal distance from the body vertex to the center of rotation.

2) Moment pitching coefficient

The moment pitching coefficient based on maximum section area and body length is given by

$$c_{m_q} = 2c_{m_\alpha}\left[\frac{\left(1-\frac{x_m}{l_B}\right)^2 - \frac{V_B}{S_b l_B}\left(\frac{x_c}{l_B}-\frac{x_m}{l_B}\right)}{\left(1-\frac{x_m}{l_B}\right)-\frac{V_B}{S_b l_B}}\right]\frac{V_B}{S_B l_B} \tag{2.36}$$

where, c_{m_α} is the body moment curve slope from equation (2.30), x_c is the longitudinal distance from the vertex to the center of the volume.

2.5.1.4 Simplification of the hydrodynamic coefficients

The transverse forces on the remaining portion of the body (x_o to l_B) is much smaller than the forward portion, and to simplify the expression all these terms are ignored. Usually the middle section of the hull of torpedo shaped AUV is a cylinder, and cross section area of the cylinder is the always the maximum

section area of the AUV. So the diameter of the middle section cylinder d_B is selected as reference length. Then, these coefficients can be written as,

$$\begin{aligned} C_m &= \frac{(k_2-k_1)2\alpha}{S_B d_B}\int_0^{x_o}\frac{dS_x}{dx}(x_m-x)dx+\frac{l_B}{d_B}\frac{l_B\omega}{2V_\infty}c_{m_q},\ \text{(based on } S_B d_B) \\ C_L &= \frac{(k_2-k_1)2\alpha}{S_B}\int_0^{x_o}\frac{dS_x}{dx}dx+\frac{l_B\omega}{2V_\infty}c_{L_q},\ \text{(based on } S_B) \\ C_D &= C_{D_0}+\frac{(k_2-k_1)2\alpha^2}{S_B}\int_0^{x_o}\frac{dS_x}{dx}dx,\ \text{(based on } S_B) \end{aligned} \tag{2.37}$$

where, V_∞ is relative free stream velocity, ω is the rotational velocity.

The curve slopes are defined as follows to simplify the equations.

$$\begin{aligned} C_{m_\alpha} &= \frac{2(k_2-k_1)}{S_B d_B}\int_0^{x_o}\frac{dS_x}{dx}(x_m-x)dx \\ C_{L_\alpha} &= \frac{2(k_2-k_1)}{S_B}\int_0^{x_o}\frac{dS_x}{dx}dx \\ C_{L_q} &= l_B c_{L_q}/2 \\ C_{m_q} &= l_B^2 c_{m_q}/(2d_B) \end{aligned} \tag{2.38}$$

Then, the hydrodynamic coefficients of the hull can be written in the simplified form as

$$\begin{aligned} C_m &= C_{m_\alpha}\alpha+\frac{\omega}{V_\infty}C_{m_q},\ \text{(based on } S_B d_B) \\ C_L &= C_{L_\alpha}\alpha+\frac{\omega}{V_\infty}C_{L_q},\ \text{(based on } S_B) \\ C_D &= C_{D_0}+C_{L_\alpha}\alpha^2,\ \text{(based on } S_B) \end{aligned} \tag{2.39}$$

2.5.2 Fin Hydrodynamic Coefficients

2.5.2.1 Lift and drag coefficients

An empirical method is used for calculating the forces for low-aspect ratio control surfaces as follows[65, 75],

$$C_L = \left(\frac{2\pi a_0 a_e}{\sqrt{a_e{}^2 + 4} + 2a_0} \right) \alpha + \frac{C_{D_c}}{a_e} \alpha^2$$
$$C_D = C_{D_0} + \frac{C_L{}^2}{\pi a_e e} \tag{2.40}$$

where, C_L is the lift coefficient based on the area of the fin, C_D is the drag coefficient based on the area of the fin, a_0 is the section lift-curve slope corrected from experimental observations with the value of 0.9, a_e is the effective aspect ratio, α is the angle of attack, C_{D_0} is the zero lift drag coefficient, e is the Oswald efficiency factor with the value of 0.9, C_{D_c} is the cross flow-drag coefficient, which is a function of the tip shape and taper ratio r_{TAP}. For fins with squared tip, $C_{D_c} = 0.1 + 1.6 r_{TAP}$.

2.5.2.2 Zero-lift drag coefficient

Based on the empirical expression proposed by[76] for streamlined shapes at low Reynolds numbers, the zero lift drag coefficient is calculated by,

$$C_{D_0} = 2C_f \left[1 + t/c + (t/c)^2 \right] \tag{2.41}$$

where, C_f is the skin-friction coefficient, t is the maximum thickness of the plane, c is the corresponding chord.

The curve slopes are defined as follows.

$$C_{L_{\alpha 1}} = \frac{2\pi a_0 a_e}{\sqrt{a_e{}^2 + 4} + 2a_0},$$
$$C_{L_{\alpha 2}} = \frac{C_{D_c}}{a_e} \tag{2.42}$$
$$C_{D_L} = \frac{1}{\pi a_e e}$$

Then, the lift and drag coefficients of a fin can be simplified as follows.

$$C_L = C_{L_{\alpha 1}} \alpha + C_{L_{\alpha 2}} \alpha^2$$
$$C_D = C_{D_0} + C_{D_L} C_L{}^2 \tag{2.43}$$

2.5.3 Hydrodynamic Damping Forces and Moments Modeling

Here, we present a vector based damping forces and moments model for the decomposed components including the main body and control fins of a torpedo shaped AUV in 3D underwater motion. It should be noted that the symbols of lift and drag coefficients for the hull and the fins are all C_L and C_D. We don't want to adopt complicated indexes to separate them. It is assumed that when the forces and moments acting on the hull are calculated, the coefficients used are related to the hull, and so to the fins.

2.5.3.1 Damping forces and moments acting on the hull

For the streamlined body with 3D motion, in order to calculate the damping forces and moments, the effective rotation axis and the effective attack angle should be determined first.

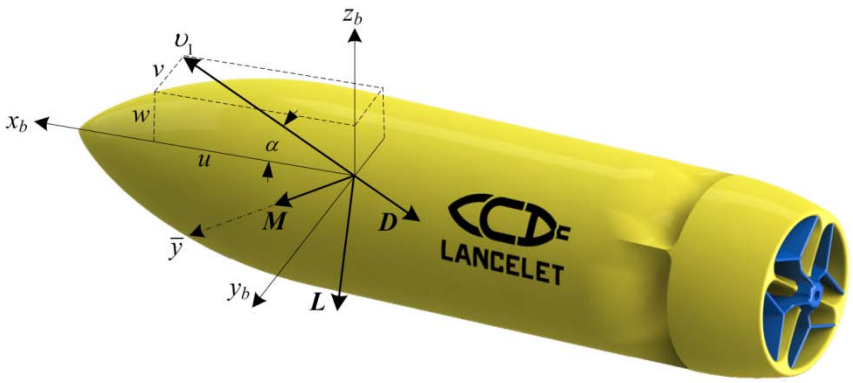

Figure 2.4 Hydrodynamic damping acting on the hull in 3D motion

The positive direction of the attack angle and pitching angular velocity of the hull can be calculated as follows and shown in Figure 2.4.

$$\bar{y} = \left(\boldsymbol{\upsilon}_1 \times [1,0,0]^T\right) \Big/ \left\|\boldsymbol{\upsilon}_1 \times [1,0,0]^T\right\| \tag{2.44}$$

The magnitude of the attack angle is,

$$\alpha = \sqrt{v^2 + w^2} \Big/ \left\|\boldsymbol{\upsilon}_1\right\| \tag{2.45}$$

And the effective pitching angular velocity is,

$$\omega = \boldsymbol{\upsilon}_2 \cdot \bar{y} \tag{2.46}$$

Then, according to the equation (2.39) the damping force $\boldsymbol{F}$ and moment $\boldsymbol{M}$ acting on the hull are as follows.

$$\begin{cases} \boldsymbol{L} = \frac{1}{2}\rho \|\boldsymbol{\upsilon}_1\| S_B C_L \left(\overline{y} \times \boldsymbol{\upsilon}_1\right) \\ \boldsymbol{D} = -\frac{1}{2}\rho \|\boldsymbol{\upsilon}_1\| S_B C_D \boldsymbol{\upsilon}_1 \\ \boldsymbol{F} = \boldsymbol{L} + \boldsymbol{D} \\ \boldsymbol{M} = \frac{1}{2}\rho \|\boldsymbol{\upsilon}_1\|^2 S_B d_B C_m \overline{y} \end{cases} \tag{2.47}$$

2.5.3.2 Damping forces and moments acting on the fin

For the plate fin mounted not at the origin of the body-fixed frame, the angular velocity is the same as that of the main body, but the translational velocity is different. First we should find the translational velocity of the fin as

$$\boldsymbol{V}_{FIN} = \boldsymbol{\upsilon}_1 + \boldsymbol{\upsilon}_2 \times \boldsymbol{r}_{FIN} \tag{2.48}$$

where $\boldsymbol{r}_{FIN}$ is the vector of the coordinates of the pressure center of the fin in the body-fixed frame.

For horizontal fins, the positive direction of the attack angle is,

$$\overline{y} = \left(\boldsymbol{V}_{FIN} \times \left[-\sin(\delta_H), 0, -\cos(\delta_H)\right]^T\right) \Big/ \left\| \boldsymbol{V}_{FIN} \times \left[-\sin(\delta_H), 0, -\cos(\delta_H)\right]^T \right\| \tag{2.49}$$

where δ_H is the deflection angle of the horizontal fin. And the effective attack angle is,

$$\alpha = w_{FIN} / \|\boldsymbol{V}_{FIN}\| + \delta_H \tag{2.50}$$

For vertical fins, the positive direction of the attack angle is,

$$\overline{y} = \left(\boldsymbol{V}_{FIN} \times \left[-\sin(\delta_V), -\cos(\delta_V), 0\right]^T\right) \Big/ \left\| \boldsymbol{V}_{FIN} \times \left[-\sin(\delta_V), -\cos(\delta_V), 0\right]^T \right\| \tag{2.51}$$

where δ_V is the deflection angle of the vertical fin. And the effective attack angle is,

$$\alpha = v_{FIN} / \|\boldsymbol{V}_{FIN}\| + \delta_V \tag{2.52}$$

Then, according to the equation (2.43) the damping force $\boldsymbol{F}$ and moment $\boldsymbol{M}$ acting on the fins of the AUV are as follows.

$$\begin{cases} \boldsymbol{L} = \frac{1}{2}\rho \left\| \boldsymbol{V}_{FIN} \right\| S_{FIN} C_L \left(\overline{y} \times \boldsymbol{V}_{FIN} \right) \\ \boldsymbol{D} = -\frac{1}{2}\rho \left\| \boldsymbol{V}_{FIN} \right\| S_{FIN} C_D \boldsymbol{V}_{FIN} \\ \boldsymbol{F} = \boldsymbol{L} + \boldsymbol{D} \\ \boldsymbol{M} = \boldsymbol{r}_{FIN} \times \boldsymbol{F} \end{cases} \tag{2.53}$$

2.6 Hydrodynamic Derivatives Calculation

The equations to calculate the hydrodynamic damping forces and moments from the hydrodynamic coefficients by equations (2.47) and (2.53) are nonlinear and coupling function of the velocities and the control fin angles of the AUV. The results can be used directly for the simulation of the AUV, but the controller cannot be designed based on this damping model easily. After the forces and moments are calculated from the hydrodynamic coefficients, the related hydrodynamic derivatives can be reached by calculating the derivatives of the forces and moments with respect to the velocities of the AUV. A generalization makes use of second order Taylor series expansion to describe the damping forces and moments $\tau_D = \left[X, Y, Z, K, M, N \right]^T$ which is the function of υ. For one component $X = X\left(\upsilon\right)$, the second-order Taylor series expansion of the scalar-valued function of vector variable can be compactly written as,

$$X = X\left(\upsilon_0\right) + \nabla X^T \left(\upsilon - \upsilon_0\right) + \frac{1}{2}\left(\upsilon - \upsilon_0\right)^T H_X \left(\upsilon - \upsilon_0\right) \tag{2.54}$$

where ∇X is the gradient and H_X is the Hessian matrix.

$$\nabla X = \left[\frac{\partial X}{\partial u}, \frac{\partial X}{\partial v}, \frac{\partial X}{\partial w}, \frac{\partial X}{\partial p}, \frac{\partial X}{\partial q}, \frac{\partial X}{\partial r} \right]^T \tag{2.55}$$

$$H_X = \begin{bmatrix} \frac{\partial^2 X}{\partial u^2} & \frac{\partial^2 X}{\partial u \partial v} & \frac{\partial^2 X}{\partial u \partial w} & \frac{\partial^2 X}{\partial u \partial p} & \frac{\partial^2 X}{\partial u \partial q} & \frac{\partial^2 X}{\partial u \partial r} \\ \frac{\partial^2 X}{\partial v \partial u} & \frac{\partial^2 X}{\partial v^2} & \frac{\partial^2 X}{\partial v \partial w} & \frac{\partial^2 X}{\partial v \partial p} & \frac{\partial^2 X}{\partial v \partial q} & \frac{\partial^2 X}{\partial v \partial r} \\ \frac{\partial^2 X}{\partial w \partial u} & \frac{\partial^2 X}{\partial w \partial v} & \frac{\partial^2 X}{\partial w^2} & \frac{\partial^2 X}{\partial w \partial p} & \frac{\partial^2 X}{\partial w \partial q} & \frac{\partial^2 X}{\partial w \partial r} \\ \frac{\partial^2 X}{\partial p \partial u} & \frac{\partial^2 X}{\partial p \partial v} & \frac{\partial^2 X}{\partial p \partial w} & \frac{\partial^2 X}{\partial p^2} & \frac{\partial^2 X}{\partial p \partial q} & \frac{\partial^2 X}{\partial p \partial r} \\ \frac{\partial^2 X}{\partial q \partial u} & \frac{\partial^2 X}{\partial q \partial v} & \frac{\partial^2 X}{\partial q \partial w} & \frac{\partial^2 X}{\partial q \partial p} & \frac{\partial^2 X}{\partial q^2} & \frac{\partial^2 X}{\partial q \partial r} \\ \frac{\partial^2 X}{\partial r \partial u} & \frac{\partial^2 X}{\partial r \partial v} & \frac{\partial^2 X}{\partial r \partial w} & \frac{\partial^2 X}{\partial r \partial p} & \frac{\partial^2 X}{\partial r \partial q} & \frac{\partial^2 X}{\partial r^2} \end{bmatrix} \tag{2.56}$$

If $\upsilon_0 = 0$, we will have, $X(\upsilon_0) = 0$ and $\upsilon - \upsilon_0 = \upsilon$. Then we will have,

$$\tau_D = \begin{bmatrix} \nabla X^T \\ \nabla Y^T \\ \nabla Z^T \\ \nabla K^T \\ \nabla M^T \\ \nabla N^T \end{bmatrix} \upsilon + \frac{1}{2} \begin{bmatrix} \upsilon^T H_X \\ \upsilon^T H_Y \\ \upsilon^T H_Z \\ \upsilon^T H_K \\ \upsilon^T H_M \\ \upsilon^T H_N \end{bmatrix} \upsilon \tag{2.57}$$

The first order derivative matrix is called Jacobian matrix, and the second order derivative matrix is noted as augmented Hessian matrix. Both the Jacobian matrix and the augmented Hessian matrix can be simplified for symmetrical AUVs similar to the simplification of the added mass matrix. And based on the notations from literature[6, 69, 77], the damping forces and moment in the form of hydrodynamic derivatives for horizontal and vertical plane motion of a AUV with symmetry about *xz*-plane and *xy*-plane are always written as following forms. The relations between the hydrodynamic derivatives and the hydrodynamic coefficients can be calculated based on the damping forces and moments model expressed by equations (2.47) and (2.53).

1) Damping forces and moment for horizontal plane motion

$$\begin{cases} X = X_{uu}u^2 + X_{vv}v^2 + X_{rr}r^2 + X_{vr}vr + X_{\delta_V \delta_V}\delta_V^2 \\ Y = Y_v v + Y_r r + Y_{v|v|}v|v| + Y_{r|r|}r|r| + Y_{v|r|}v|r| + Y_{\delta_V}\delta_V + Y_{|r|\delta_V}|r|\delta_V \\ N = N_v v + N_r r + N_{v|v|}v|v| + N_{r|r|}r|r| + N_{|v|r}|v|r + N_{\delta_V}\delta_V + N_{|r|\delta_V}|r|\delta_V \end{cases} \tag{2.58}$$

where, $Y_v = \frac{\partial Y}{\partial v}$, $Y_r = \frac{\partial Y}{\partial r}$, $N_v = \frac{\partial N}{\partial v}$, $N_r = \frac{\partial N}{\partial r}$,

$$X_{uu} = \frac{1}{2}\frac{\partial^2 X}{\partial u^2}, X_{vv} = \frac{1}{2}\frac{\partial^2 X}{\partial v^2}\ X_{rr} = \frac{1}{2}\frac{\partial^2 X}{\partial r^2}, X_{vr} = \frac{\partial^2 X}{\partial v \partial r}$$

$$Y_{v|v|} = \frac{1}{2}\frac{\partial^2 Y}{\partial v^2}, Y_{r|r|} = \frac{1}{2}\frac{\partial^2 Y}{\partial r^2}, Y_{v|r|} = \frac{\partial^2 Y}{\partial v \partial r}$$

$$N_{v|v|} = \frac{1}{2}\frac{\partial^2 N}{\partial v^2}, N_{r|r|} = \frac{1}{2}\frac{\partial^2 N}{\partial r^2}, N_{|v|r} = \frac{\partial^2 N}{\partial v \partial r}$$

$$Y_{\delta_V} = \frac{\partial Y}{\partial \delta_V}, N_{\delta_V} = \frac{\partial N}{\partial \delta_V}, X_{\delta_V \delta_V} = \frac{1}{2}\frac{\partial^2 X}{\partial \delta_V^2}, Y_{|r|\delta_V} = \frac{\partial^2 Y}{\partial r \partial \delta_V}, N_{|r|\delta_V} = \frac{\partial^2 N}{\partial r \partial \delta_V}$$

2) Damping forces and moment for vertical plane motion

$$\begin{cases} X = X_{uu}u^2 + X_{ww}w^2 + X_{qq}q^2 + X_{wq}wq + X_{\delta_H \delta_H}\delta_H^2 \\ Z = Z_w w + Z_q q + Z_{w|w|}w|w| + Z_{q|q|}q|q| + Z_{w|q|}w|q| + Z_{\delta_H}\delta_H + Z_{|q|\delta_H}|q|\delta_H \\ M = M_w w + M_q q + M_{w|w|}w|w| + M_{q|q|}q|q| + M_{|w|q}|w|q + M_{\delta_H}\delta_H + M_{|q|\delta_H}|q|\delta_H \end{cases} \quad (2.59)$$

All the derivatives are defined similarly as horizontal plane motion as follows.

$$Z_w = \frac{\partial Z}{\partial w}, Z_q = \frac{\partial Z}{\partial q}, M_w = \frac{\partial M}{\partial w}, M_q = \frac{\partial M}{\partial q},$$

$$X_{ww} = \frac{1}{2}\frac{\partial^2 X}{\partial w^2}\ X_{qq} = \frac{1}{2}\frac{\partial^2 X}{\partial q^2}, X_{wq} = \frac{\partial^2 X}{\partial w \partial q}$$

$$Z_{w|w|} = \frac{1}{2}\frac{\partial^2 Z}{\partial w^2}, Z_{q|q|} = \frac{1}{2}\frac{\partial^2 Z}{\partial q^2}, Z_{w|q|} = \frac{\partial^2 Z}{\partial w \partial q}$$

$$M_{w|w|} = \frac{1}{2}\frac{\partial^2 M}{\partial w^2}, M_{q|q|} = \frac{1}{2}\frac{\partial^2 M}{\partial q^2}, M_{|w|q} = \frac{\partial^2 M}{\partial w \partial q}$$

$$Z_{\delta_H} = \frac{\partial Z}{\partial \delta_H}, M_{\delta_H} = \frac{\partial M}{\partial \delta_H}, X_{\delta_H \delta_H} = \frac{1}{2}\frac{\partial^2 X}{\partial \delta_H^2}, Z_{|q|\delta_H} = \frac{\partial^2 Z}{\partial q \partial \delta_H}, M_{|q|\delta_H} = \frac{\partial^2 M}{\partial q \partial \delta_H}$$

2.7 Summary

In this chapter, the kinematic and dynamic models of AUV are outlined first in order to review the basis equations and the related symbols which will be used in the subsequent chapters. And the empirical methods for the hydrodynamic coefficients and added mass estimation are reviewed. Then, a vector based damping forces and moments model for the torpedo shaped AUV in 3D underwater motion is established. This damping forces and moments model is suitable for parameter estimation and modular dynamic modeling and will be used in the subsequent chapters too. The relationship between hydrodynamic coefficients and hydrodynamic derivatives obtained in this chapter will be used in chapter 5 for estimation of hydrodynamic derivatives.

Chapter 3 Design and Field Test of Micro AUV Lancelet

The development and the field tests of a finless torpedo shaped micro AUV named Lancelet are presented in this chapter. A novel multi-jet drive vectoring propulsion and control system is designed and implemented. This propulsion mechanism is robust and compact and extremely suitable for torpedo shaped micro underwater vehicles, and can provide the Lancelet with high maneuverable capabilities such as turn in place and pitch in place. Rapid prototypes of the Lancelet with the designed multi-jet propulsion systems are built and tested. The performance of the propulsion system is studied, and open loop free swimming trials are carried out to explore the Lancelet's special maneuverability.

3.1 Mechanical Structure design

3.1.1 Hull Shape Selection

The proposed micro AUV will follow the traditional torpedo shape as this is seen to be the best compromise between size, usable volume, hydrodynamic efficiency and ease of handling. And the Myring hull is the most widely adopted for torpedo shaped AUVs, due to its minimal drag coefficient profile for a given fineness ratio (body length/maximum diameter)[64, 78]. The Myring hull consists of a nose-section, a constant-radius center-section and a tail-section with length of *a*, *b*, *c* respectively as seen in Figure 3.1. The Myring hull shape is axis symmetric and the specific section profile is described by the equations of radius distribution along the main axis with the origin set at the front nose point of the hull as follows.

Nose section: $r(x)=\frac{1}{2}d\left[1-\left(\frac{x-a}{a}\right)^2\right]^{\frac{1}{n}},\left(0\le x\le a\right)$

Middle section: $r(x)=d,\left(a\le x\le a+b\right)$

Tail section:

$$r(x)=\frac{d}{2}-\left(\frac{3d}{2c^2}-\frac{\tan\theta}{c}\right)\left(x-a-b\right)^2+\left(\frac{d}{c^3}-\frac{\tan\theta}{c^2}\right)\left(x-a-b\right)^3,\left(a+b\le x\le a+b+c\right)$$

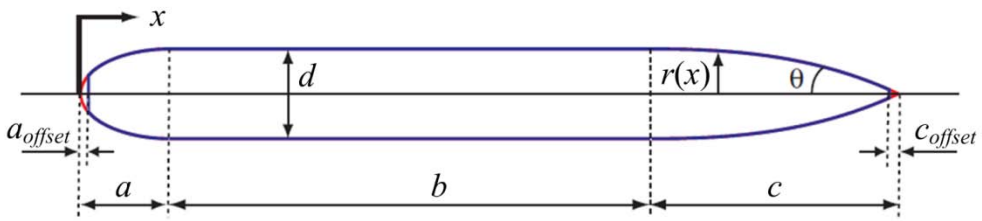

Figure 3.1 Myring hull profile and geometric parameter definition

In our design, the Type B Myring hull form[79] with a diameter of 60 mm is adopted. And the constant radius section of the Myring hull makes the modular design methods easily implemented on this hull shape.

3.1.2 Propulsion System Design

AUVs can rely on a number of propulsion techniques. So far the propeller based thrusters are the most commonly used propulsion method. For typical torpedo shaped AUVs, elevators and rudders are widely used for yaw and pitch control like the REMUS AUV[77]. The fin control method is simple and usually efficient, but it requires a minimum forward velocity for the control surfaces to be effective[80]. And the fin control system will become extremely fragile if they are scaled down to the dimension of the micro AUV.

The Bluefin AUV is equipped with an articulated, ducted thruster known as the tailcone for vehicle propulsion, as well as yaw and pitch control[81]. The design of the tailcone has eliminated the protruding dive planes and control fins common to many AUVs. The sleek design reduces the likelihood of damage and biofouling while simplifying the entire assembly down to a single easily replaceable module. The resulting ducted thruster design is also more hydrodynamically advantageous than the commonly used fin design. But the internal structure of the tailcone is complex, which makes it is only suitable for large AUVs.

On MARES, four independent COTS thrusters provide attitude control both in the horizontal and in the vertical plane[48]. Two horizontal thrusters located at the tail control both forward velocity and rotation in the horizontal plane, while another set of thrusters, in the vertical direction, control vertical velocity and pitch angle. This arrangement permits operations in very confined areas, with virtually independent horizontal and vertical motion at velocities starting

at 0 m/s. Furthermore, the modularity of the system allows the integration of other thrusters, for example to provide full control of the lateral motion. But there is no micro thruster available in the commercial market now, and the inertial volume of a micro AUV is quite limited where there is no space for two vertical thrusters mounted in the main body of the hull. As a result we cannot borrow this idea for our micro AUV design directly.

Usually the surging thruster is mounted parallel to the forward axis of the vehicle which is also the main axis of the streamlined vehicle such as the REMUS. If a thruster is mounted parallel to the main axis of the vehicle, but not on this axis like the design of MARES, it will generate a torque which can be used for the yaw control or the pitch control of the vehicle depending on the location of the thruster. But the offset value from the main axis of the vehicle to the axis of the thruster must be big enough to generate enough torque to overcome the hydrodynamic damping moment opposite to the direction of rotation. This may seriously affect the streamline hull shape of the vehicle and increase the transverse dimension and drag.

In this thesis a novel vector propulsion system which is composed of three or four jet drives is designed to solve the above problem. In Figure 3.2 only one jet drive is drawn to illustrate the mechanism of the propulsion system. Each jet drive is composed of a propeller, a stator (not shown in Figure 3.2) and a nozzle. The stator is used to convert the rotational velocity components of the jetting water into the direction of propeller axis, which could counteract the motor torque reaction and at the same time increase the propeller efficiency. The nozzle is used to guide the water to jet in a direction with a little angle β with respect to the main axis of the vehicle. The angle will make this jet drive to generate a sufficient torque to be used for yaw or pitch control. The reaction thruster force from one water jet drive is defined as F. The offset value from the center of outlet of the nozzle to the main axis is defined as a. The distance from the outlet of the nozzle to the origin of the body-fixed frame in the main axis direction of the vehicle is l. Then the forces and moment acting on the AUV in the body-fixed frame from one jet drive can be calculated as follows.

$$\begin{cases} X = F\cos(\beta) \\ Z = F\sin(\beta) \\ M = F\cos(\beta)\left(a + l\tan(\beta)\right) \end{cases} \tag{3.1}$$

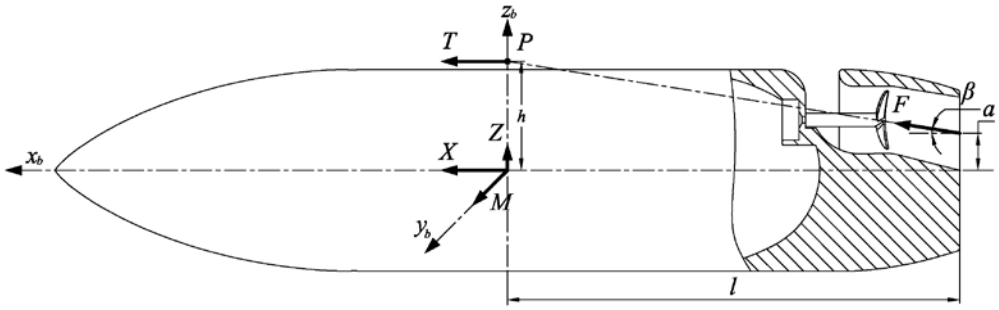

Figure 3.2 Multi-jet drive thruster mechanism

l is approximately half of the length of the AUV, and a is no more than half of the radius of the AUV, which means that l is much bigger than a for the torpedo shaped AUV. Even after l is multiplied by tan(β), it still a big component of the moment arm of the thruster force. And the range of magnitude of the torque can be designed by adjusting the angle β. For small β, the lateral influence of the jet drive on the AUV can be ignored. If we define the forward (backward) thruster force as $T = F\cos(\beta)$ and the arm of the torque of the thruster force with respect to the origin of the boy fixed frame as $h = a + l\tan(\beta)$, the force and moment from one jet drive can be simplified as $\{T, Th\}$. This equals to a thruster force T acting at point P on the z_b axis of the body-fixed frame along x_b axis direction as shown in Figure 3.2.

A. Three jet drive propulsion system

For basic maneuverability of the AUV, the propulsion system is composed of three jet drives, which are grouped on a circle each 120° apart as in Figure 3.4. The thruster forces and corresponding torques generated by this propulsion system can be transferred to the y_bz_b plane of the body-fixed frame show in Figure 3.3. T_1, T_2, T_3 are the thruster forces from these three jet drives, and M_1, M_2, M_3 are the corresponding generated torques separately with respect to the origin of the boy fixed frame, where $M_i = T_i h, (i = 1, 2, 3)$.

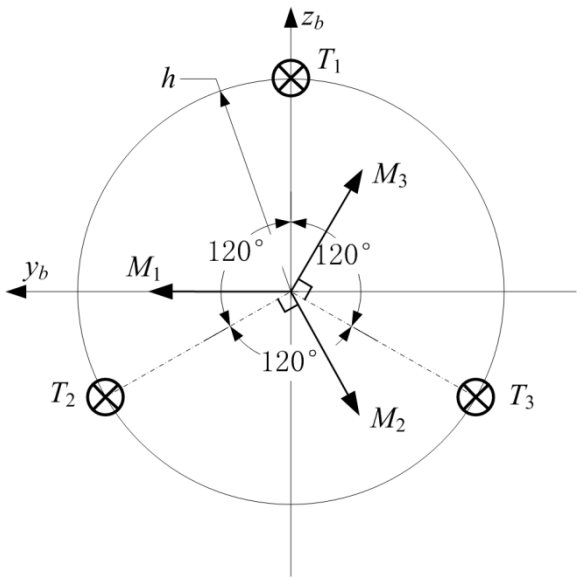

Figure 3.3 Forces and moments of the three jet drive propulsion system

Figure 3.4 Micro AUV Lancelet with three jet drive propulsion system

Then the total forces and moments from this three jet drive propulsion system can be summarized as follows.

$$\begin{cases} X = T_1 + T_2 + T_3 \\ M = T_1 h - \left(T_2 h + T_3 h\right)/2 \\ N = \left(T_3 h - T_2 h\right)\sqrt{3}/2 \end{cases} \tag{3.2}$$

The forces and moments from the three jet drive propulsion system can be written in the matrix form as follows.

$$[X, M, N]^T = A\left[T_1, T_2, T_3\right]^T \tag{3.3}$$

where $A = \begin{bmatrix} 1 & 1 & 1 \\ h & -h/2 & -h/2 \\ 0 & -h\sqrt{3}/2 & h\sqrt{3}/2 \end{bmatrix}$.

Since $\det(A) = -3\sqrt{3}h^2/2$, if $h>0$, this matrix is invertible, which means this propulsion system can generate the force and moments required for the control of the AUV with proper drive forces from these three jet drives before any of them gets saturated. From the design of this propulsion system, it can be seen that the AUV has six degree of freedoms but only three independent inputs from these three jet drives, which means that the AUV is underactuated. This can be verified from the formulas above, where there are only three independent inputs for the AUV, leaving the translational motion of y_b and z_b direction and the rotation around x_b direction not controlled directly.

B. Four jet drive propulsion system

Usually the stator in the jetting nose cannot counteract the reaction torque from the propeller completely, which gives the propulsion system the ability of the active roll control. If we do not need the active roll control, which is the case of most of the torpedo shaped underwater vehicles, we can prolong the fins of the stator to minimize the reaction torque. On the contrary, if we need active roll control, we can shorten the fins of the stator or even remove the stator to increase the reaction torque. Additionally, we should extend the design of the propulsion system to four jet derives as show in Figure 2.1, with its four jet drives distributed as shown in Figure 3.5 to provide enough independent control inputs for yaw, pitch, roll and surge control. And the active roll control of the vehicle is analyzed as follows.

The propeller of each jet drive produces both a reaction force and a reaction torque with respect to the axis of rotation. If all propellers are spinning at the same angular velocity, with propellers one and three rotating counterclockwise and propellers two and four clockwise, the net reaction torque and hence the angular acceleration about the x_b axis is zero. The torque for roll control is induced by mismatching the balance in reaction torques (i.e., by offsetting the cumulative thrust commands between the counter-rotating propeller pairs). The pitch and yaw axes can be controlled separately without impacting the roll

axis. Each pair of propellers rotating in the same direction controls one axis, either yaw or pitch, and increasing thrust for one propeller while decreasing thrust for the other will maintain the torque balance needed for roll stability and induce a net torque about the yaw or pitch axes.

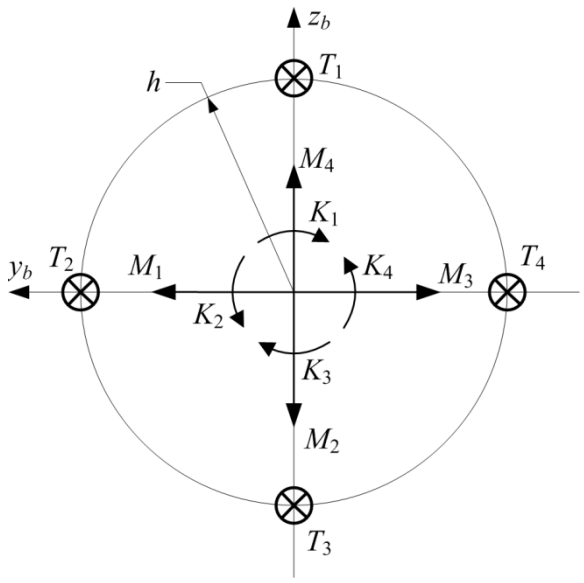

Figure 3.5 Forces and moments of the four jet drive propulsion system

The forces and torques can be transferred to the y_bz_b plane of the body-fixed frame show in Figure 3.5. T_1, T_2, T_3, T_4 are the thruster forces from these four jet drives, and M_1, M_2, M_3, M_4 are the corresponding generated torques separately with respect to the origin of the boy fixed frame, where $M_i = T_i h$, $(i = 1,2,3,4)$. The reaction torque K_i from each of these four jet drives is proportional to the corresponding thrust force T_i, as $K_i = \lambda T_i \ \ (i = 1,2,3,4)$. λ is the proportional factor between the thruster force and reaction torque of the jet drive which is mainly determined by the shape of the stator. Then the total forces and moments from this four jet drive propulsion system can be summarized as follows.

$$\begin{cases} X = T_1 + T_2 + T_3 + T_4 \\ K = \lambda\left(T_1 - T_2 + T_3 - T_4\right) \\ M = T_1 h - T_3 h \\ N = T_4 h - T_2 h \end{cases} \tag{3.4}$$

The forces and moments from the four jet drive propulsion system can be written in the matrix form as follows,

$$[X, K, M, N]^T = A[T_1, T_2, T_3, T_4]^T \tag{3.5}$$

where $A = \begin{bmatrix} 1 & 1 & 1 & 1 \\ \lambda & -\lambda & \lambda & -\lambda \\ h & 0 & -h & 0 \\ 0 & -h & 0 & h \end{bmatrix}$.

Since $\det(A) = 8\lambda h^2$, if h>0 and $\lambda > 0$ this matrix is invertible, which means this propulsion system can generate the force and moments required for the control of the AUV with proper drive forces from these four jet drives. But the AUV is still underactuated, leaving the translation motions of y_b and z_b direction not controlled directly.

The reaction torque of the propeller can be counteracted mostly by the proper designed stator behind the propeller. And the four jet drive propulsion system is a redundant system, if we can abandon the active roll control of the vehicle as most torpedo shaped underwater vehicles do. Then, if one of these motors is down, the whole vehicle is still under control. For example, if the forth motor is down, the forces and moments from this propulsion can be summarized as follows.

$$\begin{cases} X = T_1 + T_2 + T_3 \\ M = T_1 h - T_3 h \\ N = -T_2 h \end{cases} \tag{3.6}$$

The forces and moments from this propulsion system can be written in the matrix form,

$$[X, M, N]^T = A[T_1, T_2, T_3]^T \tag{3.7}$$

where $A = \begin{bmatrix} 1 & 1 & 1 \\ h & 0 & -h \\ 0 & -h & 0 \end{bmatrix}$.

For $\det(A) = -2h^2$, if h>0 this matrix is invertible, which means this propulsion system can still generate the force and moments required for the yaw, pitch and surging control of the AUV with proper drive forces from the left three jet drives.

The design of the propulsion system is simple, compact and robust. It has no moving surfaces, or other unprotected moving parts, that can be easily damaged. The propulsion system can be used for big AUVs too, but extremely suitable for micro AUVs, and is very easy to fabricated and controlled.

3.2 Control Electronics Design

The limited space of the hull of the Lancelet cannot accommodate a generic embedded computer board. The control electronics boards must be very compact, so the on-board control system has to be custom designed. Structurally the Lancelet is modular designed, and the control electronics system is modular designed too. The hardware structure of the control electronics is composed of three basic modules, which are the sensor board, the main control board, and the motor driver board. And it can be expanded to accommodate additional modules with the interfaces reserved on the main control board.

3.2.1 Main Control Board Design

As the Lancelet is underactuated, some nonlinear controllers may be necessary for the trajectory tracking control or other control tasks, and that may need to deal with plenty of floating point calculation[67]. At the same time the processor must have rich interfaces for the motor control, the sensor data acquisition, the data logging, the wireless commutation, the USB programming, ect. As a result a high performance 32 bits microcontroller will make the design of control electronics boards compact and easy.

An AVR32 microcontroller AT32UC3B0256 is used as the main processor. It can run at 60 Mhz and has all the necessary interfaces. The main control board is designed as shown in the block diagram in Figure 3.6. The Bluetooth module and the Flash card socket are used for wireless communication and data logging separately. The USB and JATC interfaces are used for programming and debugging. The I^2C, SPI interface are designed for data acquisition from the sensors board with digital ports. The ADC interface is designed for read data from analog sensors. The PWM outputs are designed for the DC motor control. There are still some GPIO (general port IO) ports reserved for the digital inputs and outputs.

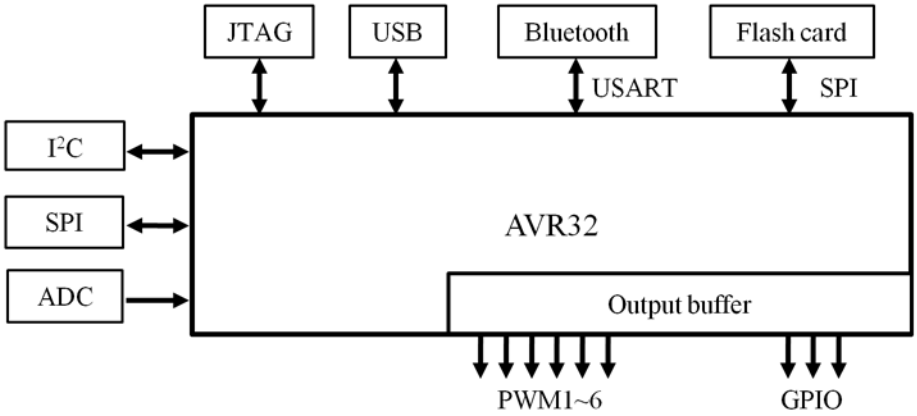

Figure 3.6 Main control board architecture and interfaces

3.2.2 Sensor Board Design

The sensor board is composed of an IMU (Inertial Measurement Unit) and a pressure sensing unit and an AVR 8-bit microcontroller ATmega328. The IMU is used to estimate orientation of the AUV relative to the earth. The commercial IMU modules are usually too big and hunger for power [82]. In this system a small size IMU consisting of a 3-axis accelerometer, a 3-axis magnetometer, and a 3-axis gyro is adopted.

The pressure sensing unit is used to measure the depth and velocity of the AUV. The depth of vehicle is measured by an absolute pressure sensor MPXH6300A with a range of 20 to 304 kPa allowing a measurable depth range of about 20 m which is appropriate for our shallow water micro AUV.

Due to the inherent cumulative error in IMU devices, it is very difficult for the AUV to cruise with high precision for a long time autonomously. This drift issue can be compensated via direct measurement of the vehicle velocity. Therefore the vehicle should have a hybrid system which combines the IMU and the velocity information. This velocity measurement is commonly achieved by one of the following four measurements, Pitometer, rotor type velocity logs, Doppler velocity logs (DVLs), correlation velocity logs (CVLs)[82-84]. The rotor type velocity log is good in the measurement of the low speed range. The influences of temperature and the density of the water on it are small. Its measurement accuracy is low and affected by turbulence. In addition, the rotor will affect the performance of our micro AUV due to its drag force. Hence, it is not suitable for our design. The DVL has effective

ranges from low speed to high speed. It has small influence of the turbulence and small error when the vehicle turns. Also, it can measure against water or seafloor alternatively and correct influence of temperature and the density of the water. The DVL is suitable for the cruising type underwater vehicle. CVLs offer advantages over DVLs in many AUV applications, since they can achieve high accuracy at low velocities even during hover manoeuvres. And DVLs require narrow beam widths, whilst ideal CVL transmitters have wide beam widths. This gives CVLs the potential to use lower frequencies thus permitting operation in deeper water, reducing power requirements for the same depth, and allowing the use of smaller transducers[85-87]. However, the Doppler sonar and correlation velocity sonar are all too large and costly and require too much power to be employed on our micro AUV.

The Pitometer has good accuracy in middle range speed measurement. Although it is influenced by turbulence and currents, and it has some errors when the vehicle turns. But the implementation of Pitometer is very simple. As it only needs two outlets for sampling the total pressure and the static pressure of the water and one differential pressure sensor to measure the difference of these two pressures. As a result, the Pitometer is very easily scaled down to a small size, and it is the best choice of velocity measurement for our micro AUV now. The pressure sensing system for both depth and velocity measurements is show in Figure 3.7. A differential pressure sensor MPXV5004 is used for the Pitometer, which will give a velocity measurement from 0 to 2.8 m/s.

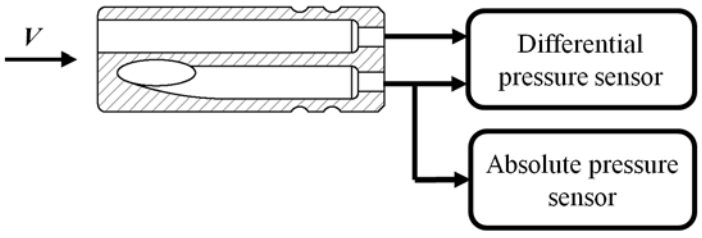

Figure 3.7 Pressure sensing system for the depth and velocity measurement, *V* is the relative fluid velocity

The data from these sensors are periodically acquired and processed by the AVR 8-bit microcontroller. The data of the IMU is used to estimate the orientation of the vehicle with a complementary filter which will be discussed

in next subsection. And the depth and velocity of the vehicle is calculated from the data of the pressure sensing system. Then the results are feed to the main control board via I^2C interrupts.

3.2.3 Motor Driver Board Design

After testing of a dozen of different micro DC motors, a 10 mm diameter coreless brushed DC motor NAMIKI 10CL-1801 is selected for the three jet drive propulsion system and a brushed DC motor FK-050SH-13130 is adopted to drive the propellers of four jet drive propulsion system. The selected brushed DC motors match well with the designed propeller. Additionally, it is observed from the field test that these motors have a much longer stable lifetime than those metal brush motors used in other micro AUV design[43]. And the rated voltages and power consumptions of these two types of DC motors are listed in Table 3.1. Texas Instruments' DRV8835 is a tiny dual H-bridge motor driver IC that can be used for bidirectional control of two brushed DC motors at 2 to 11 V. It can supply up to about 1.2 A per channel continuously and can tolerate peak currents up to 1.5 A per channel for a few seconds, making it an ideal driver for the selected motors. The size of assembled the entire control electronics is show Figure 3.8.

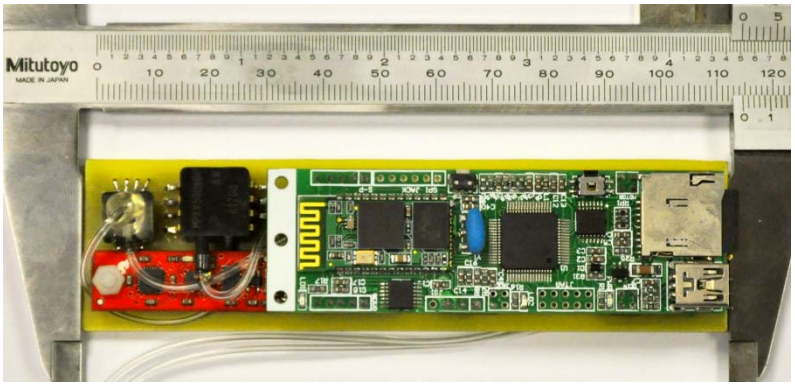

Figure 3.8 Assembled control electronics

3.2.4 Power System Design

According to the power consumption values listed in Table 3.1 (worst case scenario) and the hull size of the Lancelet, a 7.4 V 2 Ah lithium-polymer rechargeable battery pack SLPB834374H is adopted as the power source for the micro AUV. For different components operate at different voltage levels some of which are lower than voltage of the battery, the input supply has to be

stepped down and regulated. A synchronous rectification buck converter is used to step down the supply voltage to 5V with efficiency at around 95% shown in Figure 3.9. Then two linear regulators on the control board and the sensor board are applied to supply the needed voltage of 3.3V separately.

Table 3.1 Components power consumption

Component	Number	Voltage (V)	Current (mA)
Motor 10CL-1801	3	5	300
Motor FK-050SH-13130	4	7.4	350
Microcontroller	1	3.3	23
Bluetooth	1	3.3	35
Flash card	1	3.3	50
Accelerometer	1	3.3	0.145
Magnetometer	1	3.3	0.1
Gyro	1	3.3	0.1
Absolute pressure sensor	1	5	6
Differential pressure sensor	1	5	10

The lifespan of the micro AUV, defined as the length of time before the power supply runs out, can be estimated from Table 3.1 and the designed voltage regulation system. Under worst case conditions assuming all subsystems are on all the time the lifespan of the three jet drive Lancelet is more than 160 min, and the lifespan of the four jet drive Lancelet is more than 80 min. But the Bluetooth module is only used for programming the microcontroller. And it can be concluded from the design of the propulsion system that the motors would not all work at full speed with the maximum power consumption. Since the motors are adopted not only for surging but also for turning and pitching control, if they all work with full speed, there will be no dynamic space reserved for the turning or pitching control. As a result, the operation time of the three jet drive Lancelet is no less than 3 hours and the operation time of the four jet drive Lancelet is around 2 hours.

The power system still needs a manual power switch for rebooting the microcontroller or shutting down the whole system. And the switch must be totally water proof. In our design a bipolar latching Hall Effect magnetic sensor SS466A is used to enable/disable the buck converter and act as the on/off switch of the power system. The power system is treated as a separated

module and its schematics are shown in Figure 3.9. It can be switched on/off by a magnet from the outside of the hull of the vehicle.

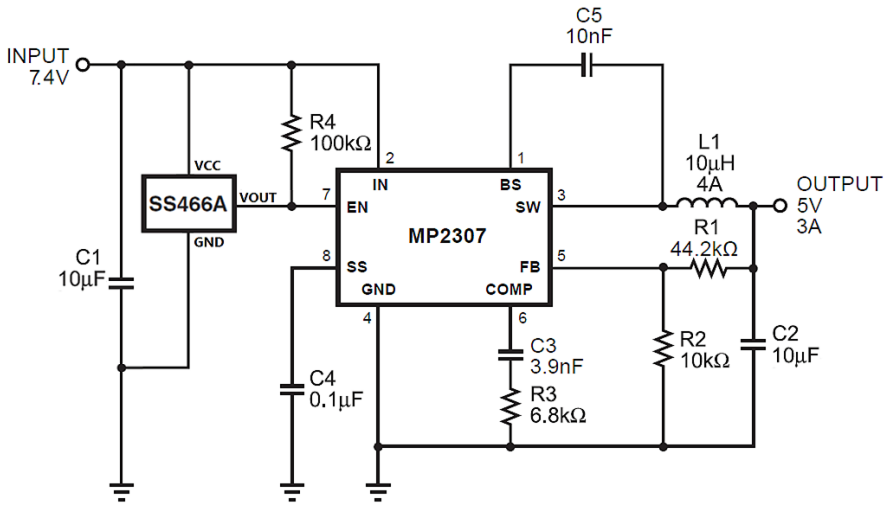

Figure 3.9 Schematics of the 5V output step down power system with Hall latching switch

3.3 Control System Architecture Design

3.3.1 Control System Program Flow

The control system works under an interrupt driven program flow logic. The main control board is programmed to stay in waiting mode until an I^2C interrupt activates it by sending the data from the sensor board. The main control board will deal with the received data in the interrupt function and store the data into the flash card, and then returns to the waiting mode.

Figure 3.10 shows the relationship between the sensor board and the main control board, which is the data transformation interrupt through I^2C interface. On startup, the main control board is programmed to initialize program variables such as the system clock frequency, and the parameters of the real-time counter for the system time. And all the necessary peripherals including the PWM for motor control, ADC for analogy inputs, SPI for the flash card, I^2C for receiving data from sensor board and the USART for Bluetooth communication are initialized and enabled as well. After setup, all interrupts are enabled. The main control board then proceeds into the main routine loop that logically stays in the waiting model for the I^2C interrupt to activate it for one control loop. In each control loop the motor speeds will be updated according to the calculation results from the control law. Then after the

program return from the I^2C interrupt function, the main routine will save the necessary data to a buffer and if the buffer is full it will be send to the flash card.

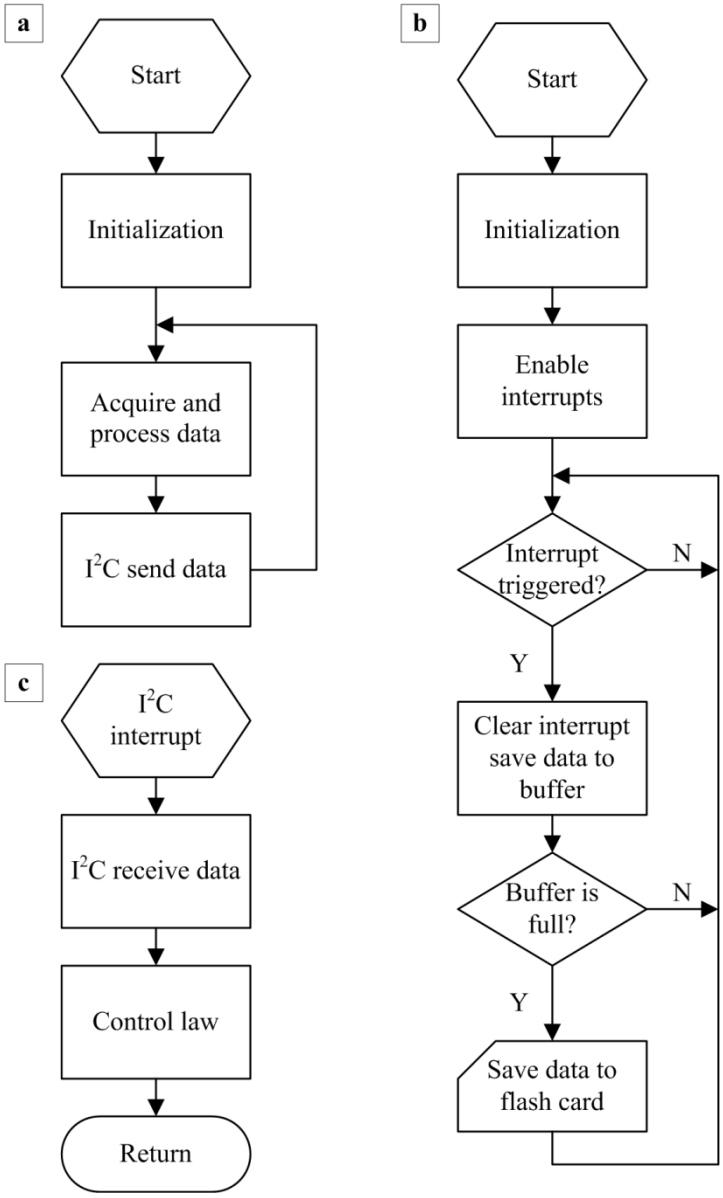

Figure 3.10 Interrupt driven control system program flow. (a) sensor board program flow, (b) main control board waiting loop, (c) main control board I^2C interrupt function

The sensor board processes the data acquired from the accelerometer, the magnetometer, the gyro and the pressure sensing system with a predefined frequency under the control of its internal timer counter. At each interval, the processed data are sent to the main control board via I^2C interface by an interrupt, which will ensure the real time characteristic of the whole control system.

3.3.2 Complementary Filter for Orientation Estimation

Compared with applying Euler angles to describe the orientation of an object in three dimensions, the method of orientation quaternion is more efficient and can avoid the problem of gimbal lock. In this research, the orientation quaternion describing the orientation of the body-fixed frame of the AUV relative to the earth-fixed frame which is defined by equation (3.8) will be estimated by a complementary filter from the data of the IMU module of the sensor board[88].

$$\boldsymbol{q} = \begin{bmatrix} q_1 & q_2 & q_3 & q_4 \end{bmatrix}^T \tag{3.8}$$

Actually, the complementary filter is a type of sensor fusion algorithm. The orientation quaternion integrated from the gyroscope is denoted as $\boldsymbol{q}_{gyo}$, and the orientation quaternion calculated from the accelerometer and the magnetometer is denoted as $\boldsymbol{q}_{acc,mag}$, then the estimated orientation quaternion with the complementary filter is obtained by equation (3.9), where γ is the complementary weight applied to each orientation calculation[89, 90].

$$\boldsymbol{q} = \gamma \boldsymbol{q}_{gyo} + (1-\gamma)\boldsymbol{q}_{acc,mag} \tag{3.9}$$

Results from[88, 91]indicate that this filter can achieve levels of accuracy exceeding that of the Kalman-based algorithm, and at the same time this filter is computationally inexpensive and effective at low sampling rates. The Euler angles corresponding to the orientation quaternion $\boldsymbol{q}$ can be calculated by the following equations.

$$\begin{bmatrix} \phi \\ \theta \\ \psi \end{bmatrix} = \begin{bmatrix} a\tan 2\left(2\left(q_0 q_1 + q_2 q_3\right), 1-2\left(q_1^2 + q_2^2\right)\right) \\ \arcsin\left(2\left(q_0 q_2 - q_1 q_3\right)\right) \\ a\tan 2\left(2\left(q_0 q_3 + q_1 q_2\right), 1-2\left(q_2^2 + q_3^2\right)\right) \end{bmatrix} \tag{3.10}$$

In this research, the orientation of the AUV is estimated and updated by the complementary filter at a frequency of 50 Hz.

3.4 Propulsion System Performance Test

In order to study the performance of the propulsion system, the thruster force of each jet drive is measured by an ATI Industrial Automation Nano17 force

sensor as shown in Figure 3.11. This force sensor is capable of measuring forces and moments along all three axes. But the lateral force and the torque with respect to the origin of the body-fixed frame from one jet drive are too small comparing to the resolution of the force and torque measurement. Here the force sensor is only used to measure the magnitude of the thruster force of each jet drive.

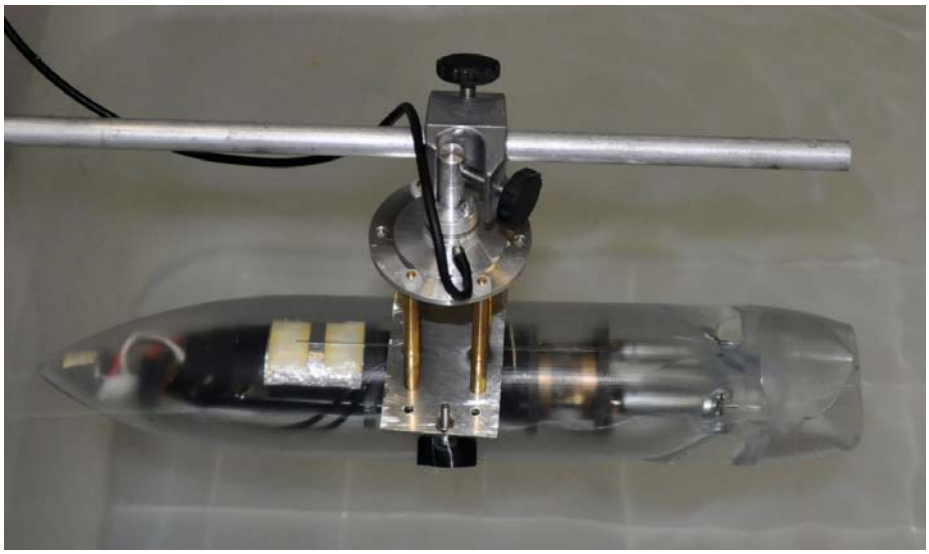

Figure 3.11 Micro AUV Lancelet with three jet drive propulsion system setup with Nano 17 force sensor

The experiment results of the thruster force of the three jet drive and the four jet drive propulsion systems are shown in Figure 3.12 and Figure 3.13 respectively. The duty cycle of the PWM signals driving the DC motors stepped up from 30% to 100% with spacing of 10%. It could be concluded that the thruster force increase almost linearly with the duty cycle, which is summarized in Figure 3.14 and Figure 3.15.

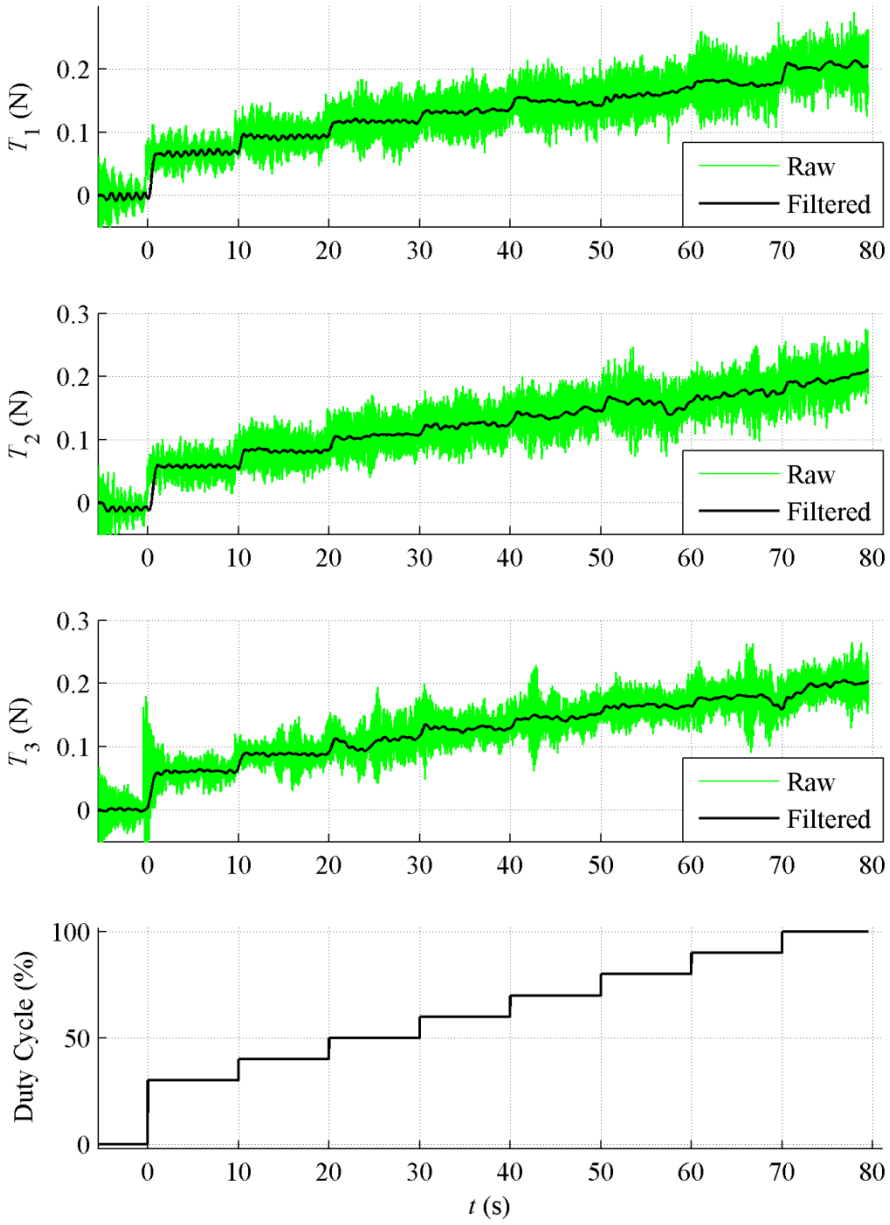

Figure 3.12 Thruster forces of three jet drives with respect to duty cycle of driven motor

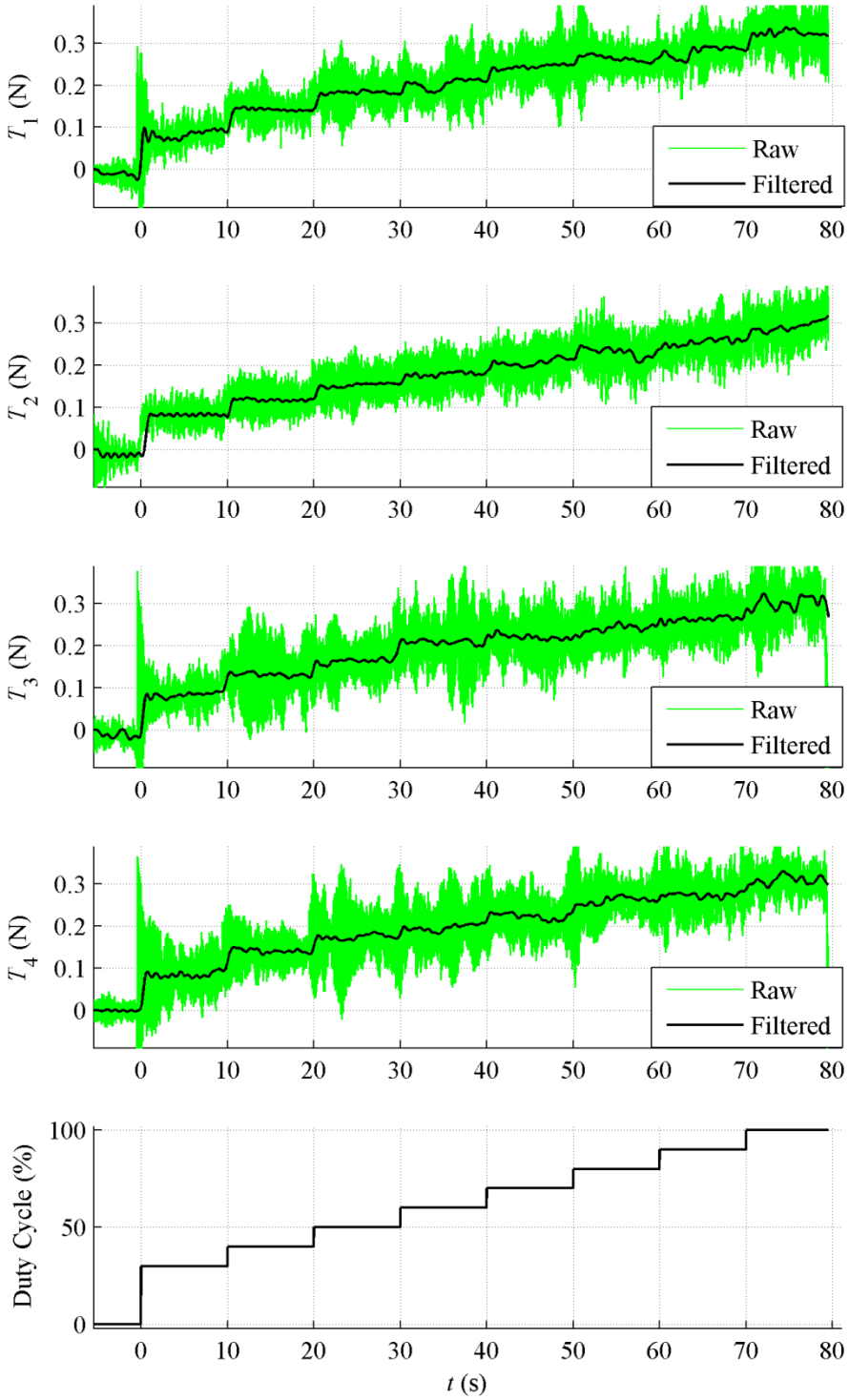

Figure 3.13 Thruster forces of four jet drives with respect to duty cycle of driven motor

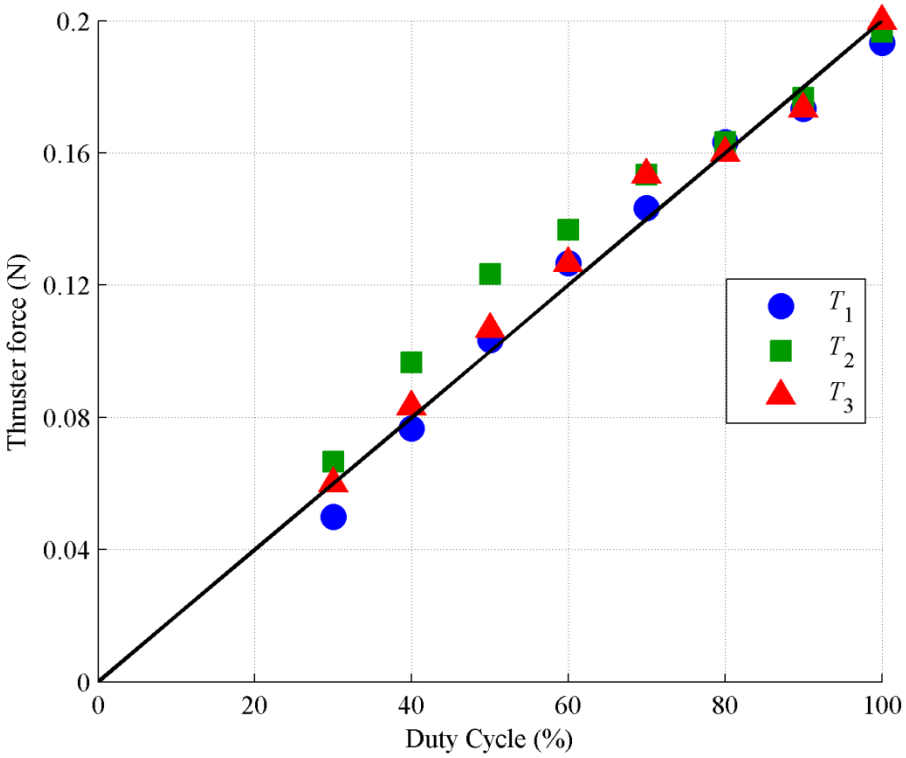

Figure 3.14 Summary of the thruster forces of three jet drive propulsion system

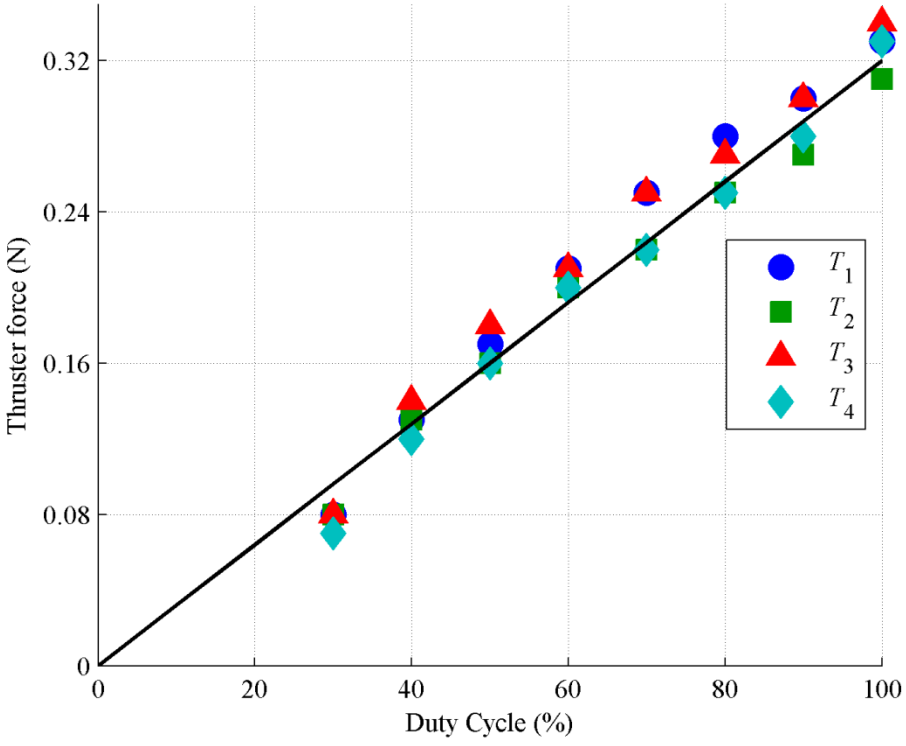

Figure 3.15 Summary of the thruster forces of the four jet drive propulsion system

The complete specification of force acting on a rigid body must include its magnitude, direction, and point of application. The magnitude of the thruster force is proportional to the motor speed and has been measured by the force sensor. The direction and point of application which are quantified as β and a shown in Figure 3.2 are determined by the shape of the nozzle of the jet drive. In this work, the nozzle is designed geometrically with β = 8° and a = 11 mm for both the three jet drive propulsion system and four jet dive propulsion system. But in order to maximize the section square of the nozzle and to minimum the pressure lost, the nozzle is not axisymmetric, the geometric center of the outlet is not necessarily the point of application of the thruster force, and the direction of the nozzle may not be the direction of the thruster force either. The real β and a may not be equal to the designed values.Here a mechanism is designed to measure the value of the moment arm h of the thruster force with respect to selected rotation center on the main axis of the AUV, and to calculate the values of β and a indirectly by the formula $h = a + l\tan(\beta)$, where l is the distance between outlet of the jet drive and selected rotation center.

This mechanism is shown in Figure 3.16, where a shaft perpendicular to the plane determined by the main axis of the vehicle and the thruster force vector of the tested jet drive supports the AUV with a ball bearing. The distance between outlet of the jet drive and selected rotation center is fixed, and the distance between the supporting shaft and the main axis of the vehicle is adjustable and defined as $\tilde{h}$. When the tested jet drive is turned on underwater, if $\tilde{h}$ less than the corresponding moment arm, the AUV will rotate counter clockwise, if $\tilde{h}$ is bigger than the corresponding moment arm, the AUV will rotate clockwise. When and only when $\tilde{h}$ equals to the corresponding moment arm, the AUV will keep steady. Thus, for the any specified distance between outlet of the jet drive and selected rotation center, the corresponding moment arm can be determined. We can set two different values of the distance between outlet of the jet drive and selected rotation center l_1 and l_2 as show in Figure 3.16. Then the corresponding moment arm can be determined separately as h_1 and h_2. Then from the following equations,

$$h_1 = a + l_1 \tan(\beta)$$
$$h_2 = a + l_2 \tan(\beta) \tag{3.11}$$

the values of β and a can be calculate. From the testing results it is found that for both the three jet drive propulsion system and four jet dive propulsion system β and a are all quiet close to their designed values. It is concluded that the direction and point of application of the thruster force is as designed.

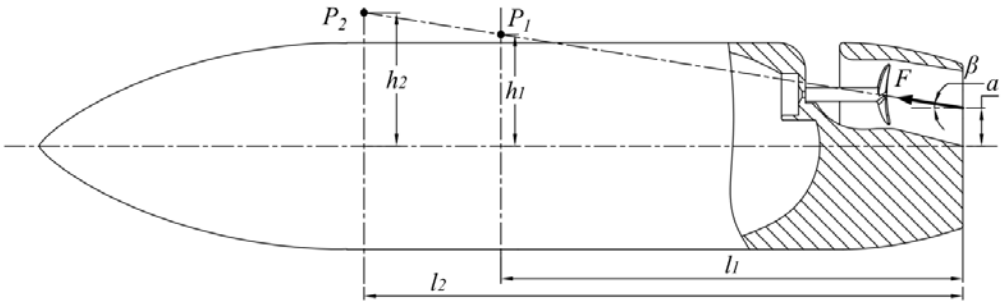

Figure 3.16 Mechanism to measure the moment arm of the thruster force

3.5 Open Loop Field Test of the Lancelet

Open loop field tests have been carried out for studying the maneuverability of the Lancelet and to provide improvement instructions of the design of the vehicle. The Lancelet is capable of not only traveling forward as traditional torpedo shaped underwater vehicles, but also has the ability to turn in place, pitch in place, and travel with any pitching angle without losing its stability even in the vertical direction. The control signals are received from a low frequency wireless transmitter, which can penetrate the water down to a depth of about 2 m. This is enough for the open loop test of our micro AUV. The received control signals is little noisy which can be seen in all the field test results.

3.5.1 Lancelet with Three Jet Drive Propulsion System

Figure 3.17 shows a process of surging acceleration, where $T_1 = T_2 = T_3$. It can be concluded from equation (3.2) that $X = T_1 + T_2 + T_3$, $M = 0$ and $N = 0$.This a pure acceleration process without turning or pitching effect. And all the three motors work below their half duty cycle and far from saturation with the total forward thruster force as a constant value of 0.24 N which gives the micro AUV a constant speed about 0.6 m/s. If all the motors work at full speed, they

will generate a total thruster force of 0.6 N which could give the Lancelet a maximum speed around 1 m/s.

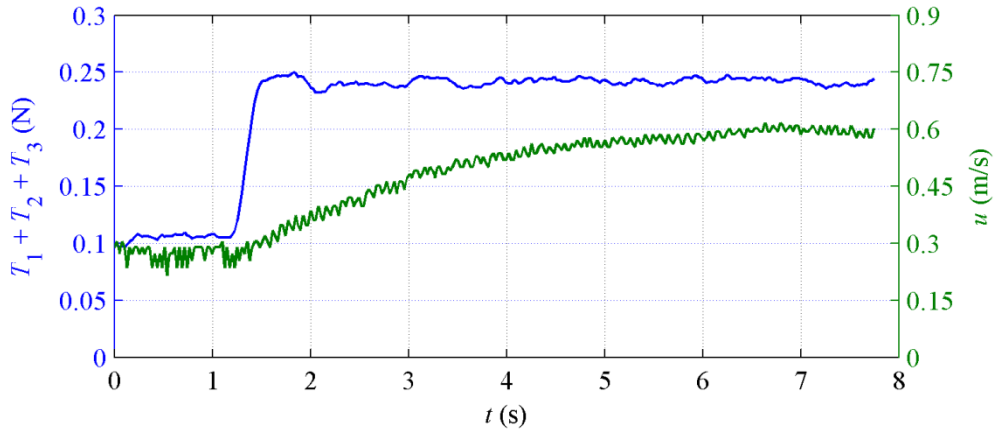

Figure 3.17 Three jet drive Lancelet thruster forces and velocity of surging acceleration process

The designed vector propulsion system of the Lancelet provides several unique propulsion capabilities, giving the Lancelet significant advantages over existing torpedo shaped AUV designs. The majority of the focus has been on the potential maneuvering capability of a zero turning radius. Turning radius in the context of AUV's refers to the minimum radius circle a vehicle can navigate; in practical terms, this is the minimum radius required for a vehicle to complete a 180° turn [92, 93]. This is a limitation of vehicle size and length, propulsion capabilities, and speed. Typical torpedo-shaped AUVs have a turning radius of anywhere from 3 m to 23 m or higher[94]. The Lancelet has a zero turning radius, meaning that the Lancelet is able to perform very tight turns even in small spaces. This is a significant advantage in situations demanding high maneuverability, particularly in exploration of unknown areas where the vehicle may be required to turn around in a small space. Figure 3.18 shows a process of turning in place, where $T_1 = 0$, $T_2 = -T_3$. It can be concluded from equation (3.2) that $X = 0$, $M = 0$ and $N = -\sqrt{3}hT_2$. The Lancelet rotates around its body-fixed z_b axis about 270° in the first half of the process, and then rotates back to its original place during the last half of the process without any surging speed.

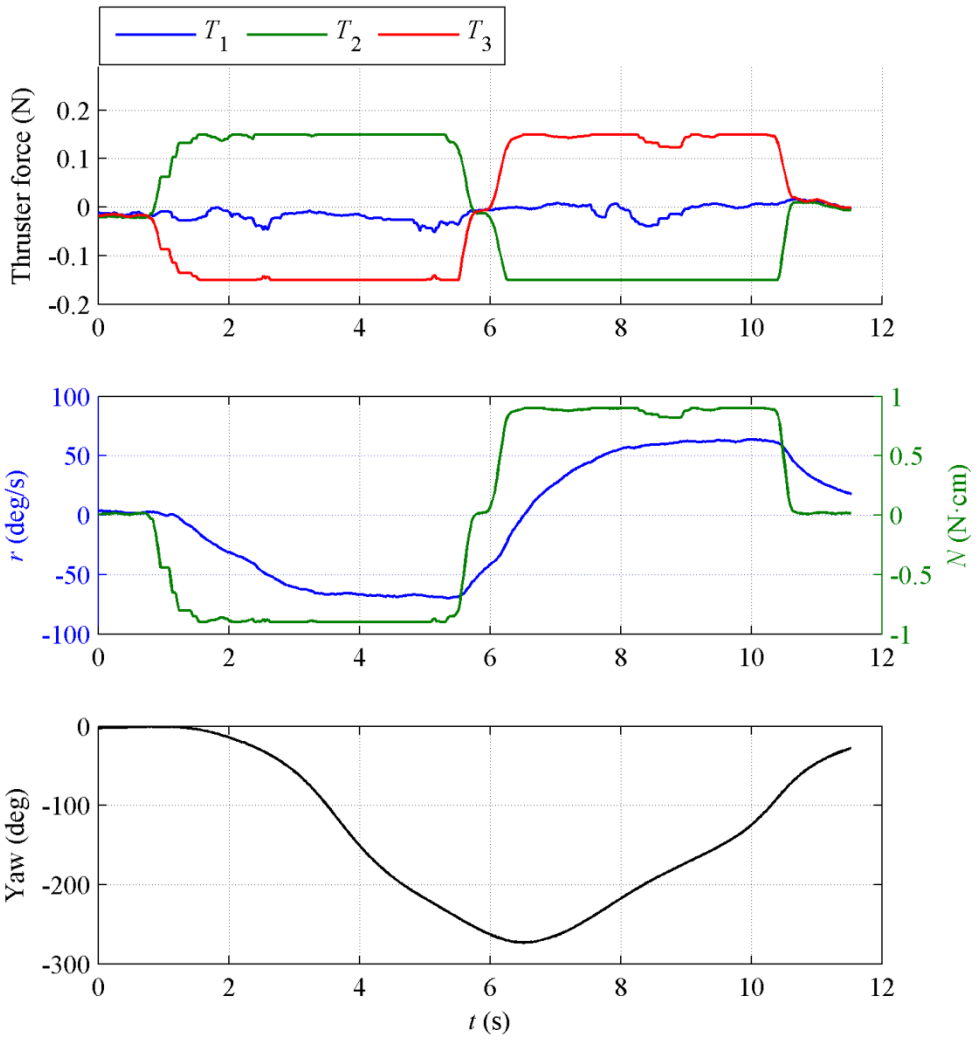

Figure 3.18 Three jet drive Lancelet turning in place process

The multi-jet drive propulsion system gives the Lancelet another potential maneuvering capability of travelling in vertical plane with any pitching angle without losing its stability. Figure 3.19shows the transition from travelling in the horizontal plane with the pitch angle near to zero to surfacing with the pitch angel near to -90°. The details of this process are shown in Figure 3.20. From 1 s to 2 s the Lancelet decelerated and stopped. Then it adjusted the pitch angle to near vertical direction without any surging speed from about 2 s to 6 s. After this process, the vehicle surfaced with the head pointing up till about 8.5 s the head of the vehicle reached the surface of the water. Finally, the vehicle returned to its normal position due to the balance between the buoyancy and the gravity of the vehicle.

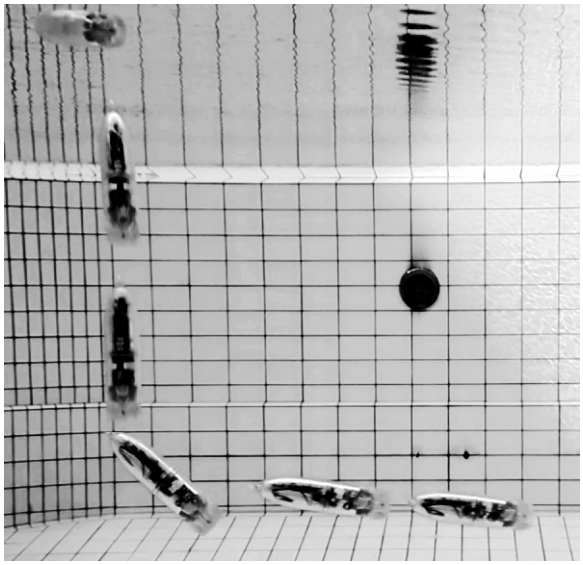

Figure 3.19 Trajectory of the process of pitching in place to surfacing vertically

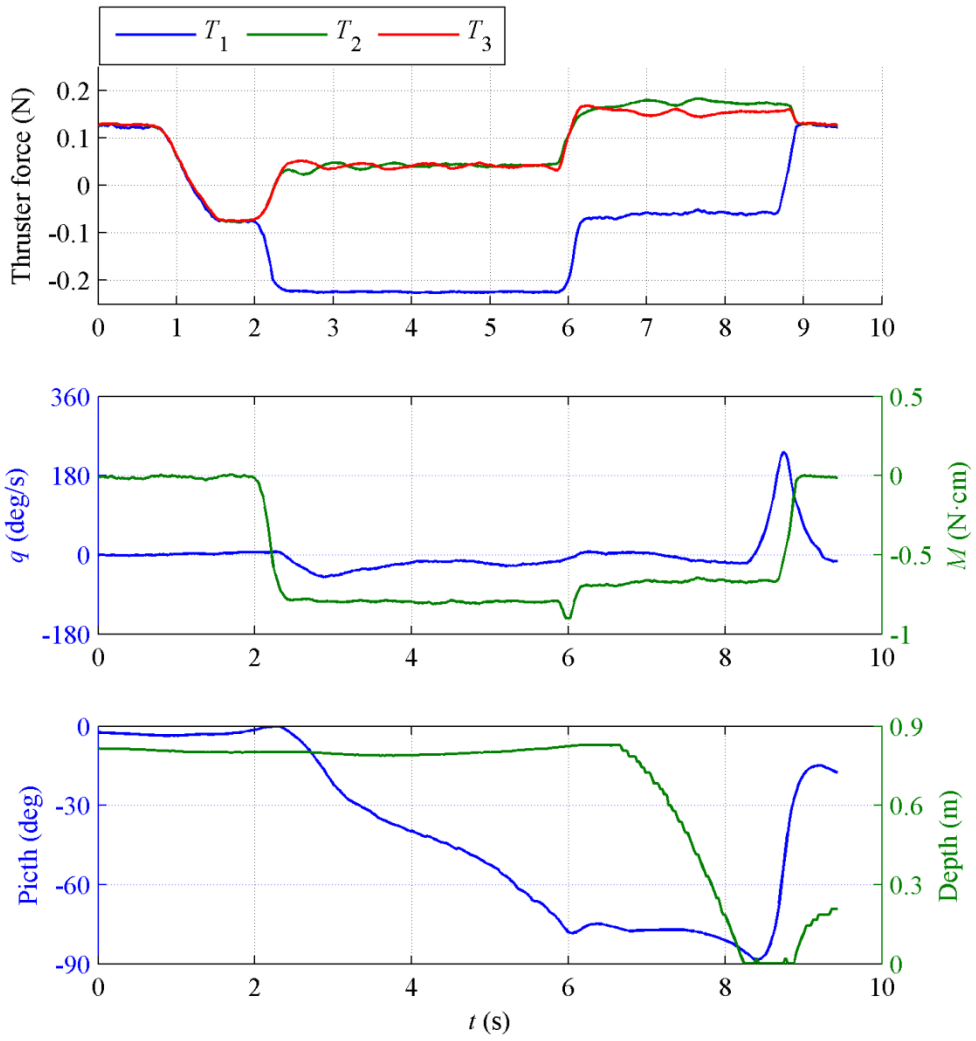

Figure 3.20 Three jet drive Lancelet pitching in place and surfacing vertically process

3.5.2 Lancelet with Four Jet Drive Propulsion System

Figure 3.21 shows a process of surging acceleration and deceleration, and turning in place of the Lancelet with the four jet drive propulsion system. From 0.5 s to 4 s the Lancelet accelerated to about 1.3 m/s which is close to the terminal velocity of the vehicle under that propulsion force. From 4 s the Lancelet made a crash stop which is process of braking by reversing the shaft speed of all these four jet drives, which could decelerated the Lancelet to nearly 0 m/s in about 1s. During the process of pure acceleration and deceleration, $T_1 = T_2 = T_3 = T_4$. It can be concluded from equation (3.4) that $X = T_1 + T_2 + T_3 + T_4$, $K = 0$, $M = 0$ and $N = 0$. The total forward thruster force is a constant value of about 0.96 N during the acceleration process which could give the micro AUV a speed of about 1.3 m/s. If all the motors work at full speed, they will generate a total thruster fore of 1.28 N which may give the Lancelet a maximum speed around 1.5 m/s. From about 6 s to 8 s the Lancelet complete a process of turning in place, where $T_1 = 0$, $T_3 = 0$, $T_2 = -T_4$. It can be concluded from equation (3.4) that $X = 0$, $M = 0$, $K = 0$ and $N = 2hT_4$. The Lancelet rotates around its body-fixed z_b axis more than 180° with zero surging speed. Then from 10 s, the Lancelet repeated the process of surging acceleration and deceleration, and turning in place. The only difference is that the vehicle turned with opposite angular velocity direction in the turning in place process.

Figure 3.22 shows the pitching in place process of the Lancelet with the four jet drive propulsion system. From 1.5 s to 3.5 s the Lancelet pitched up to about 60°, and from 3.5 s to 6 s the Lancelet pitched down to vertical direction, then the Lancelet returned to its normal balance position. During the pitching in place process, $T_2 = 0$, $T_4 = 0$, $T_1 = -T_3$. It can be concluded from equation (3.4) that $X = 0$, $K = 0$, $N = 0$ and $M = 2hT_1$ which indicated this is a pure pitching process. Because the depth sensor is mounted on the nose of the vehicle, the depth readings changes with the pitching angle as in Figure 3.22.

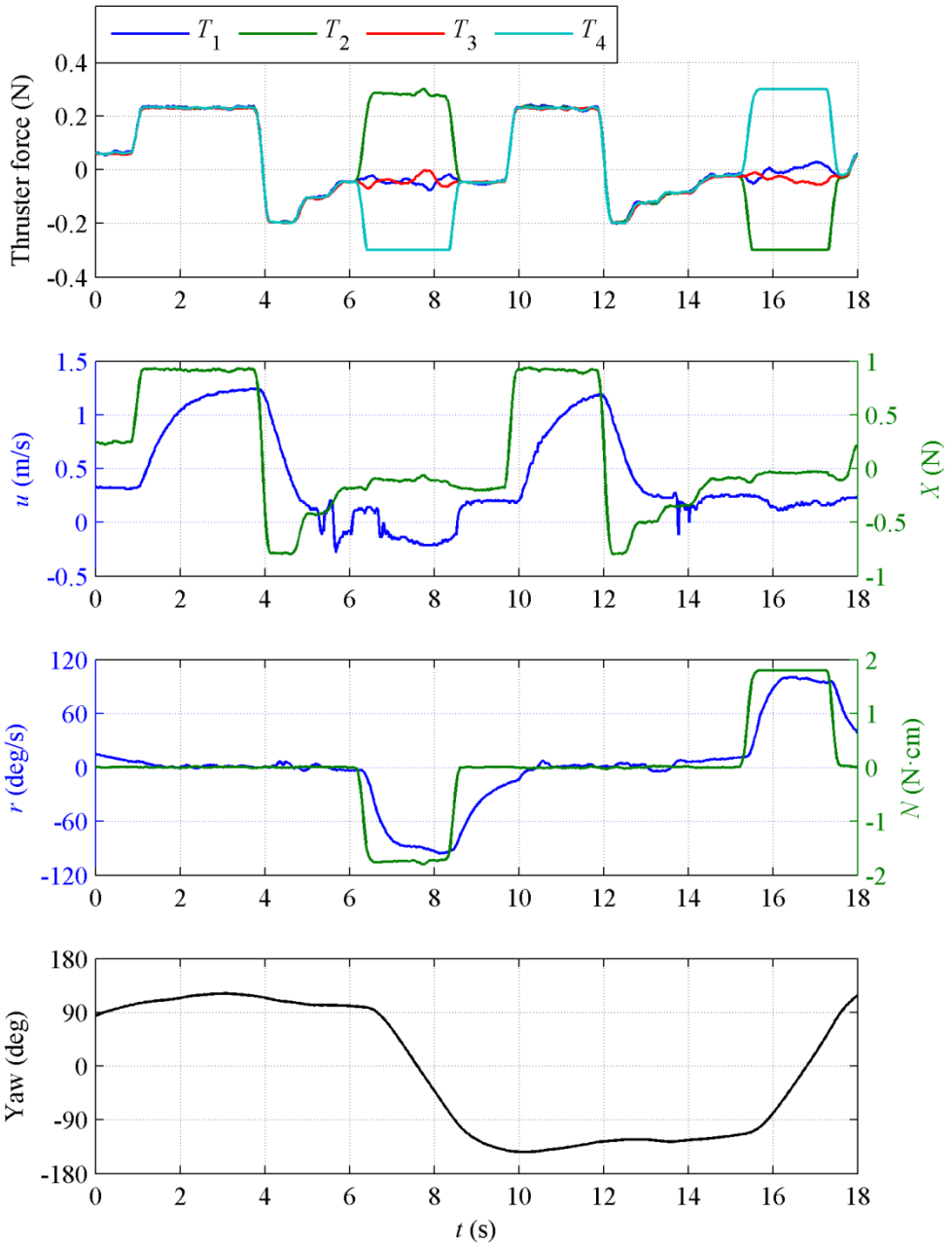

Figure 3.21 Four jet drive Lancelet surging acceleration and deceleration and turning in place process

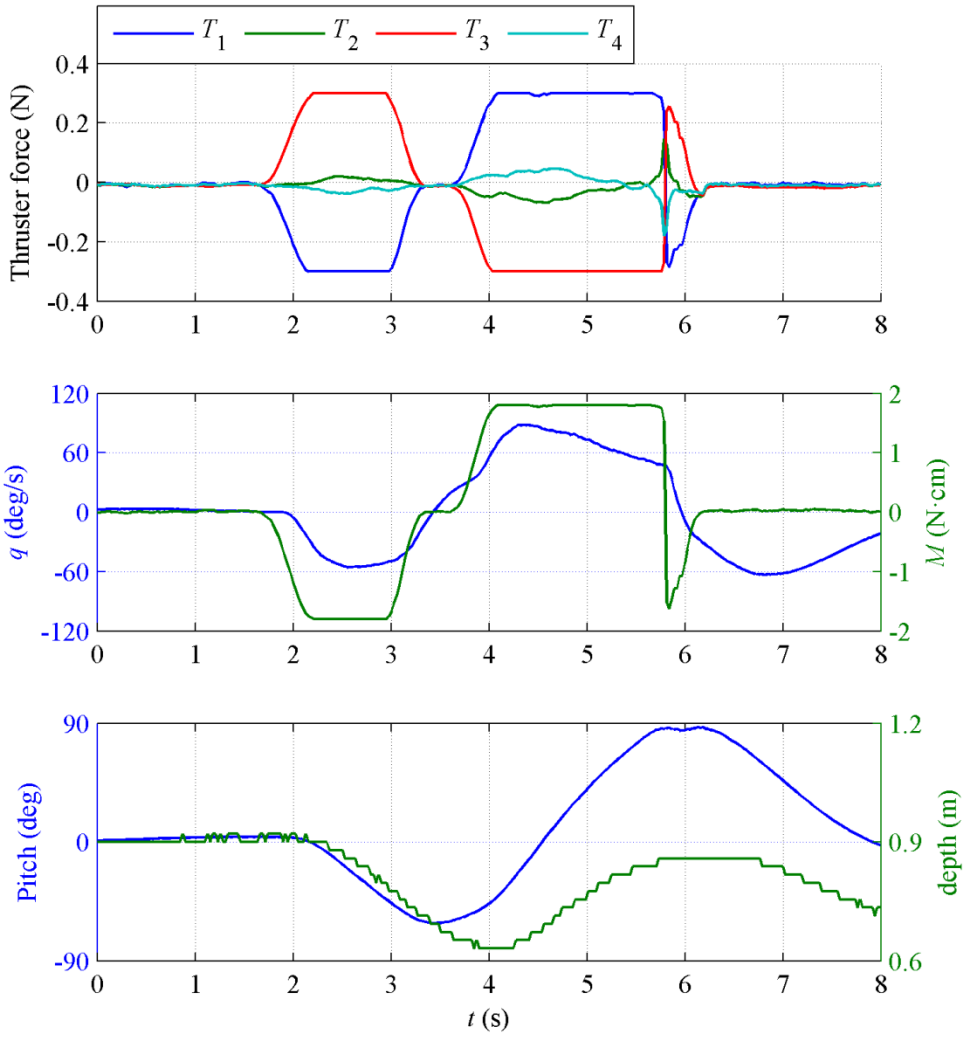

Figure 3.22 Four jet drive Lancelet pitching in place process

3.6 Summary

This chapter presents the work undertaken in the design, construction and testing of the Lancelet micro AUV which is equipped with a novel finless multi-jet drive propulsion system. Fully capable prototypes with the designed multi-jet drive propulsion systems have been built. And open loop free swimming field tests are carried out to explore their special maneuverability. From the experiment results, we have concluded that the multi-jet drive propulsion systems and the whole control electronics work well as designed. In the next two chapters, the prototypes will be used for the hydrodynamic parameter identification and the modular dynamic modeling of the AUV.

Chapter 4 Combination of Empirical and Parameter Identification Methods for Estimation of Hydrodynamic Parameters

Empirical methods of determining the hydrodynamic coefficients of the torpedo shaped AUV are discussed in Chapter 2. But some of these hydrodynamic coefficients are not easy to be estimated especially for AUVs with non-streamlined appendages on the hull[95-97]. System identification techniques are more efficient and flexible test-based method and can be applied to free-swimming model or full-size vehicle tests without complicated laboratory testing facilities[98]. In this chapter, the empirical methods are combined with the identification method for the accurate estimation of both hydrodynamic coefficients and hydrodynamic derivatives of the AUV.

4.1 Maximum Likelihood Estimation for Hydrodynamic Coefficients Identification

4.1.1 Introduction to Maximum Likelihood Estimation

Maximum likelihood estimation (MLE) is a statistical method used for fitting a statistical model to data, and providing estimates for the model's parameters[99, 100]. Consider a model parameterized by unknown parameters $\boldsymbol{\theta} \in R^n$, the MLE is about the selection of $\boldsymbol{\theta}$ which maximizes the probability of appearance of sampled output data $Y_N = (\boldsymbol{y}_1, \boldsymbol{y}_2, \cdots, \boldsymbol{y}_N), \boldsymbol{y}_i \in R^m$. The target of the parameter vector $\hat{\boldsymbol{\theta}}$ can be calculated by maximizing a likelihood function *L*,

$$\hat{\boldsymbol{\theta}} = \mathrm{ARG} \max_{\boldsymbol{\theta} \in \Theta} L(Y_N | \boldsymbol{\theta}) \tag{4.1}$$

We can use $\ln p(Y_N | \boldsymbol{\theta})$ as the likelihood function, where $p(Y_N | \boldsymbol{\theta})$ is the conditional probability of output data array Y_N under the condition of $\boldsymbol{\theta}$. Apply the Bayes' theorem,

$$p(Y_N | \boldsymbol{\theta}) = \prod_{i=1}^{N} p(y_i | Y_{i-1}, \boldsymbol{\theta}) \tag{4.2}$$

Then, we will have,

$$\hat{\boldsymbol{\theta}} = \text{ARG}\ \max_{\boldsymbol{\theta}\in\Theta} \sum_{i=1}^{N} \ln\, p(\boldsymbol{y}_i \big| Y_{i-1}, \boldsymbol{\theta}) \tag{4.3}$$

If N is big enough, it can be assumed that $p(\boldsymbol{y}_i \big| Y_{i-1}, \boldsymbol{\theta})$ is near the normal distribution, with the definitions of the expected value and the variance of $\boldsymbol{y}_i$ as follows.

$$E\left\{\boldsymbol{y}_i \big| Y_{i-1}, \boldsymbol{\theta}\right\} \equiv \hat{\boldsymbol{y}}(i \big| i-1) \tag{4.4}$$

$$\text{cov}\left\{\boldsymbol{y}_i \big| Y_{i-1}, \boldsymbol{\theta}\right\} = E\left\{\left[\boldsymbol{y}_i - \hat{\boldsymbol{y}}(i \big| i-1)\right]\left[\boldsymbol{y}_i - \boldsymbol{y}(i \big| i-1)\right]^T\right\} \equiv E\left\{e(i)e(i)^T\right\} \equiv B(i) \tag{4.5}$$

Then, the likelihood function will be as follows.

$$\hat{\boldsymbol{\theta}} = \text{ARG}\ \max_{\boldsymbol{\theta}\in\Theta}\left\{-\frac{1}{2}\sum_{i=1}^{N}\left[e(i)^T B^{-1}(i)e(i) + \ln\left|B(i)\right|\right]\right\} \tag{4.6}$$

And the MLE becomes to find $\boldsymbol{\theta}$ to minimize the likelihood cost function,

$$J = \frac{1}{2}\sum_{i=1}^{N}\left[e(i)^T B^{-1}(i)e(i) + \ln\left|B(i)\right|\right] \tag{4.7}$$

4.1.2 Output Error Method

For a nonlinear system with unknown parameters, the effect of process noise is very difficult to determine. Here we adopt the output error method (OEM) which assumes that the process noise is negligible and that the outputs are corrupted by additive measurement noise only[99]. Then, the mathematical model of the dynamic system whose parameters are to be estimated can be described by the following general nonlinear system representation with continuous states function and discrete output function,

$$\begin{aligned} \dot{\boldsymbol{x}} &= f(\boldsymbol{x}, \boldsymbol{u}, \boldsymbol{\theta}; t)\ (t \in [0, T]) \\ \boldsymbol{y}_i &\equiv \boldsymbol{y}(t_i) = h\left[\boldsymbol{x}(t_i), \boldsymbol{u}(t_i), \boldsymbol{\theta}; t_i\right] + \varepsilon(t_i)\ (i = 1, 2, \cdots, N) \end{aligned} \tag{4.8}$$

where $\boldsymbol{x}$ is the vector of state variables, $\boldsymbol{u}$ the control input vector, $\boldsymbol{y}$ is the system output vector, and $\boldsymbol{\theta}$ is the vector of system parameters. f and h are general nonlinear real-valued functions. The output error $\varepsilon(t_i)$ is assumed to be white noises with zero mean value as $E\left[\varepsilon(t_i)\right] = 0, E\left[\varepsilon(t_j)\varepsilon^T(t_k)\right] = R\delta_{jk}$, where δ_{ij} is the Kronecker symbol.

Then, the likelihood cost function can be written as,

$$J = \frac{1}{2}\sum_{i=1}^{N}\left[e(i)^T R^{-1} e(i) + \ln|R| \right] \tag{4.9}$$

where *e* is the error of the system output, and *R* can be estimated by,

$$R = \frac{1}{N}\sum_{i=1}^{N} e(i)e^T(i) \tag{4.10}$$

And the optimization problem of finding the value of $\boldsymbol{\theta}$ to minimize the likelihood cost function (4.9) can be solved by the Newton-Raphson Method. This iteration method requires $\frac{\partial J}{\partial \boldsymbol{\theta}} = 0$ as the target of optimization. If $\boldsymbol{\theta}$ is not the best value, it can be adjusted according to the following equation.

$$\frac{\partial J_{k+1}}{\partial \boldsymbol{\theta}} = \frac{\partial J(\boldsymbol{\theta}_k + \Delta\boldsymbol{\theta}_k)}{\partial \boldsymbol{\theta}} = \frac{\partial J(\boldsymbol{\theta}_k)}{\partial \boldsymbol{\theta}} + \frac{\partial^2 J(\boldsymbol{\theta}_k)}{\partial \boldsymbol{\theta}^2}\Delta\boldsymbol{\theta}_k + \Delta\boldsymbol{\theta}_k^2 = 0 \tag{4.11}$$

Neglect the second order infinitely small, we will have,

$$\Delta\boldsymbol{\theta}_k = -\left[\frac{\partial^2 J(\boldsymbol{\theta}_k)}{\partial \boldsymbol{\theta}^2} \right]^{-1} \frac{\partial J(\boldsymbol{\theta}_k)}{\partial \boldsymbol{\theta}} \tag{4.12}$$

According to the likelihood cost function(4.9), by neglecting the derivative of *J* to *R*, the elements of the right side of equation (4.12) can be calculated as follows.

$$\frac{\partial J(\boldsymbol{\theta}_k)}{\partial \boldsymbol{\theta}_j} = \sum_{i=1}^{N}\left[e(i)^T R^{-1} \frac{\partial e(i)}{\partial \boldsymbol{\theta}_j} \right] \quad (j = 1, 2, \cdots, n) \tag{4.13}$$

$$\frac{\partial^2 J(\boldsymbol{\theta}_k)}{\partial \boldsymbol{\theta}_j \partial \boldsymbol{\theta}_l} = \sum_{i=1}^{N}\left[\frac{\partial e^T(i)}{\partial \boldsymbol{\theta}_l} R^{-1} \frac{\partial e(i)}{\partial \boldsymbol{\theta}_j} \right] \quad (j, l = 1, 2, \cdots, n) \tag{4.14}$$

4.1.3 Hydrodynamic Coefficients Identification with AUV Dynamic Model

Here, we will talk about how to apply the output error method to the dynamic model of the AUV constructed by a main torpedo shaped body and several control fins to estimate its unknown hydrodynamic coefficients. And it is assumed that all the fins have the same shape, then according to equations

(2.39) and (2.43) the hydrodynamic coefficients vector and output vector are defined as follows.

$$\boldsymbol{\theta} = \left[\left(C_{D_0}, C_{L_\alpha}, C_{L_q}, C_{m_\alpha}, C_{m_q} \right)_{hull}, \left(C_{D_0}, C_{D_L}, C_{L_{\alpha 1}}, C_{L_{\alpha 2}} \right)_{fin} \right]^T \tag{4.15}$$

$$\boldsymbol{y} = \upsilon = \left[u, v, w, p, q, r \right]^T \tag{4.16}$$

Substitute (2.9) and (2.10) into (2.6), the dynamic equation of the AUV will be as

$$M\dot{\upsilon} + C(\upsilon)\upsilon = \tau_D + \tau_E + \tau - g(\eta) \tag{4.17}$$

where,

$$\begin{aligned} M &= M_{RG} + M_A \\ C(\upsilon) &= C_{RG}(\upsilon) + C_A(\upsilon) \end{aligned} \tag{4.18}$$

If we set,

$$F = \tau_D + \tau_E + \tau - g(\eta) - C(\upsilon)\upsilon \tag{4.19}$$

Then we will have

$$\dot{\upsilon} = M^{-1}F \tag{4.20}$$

By applying Euler's formula we will have,

$$\hat{\upsilon}(k+1) = \upsilon(k) + \dot{\upsilon}(k)\Delta T \tag{4.21}$$

$$e(k+1) = \upsilon(k+1) - \hat{\upsilon}(k+1) \tag{4.22}$$

where ΔT is the time interval of the calculation step. Then, we will have

$$\frac{\partial e(k+1)}{\partial \boldsymbol{\theta}_j} = -\frac{\partial \hat{\upsilon}(k+1)}{\partial \boldsymbol{\theta}_j} = -\frac{\partial \dot{\upsilon}(k)}{\partial \boldsymbol{\theta}_j}\Delta T = -M^{-1}\frac{\partial F}{\partial \boldsymbol{\theta}_j}\Delta T \tag{4.23}$$

Substitute (4.23) into (4.13) and (4.14), and we can adopt the output error method for the hydrodynamic coefficient identification.

4.2 Hydrodynamic Coefficients Identification for Starfish AUV

The Starfish AUV is a torpedo-shaped AUV with a diameter of 0.2 m, which was designed to be modular at the mechanical, electronic and software level at the Acoustic Research Laboratory of National University of Singapore[101]. The detail description of the Starfish AUV is in[102]. A surfacing process in

vertical plane from the experiment data is selected for the coefficients identification. In this process the thruster force is 37 N and the horizontal fin reflection angle is as in Figure 4.1.

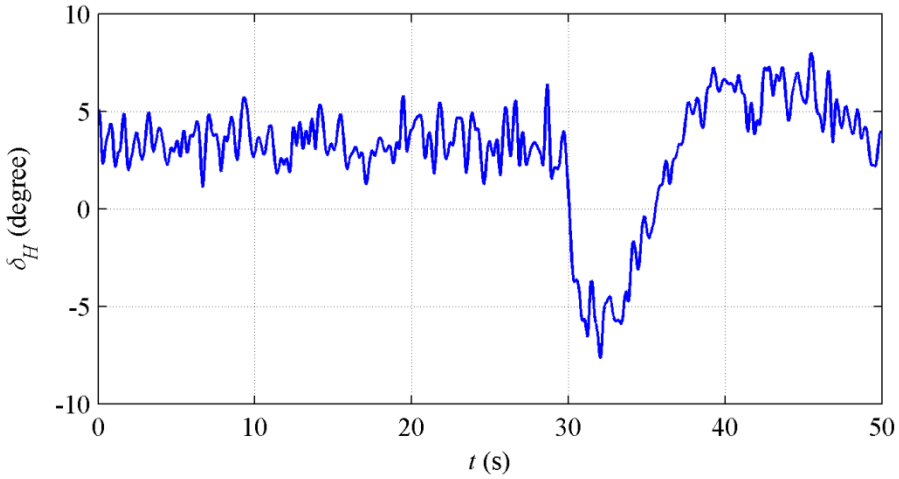

Figure 4.1 Horizontal fin reflection angle

Table 4.1 Starfish AUV hydrodynamic coefficients

	C_{D_0}	C_{L_α}	C_{L_q}	C_{m_α}	C_{m_q}	$(C_{D_L})_{fin}$	$(C_{L_{\alpha 1}})_{fin}$	$(C_{L_{\alpha 2}})_{fin}$
All identified	1.28	1.11	5.54	-28.86	-15.13	-3.01	1.29	0.79
Hull identified	1.27	1.99	9.13	-32.81	-31.24	***0.12***	***3.47***	***0.47***
Empirical estimated	***0.19***	***1.83***	***1.90***	***10.66***	***-0.31***	***0.12***	***3.47***	***0.47***

4.2.1 Identification of All Hydrodynamic Coefficients

The zero lift drag coefficient of the fin is small and has little influence on the drag force of the whole vehicle, so it is assumed to be known with the empirical value as its real value to reduce the number of coefficients to be estimated. Then the hydrodynamic coefficients vector and the output vector can be written as follows.

$$\boldsymbol{\theta} = \left[\left(C_{D_0}, C_{L_\alpha}, C_{L_q}, C_{m_\alpha}, C_{m_q} \right)_{hull}, \left(C_{D_L}, C_{L_{\alpha 1}}, C_{L_{\alpha 2}} \right)_{fin} \right]^T \tag{4.24}$$

$$\boldsymbol{y} = [u, w, q]^T \tag{4.25}$$

The identification results are shown in the first row of Table 4.1. And the identification results are also verified by simulation. Figure 4.2 and Figure 4.3 show the comparison between the simulation results of the dynamic model with the identified parameters and experiment results at the same control command. Figure 4.2 shows output comparison including the linear and angular velocities of the vehicle in the vertical plane which are the variables used directly for the parameter identification in the surfacing process. As can

be seen, the simulation results are in good agreement with field test results. This is double confirmed by the comparison between the simulation and experiment results of the pitch angle and depth values which are not used directly in the proposed parameter identification algorithm. But even this cannot guarantee the identified parameters are correct.

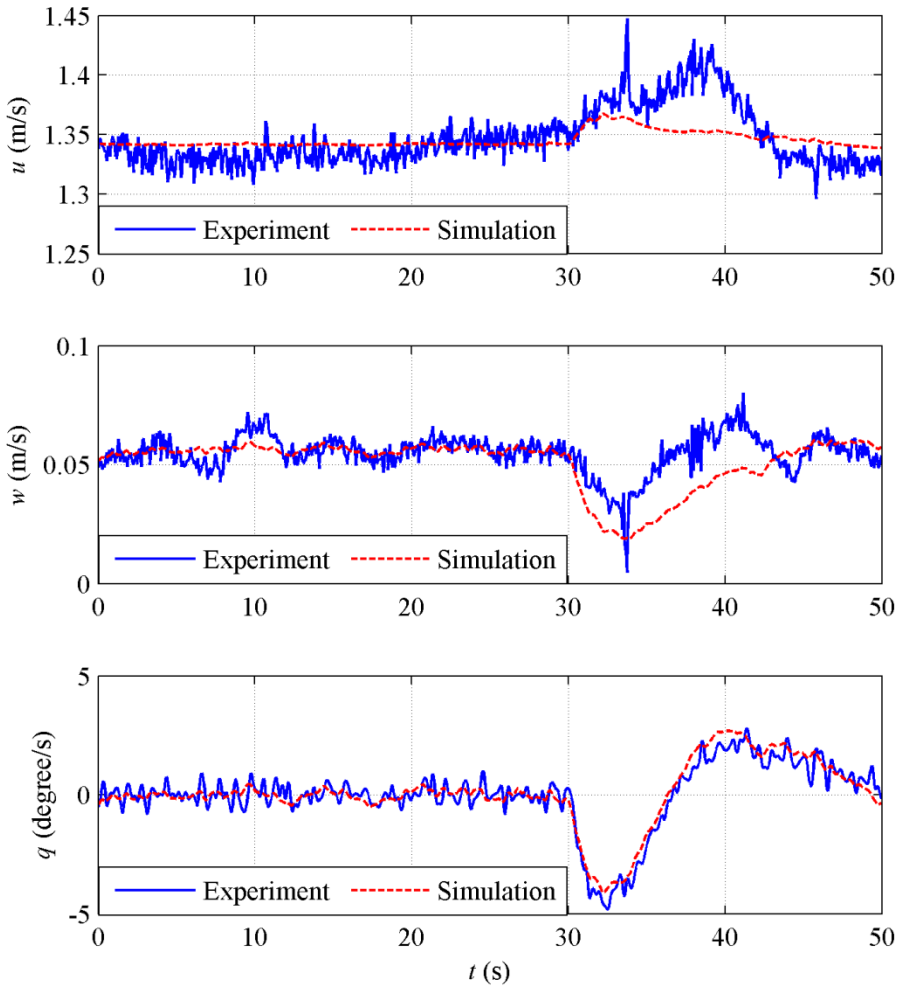

Figure 4.2 Outputs comparison between experiment and simulation of all hydrodynamic coefficients identification for Starfish AUV

The hydrodynamic coefficients estimated by empirical methods are also listed at the third row of Table 4.1 in bold Italic font. We can see from the identification results that some of the parameters identified are not reasonable, like $\left(C_{D_L}\right)_{fin}$ must be positive theoretically. The error of the identification results may due to the coupling of the hydrodynamic coefficients, which means if two parameters are all related to one force or moment acting on the

vehicle, it will be difficult or even impossible to identify both of them accurately. For example, the zero lift drag coefficients of both the hull and the fin are all related to the drag force of the vehicle at zero angle of attack. And this drag force is proportional to the square of the surging velocity of vehicle and the sum of these two coefficients. As a result, it is impossible to identify both of them simultaneously, and that is why in our identification algorithm we have assumed the zero lift drag coefficient of the fins is known. $\left(C_{L_\alpha}\right)_{hull}$ and $\left(C_{D_L}\right)_{fin}$ are all related to the drag force of the vehicle at non zero angle of attack, and the value of angle of attack for them are not always identical for the control fins have a non zero deflection angle in the surfacing process. Theoretically both of them can be identified. But the influence of drag from the fins is overwhelmed by the drag from the hull and related noise. As a result it is very difficult to identify both of them accurately. That may be the reason why the values of some of the identified parameters are unreasonable.

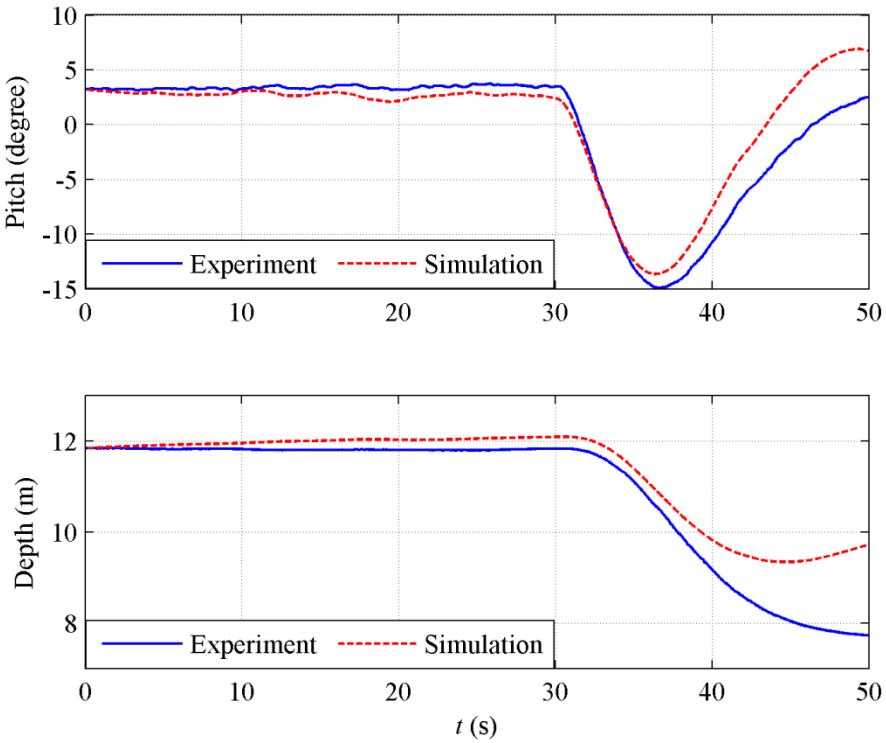

Figure 4.3 Pitch angle and depth comparison between experiment and simulation of all hydrodynamic coefficients identification for Starfish AUV

4.2.2 Identification of Hull Hydrodynamic Coefficients

Due to the coupling of the hydrodynamic coefficients, some of them cannot be identified simultaneously. And the control fins are streamlined and have quite simple shape, and their hydrodynamic coefficients can be estimated with empirical methods easily and even more accurately than the identification method. To avoid the problem of coefficient coupling, we assume the hydrodynamic coefficients of the control fins as known parameter and focus on the identification of the hydrodynamic coefficients of the hull, which are affected seriously by the non streamlined appendages. Then the hydrodynamic parameter vector to be identified can be simplified to the following form.

$$\boldsymbol{\theta} = \left[\left(C_{D_0}, C_{L_\alpha}, C_{L_q}, C_{m_\alpha}, C_{m_q} \right)_{hull} \right]^T \tag{4.26}$$

The identification results are shown in the second row of Table 4.1. The bold Italic numbers of this row are the corresponding empirical estimated hydrodynamic coefficients. Figure 4.4 and Figure 4.5 show the comparison between the simulation results and experiment results at the same control command.

As can be seen, the simulation is in better agreement with the experiment than the identification results for all hydrodynamic coefficients. And all the values of the identified coefficients are reasonable. But only the value of the identified lift coefficient is close to the empirical value. The value of the identified zero lift drag coefficient of hull is about 6 times bigger than the empirical value. This is because the Starfish is equipped with a DVL module and a wireless antenna tower. Both of them are not streamlined, and the total frontal area of them is even bigger than the section area of the main body of the AUV. They are the main source of the drag force. Non-streamlined appendages on the hull not only increase the drag force of the vehicle, but also have serious impact on the values of other hydrodynamic coefficients of the hull. For the Starfish, the identification method is the better choice of obtaining the values of the hydrodynamic coefficients of the hull than the pure empirical methods.

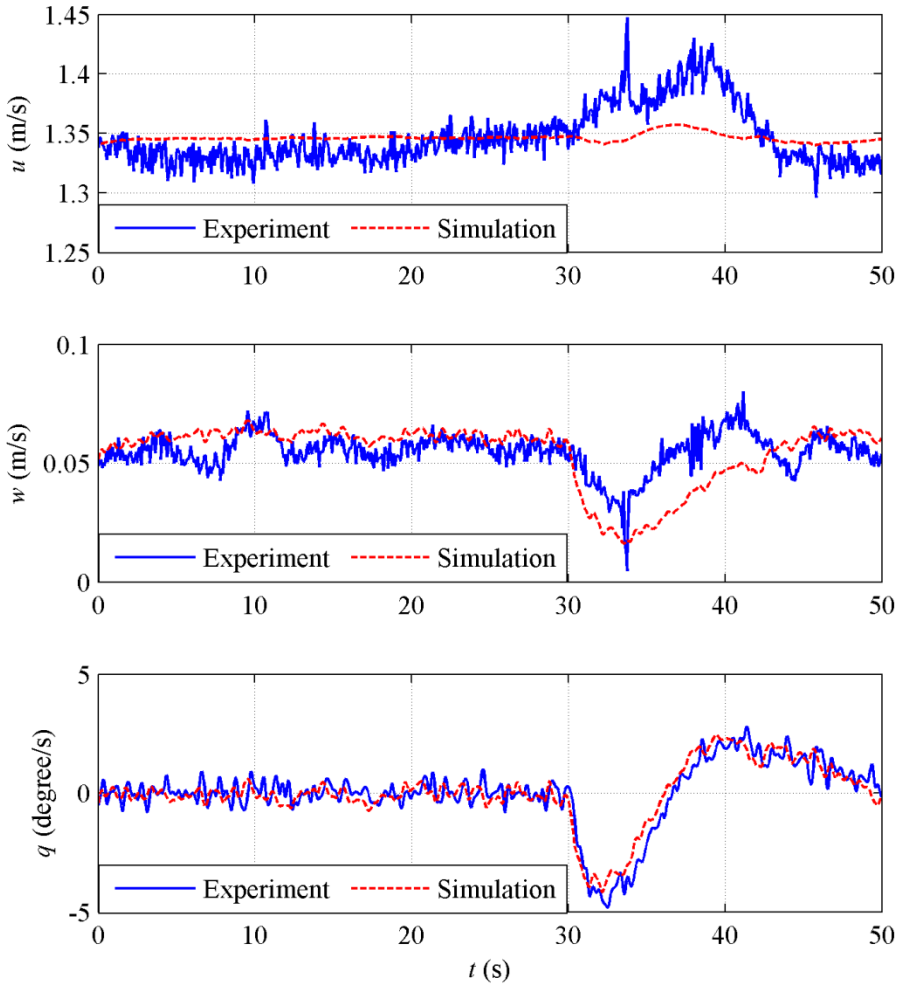

Figure 4.4 Outputs comparison between experiment and simulation of hull hydrodynamic coefficients identification for Starfish AUV

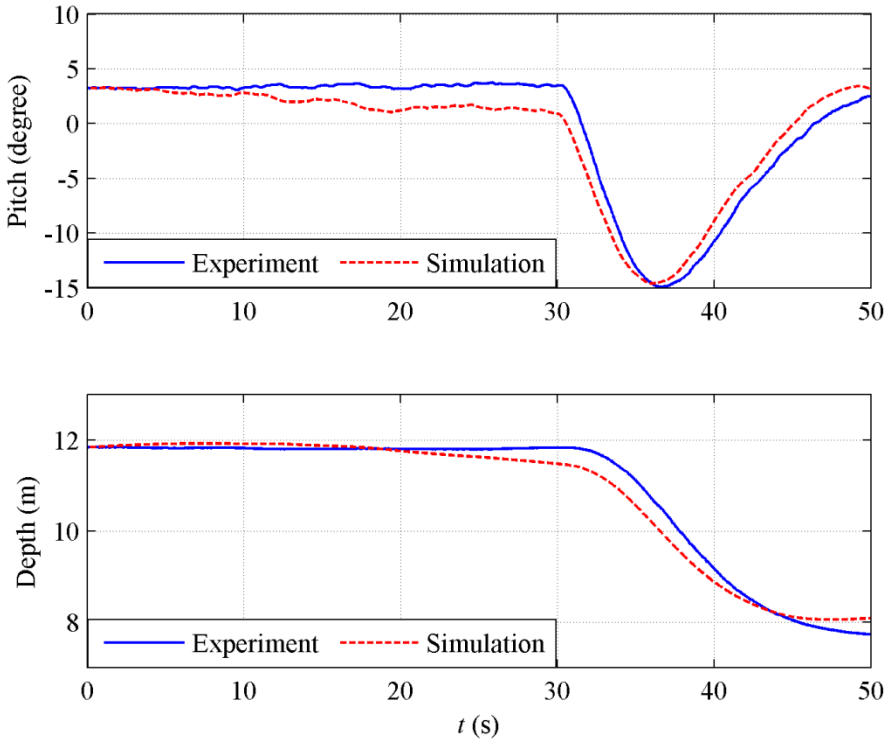

Figure 4.5 Pitch angle and depth comparison between experiment and simulation of hull hydrodynamic coefficients identification for Starfish AUV

4.3 Hydrodynamic Coefficients Identification for the Lancelet

Open loop free swimming trials are carried out to explore the Lancelet's dynamic characteristics. A turning process in horizontal plane is selected for the hydrodynamic coefficients identification of a three jet drive Lancelet. In this process the control inputs are the thruster forces from these three jet drives as shown in Figure 4.6. This micro AUV is finless, which indicates that the hydrodynamic coefficients of the hull are the only damping parameters that need to be identified. The hydrodynamic coefficients vector and the output vector can be simplified to the following form.

$$\boldsymbol{\theta} = \left[C_{D_0}, C_{L_\alpha}, C_{L_q}, C_{m_\alpha}, C_{m_q} \right]^T \tag{4.27}$$

$$\boldsymbol{y} = \left[u, v, r \right]^T \tag{4.28}$$

Table 4.2 Lancelet micro AUV hydrodynamic coefficients

	C_{D_0}	C_{L_α}	C_{L_q}	C_{m_α}	C_{m_q}
MLE identified	0.26	0.73	0.37	-10.28	0.12
Empirical estimated	***0.21***	***1.71***	***0.29***	***4.16***	***-0.37***

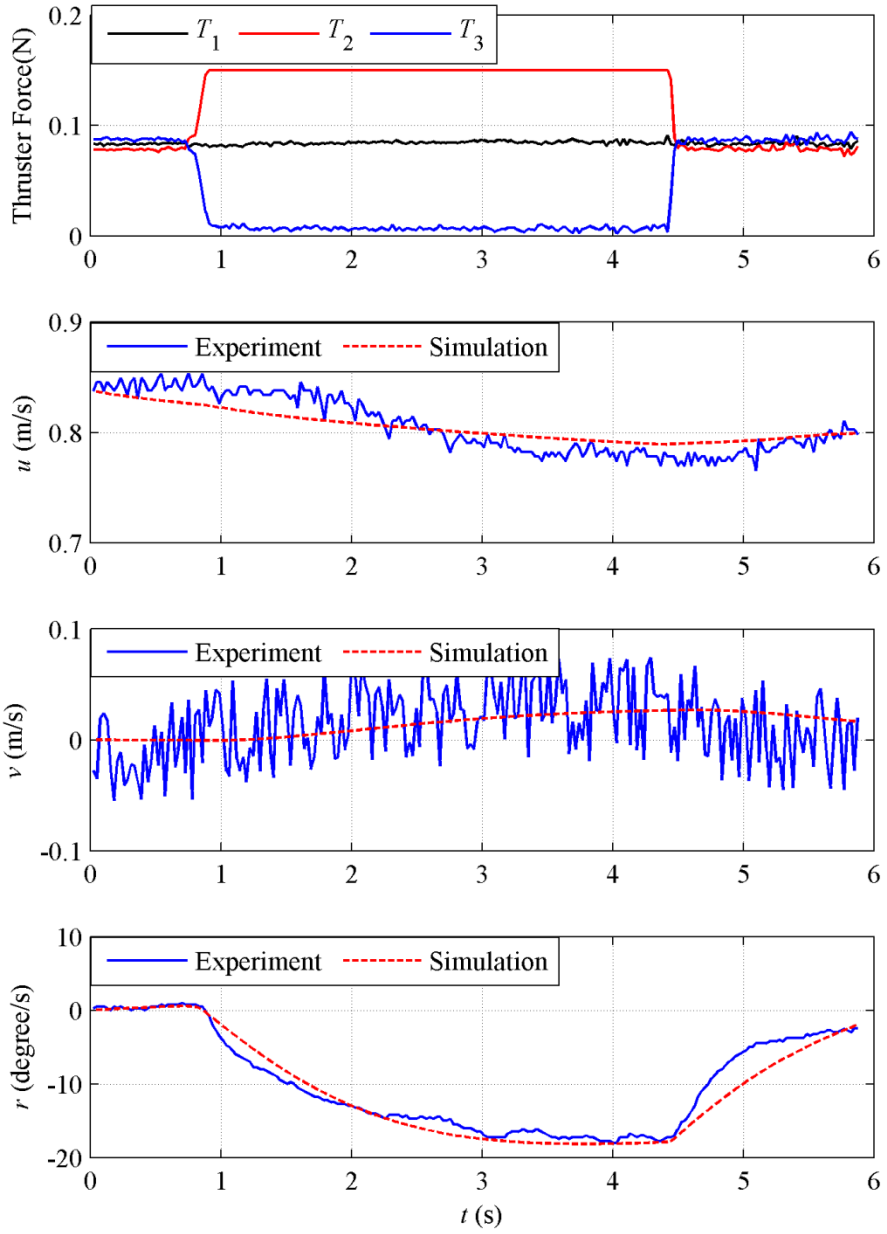

Figure 4.6 Control inputs and system outputs comparison between experiment and simulation of hydrodynamic coefficients identification for the four jet drive Lancelet

The identification results are list in the first row of Table 4.2. And the empirical estimated hydrodynamic coefficients of the hull are listed in the second row of the table in bold Italic font. It can be seen from the table that the values of the identified drag and lift coefficients are close to the empirical values, but the values of the identified moment coefficients are far from the empirical values even with different signs. This is due to the fact that the hull

of the Lancelet has a streamlined shape, but the propulsion system is not perfectly streamlined which may introduce uncertainty to the damping characteristics of the whole vehicle, especially to the position of the pressure center which will affect the moment related coefficients seriously. Figure 4.6 also shows the comparison between the simulation results and experiment results at the same control command. As can be seen, the simulation results are in good agreement with the experiment results.

4.4 Least Square Method for Hydrodynamic Derivatives Identification

4.4.1 Introduction to Least Square Method

For a dynamic model parameterized by unknown parameters $\boldsymbol{\theta} \in R^n$ as follows,

$$y(i) = \boldsymbol{H}(i)\boldsymbol{\theta} \tag{4.29}$$

where $y(i) \in R^m$ is the primary output vector, $\boldsymbol{H}(i)$ is the matrix relating the system parameters to output, and the parameter vector $\boldsymbol{\theta}$ is ideally constant. The objective the least square (LS) method is to estimate the parameters $\boldsymbol{\theta}$, which are never exactly known, so that the differences between the actual outputs and their estimated values are minimized[103-105]. This difference is called equation error and is given by,

$$e(i) = y(i) - \boldsymbol{H}(i)\hat{\boldsymbol{\theta}} \tag{4.30}$$

where $\hat{\boldsymbol{\theta}}$ is the estimate of $\boldsymbol{\theta}$. To minimize the error, the scalar positive squared error measure is defined as,

$$J = \frac{1}{2}\sum_{i=1}^{N} e^2(i) \tag{4.31}$$

and minimized by,

$$\frac{dJ}{d\hat{\theta}} = -\sum_{i=1}^{N} \boldsymbol{H}^T(i)e(i) = 0 \tag{4.32}$$

where N is the number of the sampled output data. Substituting equation (4.30) into (4.31)yields,

$$\sum_{i=1}^{N} \boldsymbol{H}^T(i)\, y(i) = \sum_{i=1}^{N} \boldsymbol{H}^T(i)\, \boldsymbol{H}(i)\, \hat{\boldsymbol{\theta}} \tag{4.33}$$

Writing the equations in matrix form and solving for the parameter vector gives,

$$\hat{\boldsymbol{\theta}} = \left[\mathbf{H}^T\mathbf{H}\right]^{-1}\mathbf{H}^T\boldsymbol{y} \tag{4.34}$$

where $\mathbf{H} = \begin{bmatrix} \boldsymbol{H}(1) \\ \boldsymbol{H}(2) \\ \vdots \\ \boldsymbol{H}(N) \end{bmatrix}$, $\boldsymbol{y} = \begin{bmatrix} y(1) \\ y(2) \\ \vdots \\ y(N) \end{bmatrix}$.

4.4.2 Hydrodynamic Derivatives Identification with Vertical Plane Motion

For vertical plane motion, the dynamic equations of the AUV with port-starboard and bottom-up symmetry are as follows,

$$\begin{cases} m\left(\dot{u} - wq\right) - X_{\dot{u}}\dot{u} + Z_{\dot{w}}wq + Z_{\dot{q}}q^2 - X_T = X_D \\ m\left(\dot{w} + uq\right) - Z_{\dot{w}}\dot{w} - Z_{\dot{q}}\dot{q} - X_{\dot{u}}uq - Z_T = Z_D \\ I_y\dot{q} - M_{\dot{w}}\dot{w} - M_{\dot{q}}\dot{q} - Z_{\dot{w}}wu - Z_{\dot{q}}qu + X_{\dot{u}}uw - M_T = M_D \end{cases} \tag{4.35}$$

where I_y is moments of inertia relative to the axis of y_b in the body-fixed frame. The index '*D*' denotes hydrodynamic damping and '*T*' denotes thrusters. It is assumed that all the parameters ($m, I_y, X_{\dot{u}}, Z_{\dot{w}}, Z_{\dot{q}}, M_{\dot{w}}, M_{\dot{q}}$) and variables ($u, w, q, \dot{u}, \dot{w}, \dot{q}$) on the left side of the above equation are known, and the thruster forces (X_T, Z_T, M_T) are known too. As a result, X_D, Z_D and M_D can be calculated. And the hydrodynamic damping forces and moment can be written as the function of the hydrodynamic derivatives as follows.

$$\begin{cases} X_D = X_{uu}u^2 + X_{ww}w^2 + X_{qq}q^2 + X_{wq}wq + X_{\delta_H\delta_H}\delta_H^2 \\ Z_D = Z_w w + Z_q q + Z_{w|w|}w|w| + Z_{q|q|}q|q| + Z_{w|q|}w|q| + Z_{\delta_H}\delta_H + Z_{|q|\delta_H}|q|\delta_H \\ M_D = M_w w + M_q q + M_{w|w|}w|w| + M_{q|q|}q|q| + M_{|w|q}|w|q + M_{\delta_H}\delta_H + M_{|q|\delta_H}|q|\delta_H \end{cases} \tag{4.36}$$

For one component X_D,

$$X_D = X_{uu}u^2 + X_{ww}w^2 + X_{qq}q^2 + X_{wq}wq + X_{\delta_H\delta_H}\delta_H^2 \tag{4.37}$$

If an uncoupled experiment is run taking N samples, (4.37)expands to N rows as follows.

$$\underbrace{\begin{bmatrix} X_D(1) \\ X_D(2) \\ \vdots \\ X_D(N) \end{bmatrix}}_{\boldsymbol{y}} = \underbrace{\begin{bmatrix} u^2(1) & w^2(1) & q^2(1) & w(1)q(1) & \delta_H^2(1) \\ u^2(2) & w^2(2) & q^2(2) & w(2)q(2) & \delta_H^2(2) \\ \vdots & \vdots & \vdots & \vdots & \vdots \\ u^2(N) & w^2(N) & q^2(N) & w(N)q(N) & \delta_H^2(N) \end{bmatrix}}_{\mathbf{H}} \underbrace{\begin{bmatrix} X_{uu} \\ X_{ww} \\ X_{qq} \\ X_{wq} \\ X_{\delta_H\delta_H} \end{bmatrix}}_{\boldsymbol{\theta}} \quad (4.38)$$

Hence, an equation linear in the vector of unknowns is obtained. Then $\boldsymbol{\theta}$ can be estimated by(4.34). For Z_D and M_D, similar methods can be adopted to estimate the hydrodynamic derivatives.

4.4.3 Hydrodynamic Derivatives Identification for Starfish AUV

We adopt the same surfacing process in vertical plane described in section 4.2 for the hydrodynamic derivatives identification of Starfish AUV, and the identification results are shown in the first row of Table 4.3. The hydrodynamic derivatives calculated from the hydrodynamic coefficients estimated by combining the empirical method and the MLE method discussed in subsection 4.2.2 are listed in the second row of Table 4.3. The outputs from the experiment and the simulation with the identified hydrodynamic derivatives are compared in Figure 4.7. And the comparisons between the experiment and the simulation of the pitch angle and the depth are shown in Figure 4.8.

As can be seen, the simulation results from the dynamic model with the hydrodynamic derivatives estimated by combining the MLE method with the empirical method are in better agreement with the experiment results than that of the LS method. This indicates that identifying the hydrodynamic coefficients of hull with MLE method and estimating the hydrodynamic coefficients of the fins with empirical method and then calculate the hydrodynamic derivatives from these hydrodynamic coefficients is a better way of obtain the hydrodynamic derivatives of the torpedo shaped AUVs than the direct LS identification methods. And the empirical methods can be used to analyze the reasonability of the value of some of these hydrodynamic

coefficients. As a result, the combination of empirical and identification methods for estimation of the hydrodynamic parameters could provide a more reliable and more accurate dynamic model for both simulation and controller design of torpedo shaped AUVs.

Table 4.3 Hydrodynamic derivatives identification results

X_{uu}	X_{ww}	X_{qq}	X_{wq}	$X_{\delta H\delta H}$	Z_w	Z_q	$Z_{w\|w\|}$	$Z_{q\|q\|}$	$Z_{w\|q\|}$	$Z_{\delta H}$	$Z_{\|q\|\delta H}$	M_w	M_q	$M_{w\|w\|}$	$M_{q\|q\|}$	$M_{w\|q\|}$	$M_{\delta H}$	$M_{\|q\|\delta H}$
-20.1	-212	389	139	-16.8	-62.6	-110	465	-332	-269	-0.766	-570	-127	-41	66.9	373	20.1	-14.3	232
-20.3	33.4	36.1	240	-57	-167	-310	-10	8.35	18.3	-136	24.7	-233	-245	-9.16	7.62	-16.7	-124	22.5

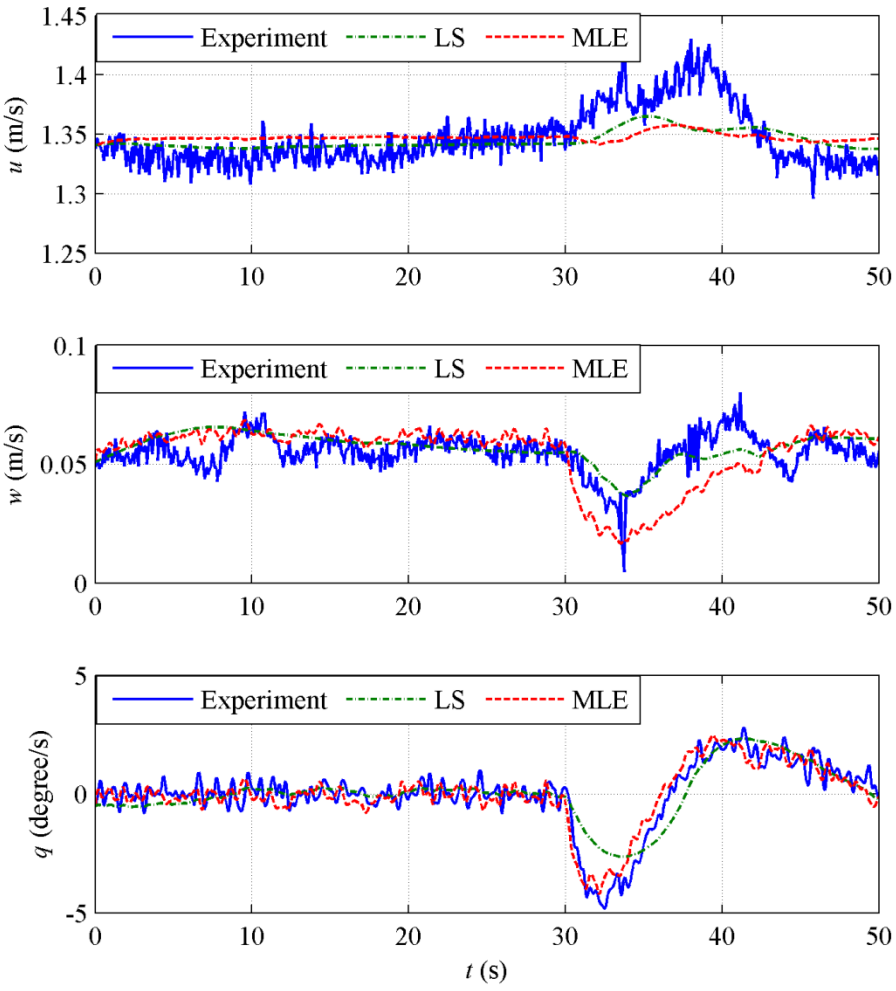

Figure 4.7 Outputs comparison of identification for hydrodynamic derivatives

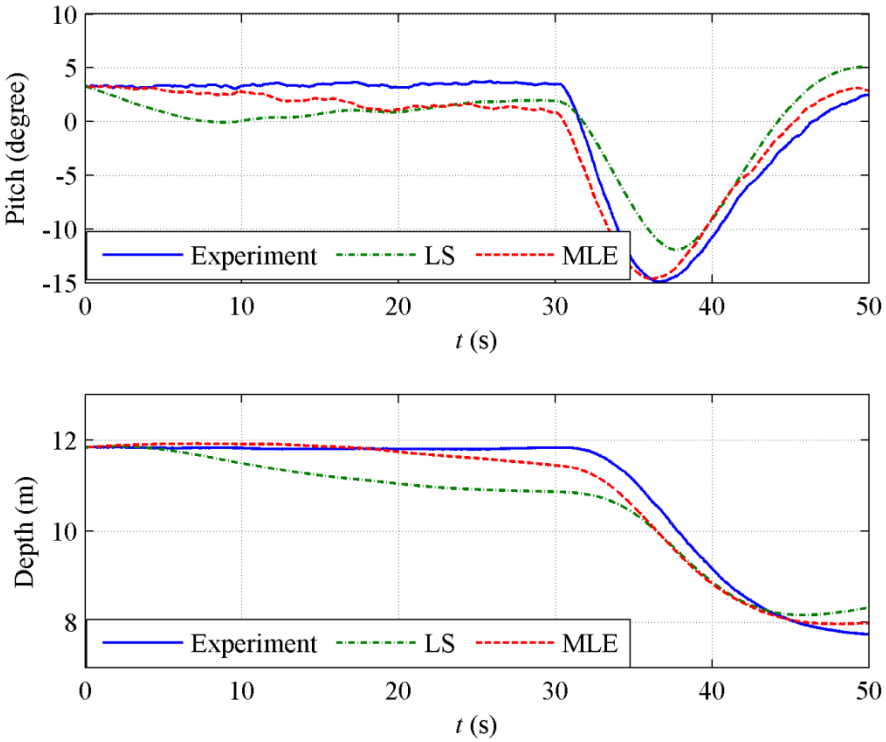

Figure 4.8 Pitch angle and the depth comparison of identification for hydrodynamic derivatives

4.5 Summary

In this chapter, the MLE method is adopted to identify the hydrodynamic coefficients of the Starfish AUV and the three jet drive Lancelet micro AUV according to the damping force model based on hydrodynamic coefficients established in Chapter 2. The Starfish AUV has four streamlined control fins which include a pair of rudders and a pair of elevators. First we try to identify all the hydrodynamic coefficients of the hull and the control fin at the same time. Due to the coupling of the hydrodynamic coefficients, some of the identification results are not reasonable compared with theoretical analysis. For the control fins are streamlined and have quite simple shape, their hydrodynamic coefficients can be estimated with empirical methods to avoid the problem of hydrodynamic coefficient coupling. And all the uncertainties of hydrodynamic damping of the AUV are concentrated on the hull. Then the hydrodynamic coefficients of the hull are identified with the output error method. It is concluded from the identification results that combining the empirical method and the identification method together is a better way of obtaining the hydrodynamic coefficients of an AUV. This technique is

particularly suitable for the AUV with non-streamlined appendages on the hull or the hull of which is not perfectly streamlined, but the control fins of which are streamlined. For the finless micro AUV Lancelet, the hydrodynamic coefficients of the whole vehicle can be identified directly. Then the hydrodynamic derivatives are identified by the LS method according to the damping force model based hydrodynamic derivatives stated in Chapter 2. It is concluded from the identification results that identifying the hydrodynamic coefficients of hull with MLE method and estimating the hydrodynamic coefficients of the fins with empirical method and then calculate the hydrodynamic derivatives from these hydrodynamic coefficients is a better way of obtain the hydrodynamic derivatives of the torpedo shaped AUVs than the direct LS identification methods, and could provide a more accurate dynamic model for the controller design.

Chapter 5 Modular Dynamic Modeling of Micro Autonomous Underwater Vehicle Lancelet

The modular designed torpedo shaped AUV usually consists of a nose section, zero or more mid-bodies, and a tail section[48, 50, 68]. For an AUV reconfigured with modular sections, rebuilding the dynamic model will be quite an effort and time consuming job, especially when some of the hydrodynamic parameters can only be obtained accurately by test based methods. In this chapter we will disscuss the problem for rebuilding the dynamic model of a modular designed AUV from modular section parameters to avoid the field tests and parameter identification processes for each newly reconfigured AUV.

5.1 Concept of Modular Modeling

Based on the dynamic model of the AUV expressed by equations (2.6) and (2.10) from Chapter 2, the problem of modular dynamic modeling can be broken down into three sub-tasks: the modularization of inertial property of the AUV, the modularization of the restoring forces, and the modularization of the hydrodynamic characteristics.

The inertial property includes the mass, the moment of inertia and the center of mass with respect to the center of buoyancy of the AUV, which is determined by the mass distribution of AUV and can be calculated directly from the inertial properties of the modular sections. The restoring forces are due to the gravity and buoyancy of the AUV, which can be calculated from the gravity and buoyancy of the modular sections with coordinates transformations.

The AUV hydrodynamic characteristics include the added mass and the hydrodynamic damping. The added mass of an torpedo shaped AUV reconfigured with modular sections can be calculated with empirical methods, if and only if the geometric parameters of the whole vehicle are known[72]. The hydrodynamic damping of the AUV quantified by hydrodynamic coefficients is the main source of the uncertainty of the dynamic model. The hydrodynamic damping of the torpedo shaped AUV is mainly from the control

fins and the hull. The fins are usually streamlined, and their hydrodynamic coefficients can be empirically calculated or experimentally tested easily and separately. By ignoring the interference between the fins and the hull, the hydrodynamic damping due to these fins can be calculated readily. Consequently the problem of modular modeling is specified on the modularization of the hydrodynamic coefficients of the hull, for some of the hydrodynamic coefficients of the hull with non-streamlined appendages can only be obtained accurately with test based methods. The modularization of the hydrodynamic coefficients of the hull is key problem for modular dynamic modeling, which will be discussed in details in the next subsections.

5.2 Hydrodynamic Coefficients in Normal Force Axis System

Usually the hydrodynamic damping force of the hull F is decomposed into drag D and lift L in the lift axis system, with the hydrodynamic coefficients in a simplified form as shown in equations (2.39) which do not satisfy the superposition property. The damping force F can be decomposed into normal force N and axis force X in the normal force axis system, shown in Figure 5.1, where α is the attack angle and V_∞ is the relative fluid velocity.

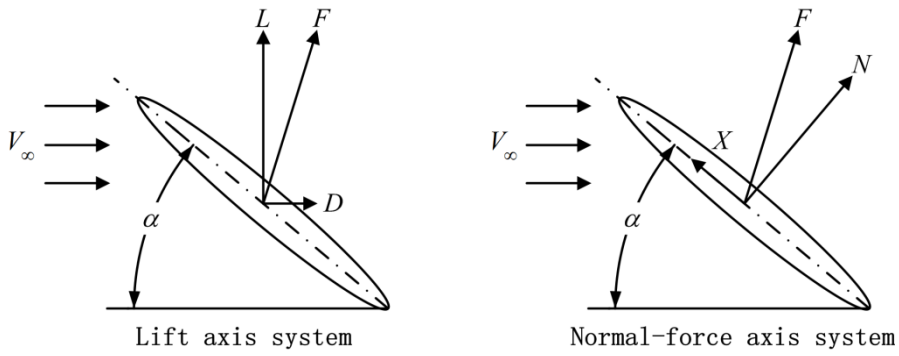

Figure 5.1 Lift axis system and the normal-force axis system

The corresponding hydrodynamic coefficients are transformed from the lift axis system into the normal-force axis system, where they can be estimated from the parameters of modular sections by the DATCOM method[74]. The equations relating the lift and drag coefficients to the normal and chord force coefficients are as follows[74].

$$\begin{cases} C_N = C_L \cos\alpha + C_D \sin\alpha \\ C_X = -C_D \cos\alpha + C_L \sin\alpha \end{cases}, \begin{cases} C_L = C_N \cos\alpha + C_X \sin\alpha \\ C_D = C_N \sin\alpha - C_X \cos\alpha \end{cases} \tag{5.1}$$

For small attack angle $\cos\alpha \approx 1, \sin\alpha \approx \alpha$. By substituting (2.39)into(5.1) we will have the following approximate equations,

$$\begin{aligned} C_N &\approx C_L + C_D\alpha = C_{L_\alpha}\alpha + C_{D_0}\alpha + C_{L_\alpha}\alpha^3 + \frac{q}{U_0}C_{L_q} \approx \left(C_{L_\alpha} + C_{D_0}\right)\alpha + \frac{q}{U_0}C_{L_q} \\ C_X &\approx -C_D + C_L\alpha = -\left(C_{D_0} + C_{L_\alpha}\alpha^2\right) + C_{L_\alpha}\alpha^2 + \frac{q\alpha}{U_0}C_{L_q} \approx -C_{D_0} \end{aligned} \tag{5.2}$$

If we set $C_{N_\alpha} = C_{L_\alpha} + C_{D_0}$ and $C_{N_q} = C_{L_q}$, the hydrodynamic coefficients in normal-force axis system will be as follows

$$\begin{aligned} C_m &= C_{m_\alpha}\alpha + \frac{q}{V_\infty}C_{m_q} \\ C_N &= C_{N_\alpha}\alpha + \frac{q}{V_\infty}C_{N_q} \\ C_X &= -C_{D_0} \end{aligned} \tag{5.3}$$

Then the hydrodynamic forces and moments of the hull can be expressed in the lift axis system with C_{m_α} C_{m_q} C_{N_α} C_{N_q} and C_{D_0} as parameters, or equally in the normal-force axis system with C_{m_α} C_{m_q} C_{L_α} C_{L_q} and C_{D_0} as parameters.

5.3 Modularization of Hydrodynamic Coefficients of the Hull

The DATCOM method summarizes the results of Newtonian impact theory presented in[106]to calculate the aerodynamic characteristics of an arbitrary body of revolution. The DATCOM method is intended to design missiles very often formed by joining two or more cone frustums end to end, which is structurally similar to modular designed AUVs. The DATCOM method is focused on dividing the missile into simple shaped modular sections and estimating its aerodynamic characteristics by summing the data of these simple shaped sections together which is not practical for modular designed AUV with appendages on the hull. In this thesis, we borrow the idea of the DATCOM method but solve the problem with our proposed method.

5.3.1 Modularization of Normal Force Coefficients

The DATCOM method for estimating the normal-force curve slope of the body of revolution is about dividing the body into *m* segments, and summing the normal-force curve slope of each segment together to get the whole normal-force curve slope of the body as follows [74],

$$C_{N_\alpha} = \sum_{n=1}^{m} C_{N_\alpha}(n) \tag{5.4}$$

The normal-force pitching derivative has the same property.

$$C_{N_q} = \sum_{n=1}^{m} C_{N_q}(n) \tag{5.5}$$

5.3.2 Modularization of Moment Coefficients

The DATCOM method for estimating the moment curve slope of the body of revolution is similar to the method of estimating the normal-force curve slope, except the influence of the normal-force from the each segment[74]. The moment-curve slope can be estimated by,

$$C_{m_\alpha} = \sum_{n=1}^{m} C_{m_\alpha}(n) + \sum_{n=1}^{m} \frac{l_n}{d_B} C_{N_\alpha}(n) \tag{5.6}$$

where d_B is the maximum body diameter, and l_n is the distance from the front face of a given segment to the desired moment reference axis of the configuration, positive aft.

The moment pitching derivative has similar property as follows.

$$C_{m_q} = \sum_{n=1}^{m} C_{m_q}(n) + \sum_{n=1}^{m} -l_n C_{m_\alpha}(n) \tag{5.7}$$

5.3.3 Modularization of Drag Coefficient

The DATCOM method for estimating the zero-lift drag coefficient is by adding the pressure-drag coefficient of each segment to the skin-friction drag coefficient of the body[74] as,

$$C_{D_0} = C_{D_f} + \sum_{n=1}^{m} C_{D_p}(n) \tag{5.8}$$

C_{D_p} is the pressure-drag coefficient for individual segment. The body skin-friction drag coefficient can be estimated as follows,

$$C_{D_f} = 1.02 C_f \frac{S_S}{S_B} \tag{5.9}$$

According to the definition in Chapter 2, S_B is the maximum body section area of the AUV which is constant for the modular designed torpedo shaped AUV.

C_f is the turbulent skin-friction coefficient which changes very slightly with the total length of the AUV and can be treated as constant. S_S is the wetted area or surface area of the body excluding the base area, which can be calculated by the summing all the wetted area of the modular sections together. This implies that the body skin-friction drag coefficient satisfies superposition properties as well. Then the modularization of the zero lift drag coefficient can be written as,

$$C_{D_0} = \sum_{n=1}^{m} C_{D_0}(n) \tag{5.10}$$

5.4 Standard Reference Model Method

The modular hydrodynamic coefficients of each individual section can be obtained by wind-tunnel or tow-tank model tests which need complicated laboratory testing facilities[106]. We want to calculate the modular hydrodynamic coefficients from the modular equations assuming the hydrodynamic coefficients of the whole hull are known. By ignoring the distance related terms in the moment coefficients, the modular equations in the normal-force axis system are simplified as follows.

$$\begin{aligned} C_{N_\alpha} &= \sum_{n=1}^{m} C_{N_\alpha}(n), C_{N_q} = \sum_{n=1}^{m} C_{N_p}(n) \\ C_{m_\alpha} &= \sum_{n=1}^{m} C_{m_\alpha}(n), C_{m_q} = \sum_{n=1}^{m} C_{m_p}(n) \\ C_{D_0} &= \sum_{n=1}^{m} C_{D_0}(n) \end{aligned} \tag{5.11}$$

The AUV can be configured by two or more modular sections, but it cannot be configured by arbitrary modular sections. For example, the AUV must and can only have one nose section and one tail section. And the equations of (5.11) are dependent linear approximate equations. As a result, it is impossible to obtain all the values of the modular coefficients from their summations.

The standard reference model method is proposed to solve this problem, which means choosing a standard configuration of the modular designed AUV with its hydrodynamic coefficients known, and all the modular sections of the standard configuration are treated as reference modular sections. Any other

modular section will be substituted into this standard reference model accordingly, and the differences between the modular hydrodynamic coefficients of the new modular section and that of the reference modular section will be calculated. Then the hydrodynamic coefficients of the AUV configured with these modular sections can be estimated by summing the offset values of these modular sections to the standard reference model.

For middle sections of the torpedo shaped AUV with a constant diameter, a virtual middle section with the length of zero can be adopted in the standard reference model. The modular hydrodynamic coefficients of this virtual section are all zero. The real middle sections can be used to substitute the virtual modular section, and the offset values of these real middle sections from the virtual section will be the modular hydrodynamic coefficient of these real middle sections. The proposed standard reference model method can be used to both the mandatory modular sections and the optional modular sections with a unified form.

For simplicity, the normal-force curve slope is chosen to elaborate the standard reference model method for a modular designed AUV composed by three modular sections: the nose section *A*, the middle section *B* and the tail section *C*. The hull configured by module A_1, B_1 and C_1 is chosen as the standard reference model. The offset values of the modular normal-force curve slope from that of the reference modular sections are defined as follows.

$$\begin{aligned}
\overline{C}_{N_\alpha}\left(A_i\right) &= C_{N_\alpha}\left(A_i\right) - C_{N_\alpha}\left(A_1\right) \\
\overline{C}_{N_\alpha}\left(B_j\right) &= C_{N_\alpha}\left(B_j\right) - C_{N_\alpha}\left(B_1\right) \\
\overline{C}_{N_\alpha}\left(C_k\right) &= C_{N_\alpha}\left(C_k\right) - C_{N_\alpha}\left(C_1\right)
\end{aligned} \tag{5.12}$$

Then we will have

$$\overline{C}_{N_\alpha}\left(A_i\right) + \overline{C}_{N_\alpha}\left(B_j\right) + \overline{C}_{N_\alpha}\left(C_k\right) = C_{N_\alpha}\left(i, j, k\right) - C_{N_\alpha}\left(1,1,1\right). \tag{5.13}$$

From the definition it is concluded that,

$$\overline{C}_{N_\alpha}\left(A_1\right) = 0, \overline{C}_{N_\alpha}\left(B_1\right) = 0, \overline{C}_{N_\alpha}\left(C_1\right) = 0. \tag{5.14}$$

In order to calculate the values of the other unknown offsets, the following equations containing one unknown parameter are used.

$$\begin{aligned}
\bar{C}_{N_\alpha}(A_i) &= C_{N_\alpha}(i,1,1) - C_{N_\alpha}(1,1,1), (i>1) \\
\bar{C}_{N_\alpha}(B_j) &= C_{N_\alpha}(1,j,1) - C_{N_\alpha}(1,1,1), (j>1) \\
\bar{C}_{N_\alpha}(C_k) &= C_{N_\alpha}(1,1,k) - C_{N_\alpha}(1,1,1), (k>1)
\end{aligned} \tag{5.15}$$

After all the offsets from the reference modular sections are obtained, we can use these offset values and the normal-force curve slope of the standard reference model to calculate the normal-force curve slope of any configuration from these modules by,

$$C_{N_\alpha}(i,j,k) = \bar{C}_{N_\alpha}(A_i) + \bar{C}_{N_\alpha}(B_j) + \bar{C}_{N_\alpha}(C_k) + C_{N_\alpha}(1,1,1) \tag{5.16}$$

The proposed method can be applied to all the five hydrodynamic coefficients in the normal-force axis system.

5.5 Modularization of Hydrodynamic Coefficients of Myring Hull

The Myring hull is adopted to verify the proposed standard reference model method with the theoretical values of the hydrodynamic coefficients of the hull calculated by empirical methods, for this hull contour is streamed and its hydrodynamic coefficients can be obtained with empirical methods accurately.

The Myring hull can be divided into two or more modular sections and at any position in the design of AUV. For simplicity, in this thesis we choose the three sections in the definition of the Myring hull in Figure 3.1 as three modular sections: the nose section *A*, the middle section *B* and the tail section *C*. We defined three modules of section *A*, *B* and *C* respectively as in Table 5.1 and Figure 5.2 to Figure 5.4.The hull configured by module A_1, B_1 and C_1 is chosen as the standard reference model.

Table 5.1 Modular section geometric parameter definition

		1	2	3
Section *A*	*a* (m)	0.191	0.248	0.135
	a_{offset} (m)	0.0165	0.0165	0.0165
	n (n/a)	2	2	2
Section *B*	*b* (m)	0.654	0.850	0.458
	d (m)	0.191	0.191	0.191
Section *C*	*c* (m)	0.541	0.703	0.379
	c_{offset} (m)	0.0368	0.0368	0.0368
	θ (rad)	0.436	0.436	0.436

Figure 5.2 Modular section A_1 B_1 and C_1 of Myring hull

Figure 5.3 Modular section A_2 B_2 and C_2 of Myring hull

Figure 5.4 Modular section A_3 B_3 and C_3 of Myring hull

Table 5.2 Offset values of normal-force curve slope

i,j,k	$\bar{C}_{N_\alpha}(A_i)$	$\bar{C}_{N_\alpha}(B_j)$	$\bar{C}_{N_\alpha}(C_k)$
2	0.0354	0.1252	0.1035
3	-0.0353	-0.1252	0.1117

Table 5.3 Offset values of normal-force pitching coefficient

i,j,k	$\bar{C}_{N_q}(A_i)$	$\bar{C}_{N_q}(B_j)$	$\bar{C}_{N_q}(C_k)$
2	0.0454	0.1943	0.1586
3	-0.0442	-0.1736	-0.0232

Table 5.4 Offset values of moment curve slope

i,j,k	$\bar{C}_{m_\alpha}(A_i)$	$\bar{C}_{m_\alpha}(B_j)$	$\bar{C}_{m_\alpha}(C_k)$
2	0.3625	0.9484	0.8095
3	-0.4937	-1.0003	-1.0477

Table 5.5 Offset values of moment pitching coefficient

i,j,k	$\bar{C}_{m_q}(A_i)$	$\bar{C}_{m_q}(B_j)$	$\bar{C}_{m_q}(C_k)$
2	-0.0068	-0.0223	-0.0183
3	0.0084	0.0203	0.0219

Table 5.6 Offsets of zero-lift coefficient from standard sections

i,j,k	$\bar{C}_{D_0}(A_i)$	$\bar{C}_{D_0}(B_j)$	$\bar{C}_{D_0}(C_k)$
2	-0.0028	-0.0082	-0.0069
3	0.0030	0.0107	0.0092

Table 5.7 Modularization of hydrodynamic coefficients of Myring hull

A_i	B_j	C_k	$C_{N\alpha}$	$(C_{N\alpha})_m$	C_{Nq}	$(C_{Nq})_m$	$C_{m\alpha}$	$(C_{m\alpha})_m$	C_{mq}	$(C_{mq})_m$	C_{D_0}	$(C_{D_0})_m$
1	***1***	***1***	**1.15**	**1.15**	**0.736**	**0.736**	**5.90**	**5.90**	**-0.082**	**-0.082**	**0.139**	**0.139**
2	***1***	***1***	**1.19**	**1.19**	**0.781**	**0.781**	**6.26**	**6.26**	**-0.089**	**-0.089**	**0.140**	**0.140**
3	***1***	***1***	**1.12**	**1.12**	**0.692**	**0.692**	**5.40**	**5.40**	**-0.074**	**-0.074**	**0.137**	**0.137**
1	***2***	***1***	**1.28**	**1.28**	**0.930**	**0.930**	**6.84**	**6.84**	**-0.105**	**-0.105**	**0.150**	**0.150**
2	***2***	***1***	1.31	1.31	0.980	0.975	7.23	7.21	-0.113	-0.111	0.152	0.151
3	***2***	***1***	1.24	1.24	0.881	0.886	6.30	6.35	-0.094	-0.096	0.148	0.148
1	***3***	***1***	**1.03**	**1.03**	**0.562**	**0.562**	**4.90**	**4.90**	**-0.062**	**-0.062**	**0.130**	**0.130**
2	***3***	***1***	1.06	1.06	0.602	0.608	5.23	5.26	-0.068	-0.069	0.131	0.132
3	***3***	***1***	0.99	0.99	0.523	0.518	4.45	4.40	-0.055	-0.054	0.130	0.129
1	***1***	***2***	**1.25**	**1.25**	**0.894**	**0.894**	**6.70**	**6.70**	**-0.101**	**-0.101**	**0.148**	**0.148**
2	***1***	***2***	1.29	1.29	0.944	0.940	7.09	7.07	-0.108	-0.107	0.150	0.149
3	***1***	***2***	1.22	1.22	0.846	0.850	6.17	6.21	-0.091	-0.092	0.146	0.146
1	***2***	***2***	1.38	1.38	1.104	1.089	7.61	7.65	-0.124	-0.123	0.160	0.159
2	***2***	***2***	1.41	1.41	1.157	1.134	8.02	8.02	-0.133	-0.130	0.162	0.160
3	***2***	***2***	1.34	1.34	1.052	1.044	7.02	7.16	-0.113	-0.115	0.157	0.157
1	***3***	***2***	1.13	1.13	0.704	0.721	5.75	5.70	-0.079	-0.080	0.137	0.139
2	***3***	***2***	1.16	1.16	0.748	0.766	6.11	6.07	-0.085	-0.087	0.139	0.141
3	***3***	***2***	1.09	1.09	0.660	0.677	5.26	5.21	-0.071	-0.072	0.136	0.138
1	***1***	***3***	**1.26**	**1.26**	**0.713**	**0.713**	**4.85**	**4.85**	**-0.060**	**-0.060**	**0.134**	**0.134**
2	***1***	***3***	1.31	1.30	0.763	0.758	5.16	5.21	-0.066	-0.067	0.135	0.136
3	***1***	***3***	1.22	1.23	0.664	0.668	4.42	4.35	-0.054	-0.052	0.134	0.132
1	***2***	***3***	1.41	1.39	0.928	0.907	5.67	5.80	-0.078	-0.083	0.143	0.145
2	***2***	***3***	1.46	1.42	0.984	0.952	6.00	6.16	-0.085	-0.089	0.145	0.147
3	***2***	***3***	1.37	1.35	0.874	0.863	5.20	5.30	-0.070	-0.074	0.141	0.143
1	***3***	***3***	1.11	1.14	0.523	0.539	3.95	3.85	-0.044	-0.040	0.130	0.125
2	***3***	***3***	1.15	1.17	0.567	0.584	4.24	4.21	-0.048	-0.047	0.128	0.127
3	***3***	***3***	1.07	1.10	0.481	0.495	3.57	3.35	-0.039	-0.032	0.132	0.124

The proposed method is applied to all the five hydrodynamic coefficients in the normal-force axis system. And it is required that the values of the hydrodynamic coefficients of seven different configurations including the standard reference model and the configurations indicated in equations (5.15) with i,j,k=2,3 are known in advance to calculate the offsets from the reference modular sections, as the bold rows in Table 5.7.

The offset values calculated by equations (5.15) are listed in Table 5.2 to Table 5.6. The values of the hydrodynamic coefficients estimated with the proposed method are compared with their theoretical values in Table 5.7, where the ‘m’ outside the bracket means values estimated from the standard reference method. For the Myring hulls configured from the modular sections

defined in Table 5.1 the relative errors of the estimated values are less than 4% for the normal-force coefficients, less than 6% for the drag coefficient, and generally no more than 10% for the moment coefficients with only one exception of $C_{m_q}(3,3,3)$. The estimated values of the normal-force coefficients are more accurate than that of the moment coefficients, which is due to the fact that in order to make the standard reference model method practical for the moment hydrodynamic coefficients the distance related terms in equations (5.6) and (5.7) are ignored.

5.6 Modularization of Hydrodynamic Coefficients of the Lancelet

The hydrodynamic coefficients obtained from the MLE identification of the four jet drive Lancelet are used to verify the proposed standard reference model method too. The simplest modular designed AUV is constructed of two kind of mandatory modular sections: the nose section *A*, the tail section *B*. The minimum number of modular sections needed to verify the standard reference model method is four, including two nose sections and two tail secretions. So we built these four modular sections shown in Figure 5.5. They can be assembled to four different configurations. A_1B_1 is adopted as the standard reference model. A_1B_2 and A_2B_1 are used to calculate the offset values of section A_2 and B_2 from the reference section A_1 and B_1 respectively. A_2B_2 is used to verify the proposed modular dynamic modeling method.

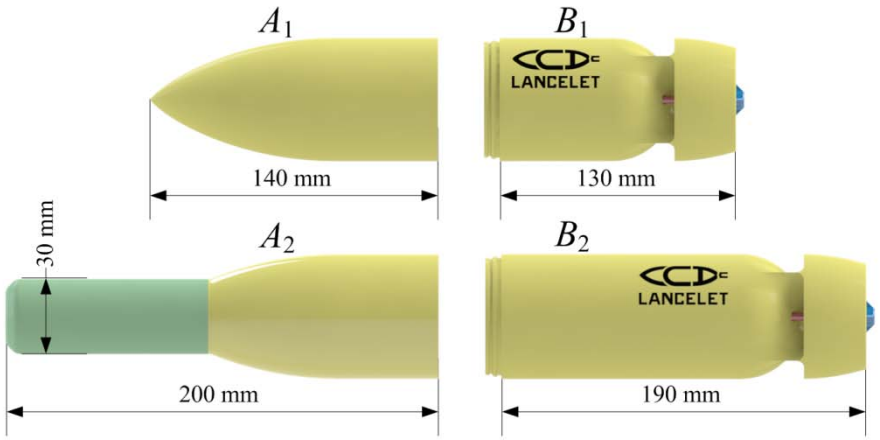

Figure 5.5 Modular sections of the Lancelet

The normal-force curve slope is chosen to elaborate the standard reference model method of the AUV constructed of two modular sections. And the other

four hydrodynamic coefficients in the normal-force axis system can be calculated with the same process. Based on the modular equation (5.11), the offset values of the modular normal-force curve slope from that of the reference modular sections can be calculated by

$$\begin{aligned} \overline{C}_{N_\alpha}(A_2) &= C_{N_\alpha}(2,1) - C_{N_\alpha}(1,1) \\ \overline{C}_{N_\alpha}(B_2) &= C_{N_\alpha}(1,2) - C_{N_\alpha}(1,1) \end{aligned} \tag{5.17}$$

After these two offset values from the reference modular sections are obtained, the normal-force curve slope of the Lancelet configured by modular section A_2 and B_2 can be calculated as follows.

$$C_{N_\alpha}(2,2) = \overline{C}_{N_\alpha}(A_2) + \overline{C}_{N_\alpha}(B_2) + C_{N_\alpha}(1,1) \tag{5.18}$$

Open loop field tests of diving process in vertical plane are adopted to identify the hydrodynamic coefficients in the lift axis system with the MLE method discussed in the Chapter 4. Then, these coefficients are transferred to the normal-force axis system and listed in Table 5.8. The identification results are also verified by simulation Figure 5.6 to Figure 5.9 show the output comparison between the simulation results of the dynamic model with the identified parameters and experiment results at the same control command. The outputs include the linear and angular velocities of the vehicle in the vertical plane which are the variables used for the MLE parameter identification of the diving process. As can be seen, the simulation results are all in good agreement with field test results.

Table 5.8 Values of indentified and predicated hydrodynamic coefficients

	C_{D_0}	C_{N_α}	C_{N_q}	C_{m_α}	C_{m_q}
A_1B_1	0.29	1.89	0.25	-7.99	-0.28
A_2B_1	0.47	1.93	0.41	-4.96	-0.38
A_1B_2	0.31	1.95	0.34	-11.27	-0.53
A_2B_2	0.51	1.78	0.44	-7.59	-0.69
$(A_2B_2)_m$	0.49	1.99	0.50	-8.24	-0.63

Table 5.9 Offset values of hydrodynamic coefficients from reference modular sections

	$\overline{C}_{D_0}$	$\overline{C}_{N_\alpha}$	$\overline{C}_{N_q}$	$\overline{C}_{m_\alpha}$	$\overline{C}_{m_q}$
A_2	0.18	0.04	0.16	3.03	-0.10
B_2	0.02	0.06	0.09	-3.28	-0.25

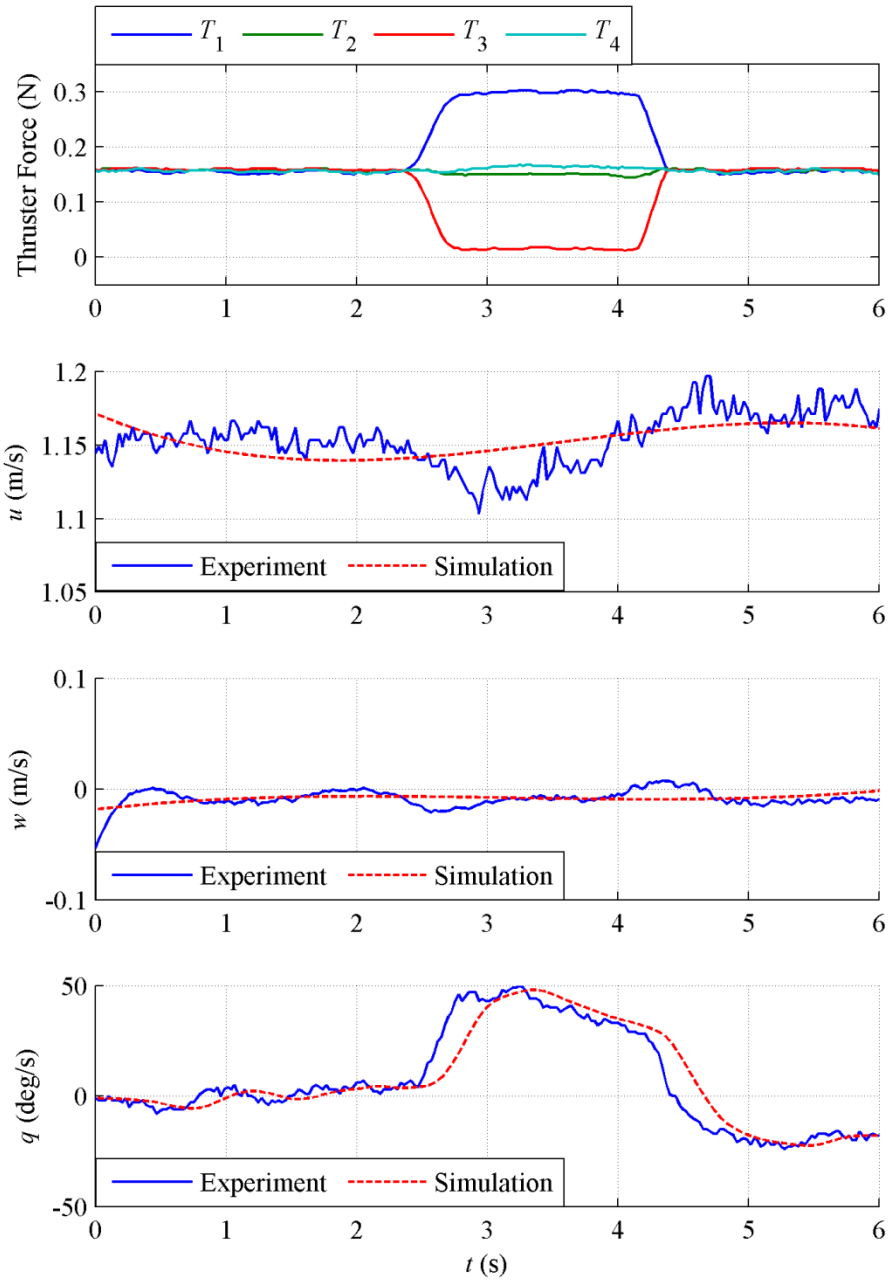

Figure 5.6 Control inputs and system outputs comparison between experiment and simulation of the configuration of A_1B_1

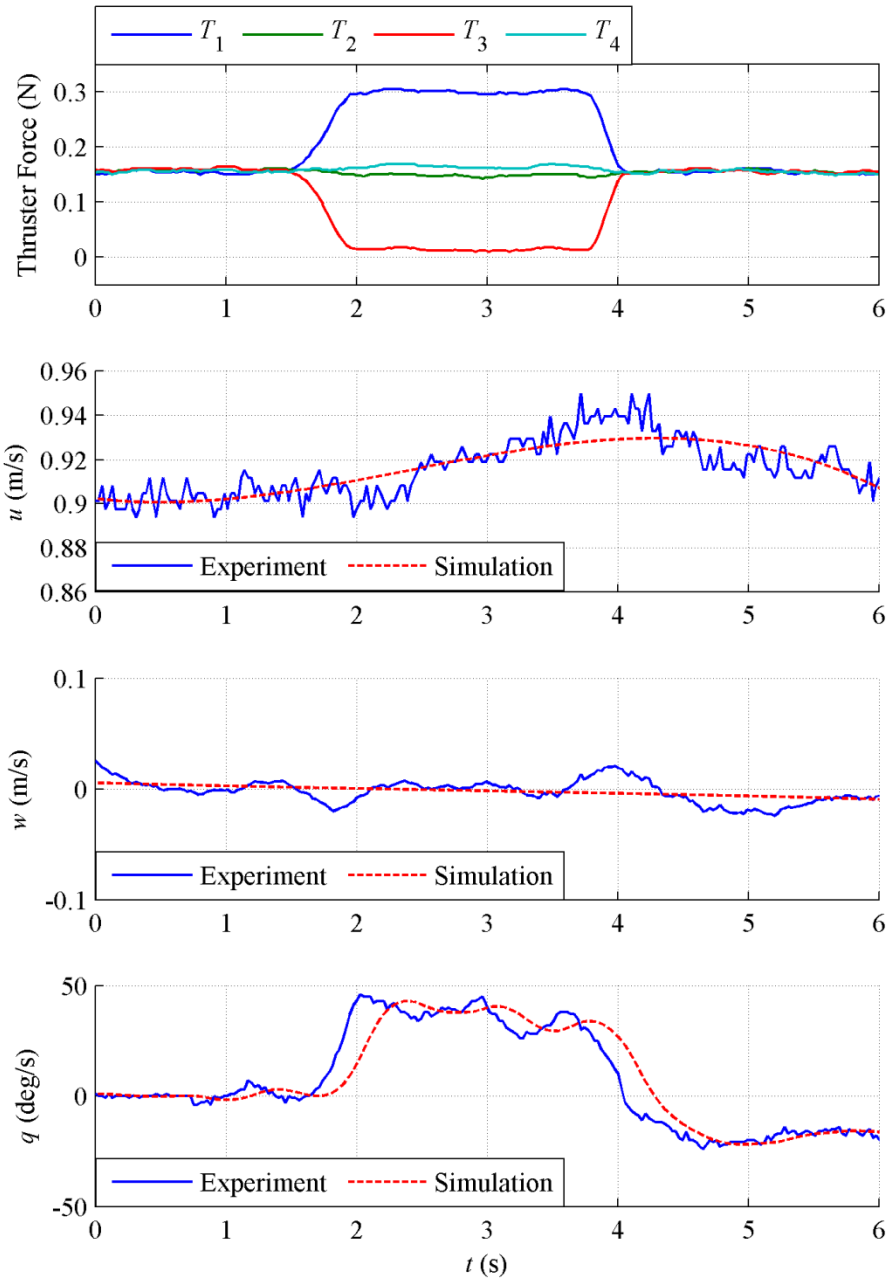

Figure 5.7 Control inputs and system outputs comparison between experiment and simulation of the configuration of A_2B_1

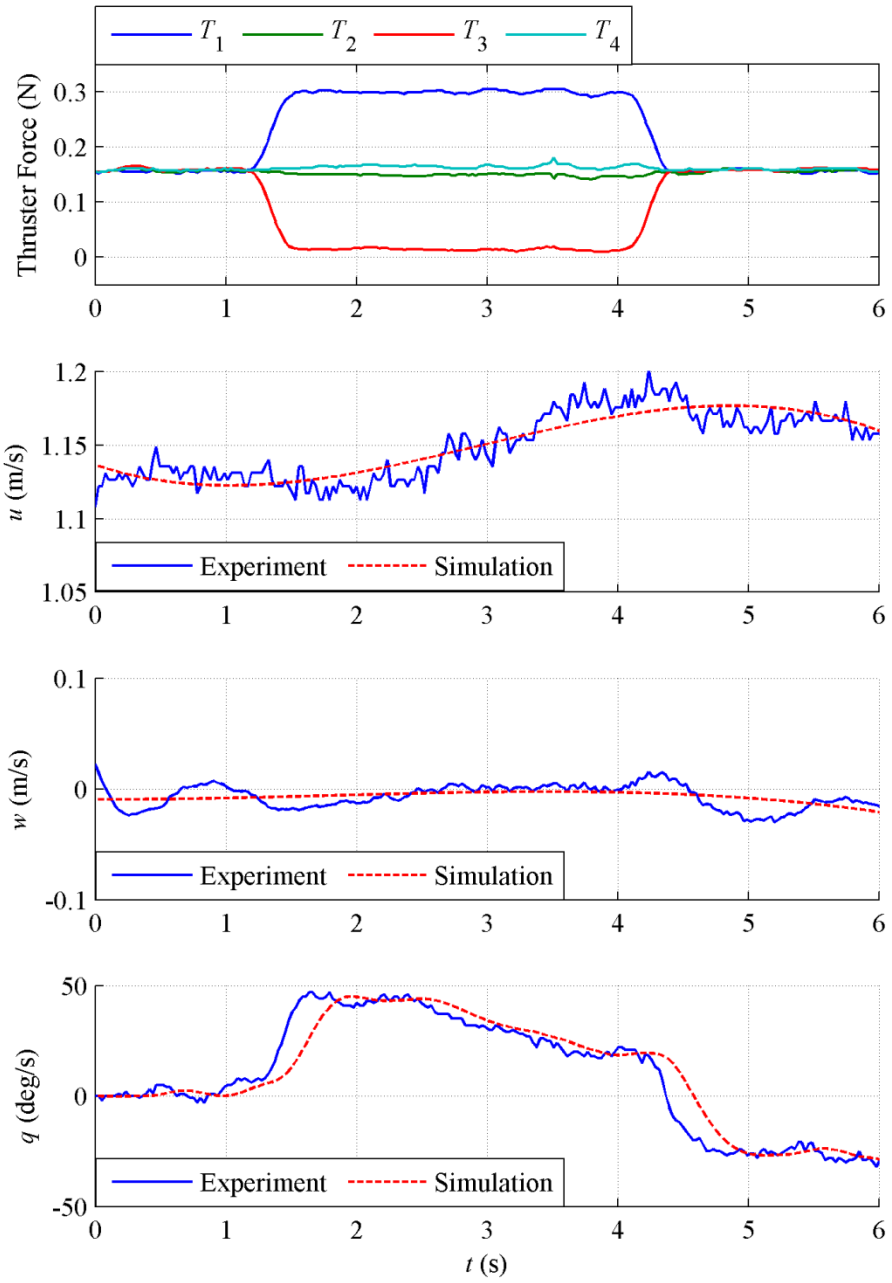

Figure 5.8 Control inputs and system outputs comparison between experiment and simulation of the configuration of A_1B_2

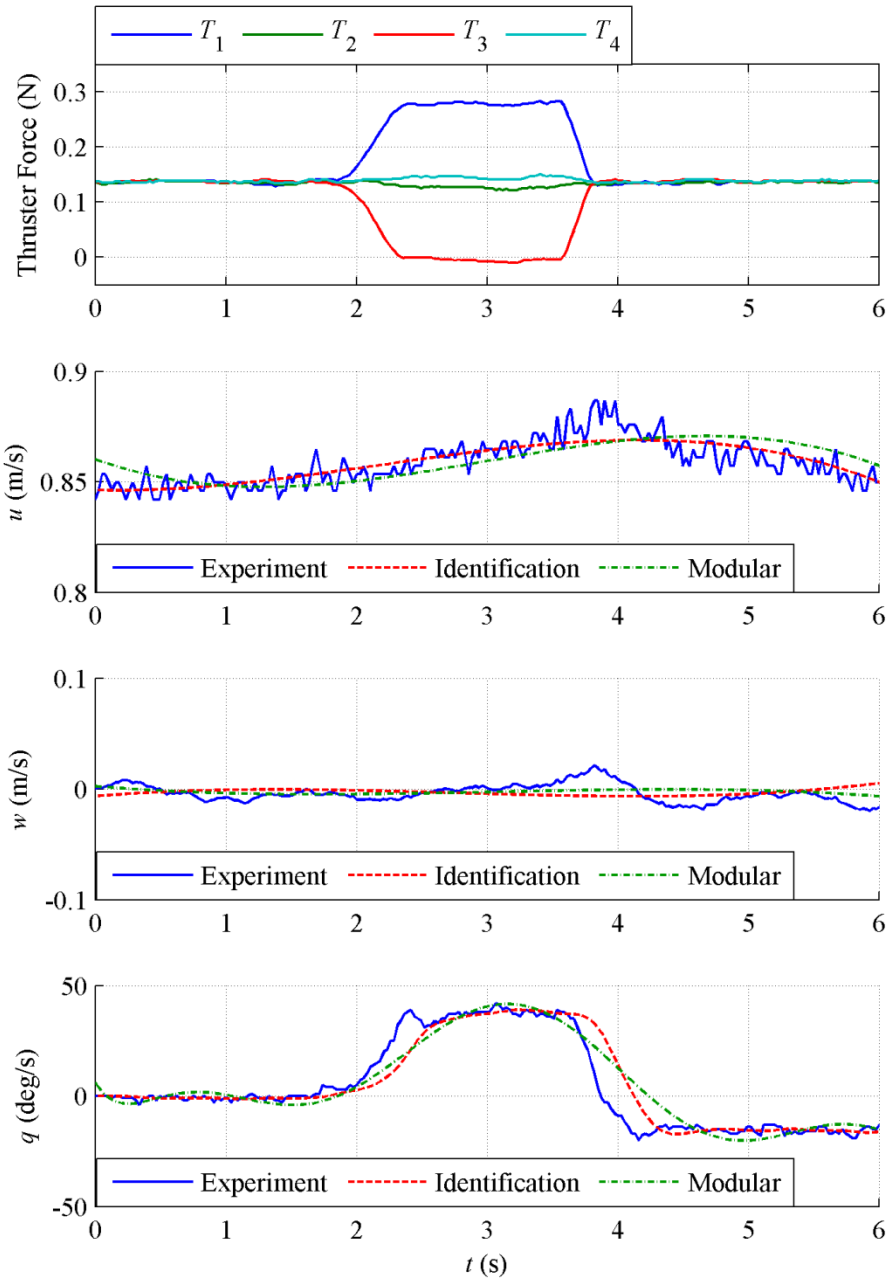

Figure 5.9 Control inputs and system outputs comparison between experiment and simulation of the configuration of A_2B_2

The offset values of the modular sections A_2 and B_2 calculated by equations (5.17) are listed in Table 5.9. The values of the hydrodynamic coefficients predicted for the configuration of A_2B_2 with the proposed method are list in the last row of Table 5.8, where the 'm' outside the bracket means values estimated with modular dynamic modeling method. The predicted values of the hydrodynamic coefficients is quite close to the identified values with the

relative error no more than 10%, which implies that the proposed the standard reference model method for modularization of the hydrodynamic coefficients are effective. And the error may due to the simplification of the modular equations, which ignored the distance related terms. The effectiveness of the modular dynamic modeling method is verified again by the simulation results shown in Figure 5.9, where the outputs of the dynamic model with the predicted parameters by the proposed method are compared with the identification results and experiment results at the same control command. It can be seen that the simulation results from the modular dynamic modeling method are in good agreement with both the identification results and the field test results.

5.7 Summary

In this chapter, the research is focused on the key problem for modular dynamic modeling of the torpedo shaped AUV, which is the modularization of the hydrodynamic coefficients of the hull. These coefficients are transformed from the lift axis system into the normal-force axis system, where they satisfy the superposition property and can be estimated from the parameters of the modular sections. The standard reference model method is proposed for the modularization of the hydrodynamic coefficients in the normal-force axis system. Then, the hydrodynamic coefficients of Myring hull estimated by empirical methods are adopted to verify the proposed standard reference model method. It is concluded from the results that theoretically the standard reference model method could give good estimation of the values of the hydrodynamic coefficients of the Myring hull by the offsets from reference modular sections in the normal-force axis system. And the MLE method is applied to identify the hydrodynamic coefficients of the four jet drive Lancelet configured by four different modular sections. The proposed standard reference model method is used to predicate the hydrodynamic coefficients, and the predicated results are compared with the identification results which shows that the proposed method works well.

Chapter 6 Conclusions and Future Works

6.1 Conclusions and Contributions

A torpedo shaped micro AUV named Lancelet is designed, constructed and tested in this research. The Lancelet is equipped with a novel finless multi-jet drive propulsion system. This propulsion mechanism is robust and compact and extremely suitable for torpedo shaped micro underwater vehicles, and can provide the Lancelet with high maneuverable capabilities such as turn in place and pitch in place. Fully capable prototypes with the designed multi-jet drive propulsion system have been built and tested. From the experiment results of open loop field tests, we have concluded that the multi-jet drive propulsion system and the whole control electronics works well as designed.

Then we focus on the estimation of hydrodynamic coefficients with both empirical and identification methods. A nonlinear dynamic model for torpedo shaped AUVs is established. In this model, a vector based algorithm to calculate the damping forces and moments directly from the hydrodynamic coefficients for the decomposed components of the vehicle is derived. Then, we study the problem of obtaining the values of these hydrodynamic coefficients which is the main uncertainty of the dynamic model of the AUV. Both of the empirical method and the parameter identification method are adopted to estimate these hydrodynamic coefficients based on the field test results of the Lancelet and the Starfish AUV. It is concluded that the best way of obtaining the hydrodynamic coefficients of an AUV is combining the empirical method and the identification method together to avoid the coupling of the coefficients and at the same time to improve the estimation accuracy. This technique is particularly suitable for the torpedo shaped AUV with non-streamlined appendages on the hull, but the control surfaces of which are streamlined.

Finally we studied the modular dynamic modeling of torpedo shaped AUV. According to the analysis of the dynamic model of the AUV, it is found that the key issue of modular dynamic modeling of the AUV is the modularization of the hydrodynamic coefficients of its hull. These hydrodynamic coefficients are transformed from the lift axis system into the normal-force axis system,

where they satisfy the superposition property. Then, the standard reference model method is proposed to calculate these hydrodynamic coefficients from the parameters of modular sections. The hydrodynamic coefficients estimated with both empirical and identification methods are used to verify the proposed method. It is concluded from the results that the standard reference model method could give good estimation of the values of the hydrodynamic coefficients of the hull by the offsets from the reference model in the normal-force axis system.

The contributions of this research are summarized as follows:

1. A dynamic model of AUV suitable for modular parameter estimation and dynamic modeling is established. The empirical methods for the hydrodynamic coefficients and added mass estimation are summarized, and the relationship between hydrodynamic coefficients and hydrodynamic derivatives is derived.

2. A palm size high maneuverable finless torpedo shaped micro AUV named Lancelet with a novel multi-jet drive propulsion system is developed. The mechanical and electronic systems of the Lancelet are designed and implemented. The performance of the designed propulsion systems is tested, and the Lancelet's special maneuverability is explored by open loop free swimming trials.

3. A method of combining the empirical and parameter identification methods for accurate estimation of the hydrodynamic coefficients of torpedo shaped AUVs is proposed, and verified by the experimental data of the Starfish AUV and the Lancelet.

4. The standard reference model method is proposed to address the modular dynamic modeling issues of the torpedo shaped AUV with empirical and experimental verification.

6.2 Future Works

The Lancelet developed in this research is still far from perfect, the possible future research directions of our work will involve more experimental

activities of field testing of the vehicle. Some suggestions of further works direction are listed as follows:

1. For the development of the micro AUV, the active roll control of the Lancelet with the four jet drive propulsion system is only discussed theoretically. In the future research, we should test the property of the active roll control mechanism, and optimize the design of the stator and nozzle, in order to provide reliable active roll control for the vehicle.

2. For hydrodynamic parameter identification, these parameters are identified based on a dynamic model assuming that the vehicle has minimum forward speed and the attack angle of the vehicle is approaching to zero. These assumptions are not valid when the Lancelet conducts the movement of turning in place or pitching in place. As a result, the identified hydrodynamic coefficients may be not correct in simulating or control of these processes. We should verify whether these hydrodynamic coefficient estimated by methods in this thesis are still valid during the turning in place or pitching in place processes, and if not we should construct a dynamic model for the Lancelet's special maneuverability and estimate the related parameters.

3. For modular modeling, we will try to establish a parameter list for each modular section of the AUV, which will generate the dynamic model for any reconfigured AUV from these modular sections more easily than the test-based methods and more accurately than the pure empirical method.

4. For control of underactuated torpedo shaped micro AUV Lancelet, we want to design a trajectory tracking control law for 3D motion of this AUV and simplify the control law to path following control, which only requires the AUV to follow the reference path without time constraints, and simplify the control law again to the point passing control which only requires the AUV to pass specific point with arbitrary path.

5. Finally, we want to integrate all the techniques discussed in this research into a program which covers four stages of the development of the modular designed AUV: parameter estimation, modular modeling, controller design and simulation. The hydrodynamic parameters will be calculated by empirical

methods in the concept design stage, but be estimated more preciously by system identification methods in the prototype experiment stage. And by applying the modular modeling method, the dynamic model for any reconfigured AUV will be generated automatically in this program from the parameters of the modular sections. Then the controllers for trajectory tracking, path following, point passing and underwater object towing will be designed, tuned and verified with visual simulations in this program.

Bibliography

1. Fjerdingen, S.A., Kyrkjeboe, E., and Transeth, A.A. *AUV pipeline following using reinforcement learning*. in *Robotics (ISR), 2010 41st International Symposium on and 2010 6th German Conference on Robotics (ROBOTIK)*. 2010.

2. Hamilton, K. and Evans, J. *Subsea pilotless inspection using an autonomous underwater vehicle (SPINAV): concepts and results*. in *Oceans 2005 - Europe*. 2005.

3. Kirkwood, W.J. *AUV technology and application basics*. in *OCEANS 2008 - MTS/IEEE Kobe Techno-Ocean*. 2008.

4. Nodland, W.E., Ewart, T.E., Bendiner, W.P., Miller, J.B., et al. *SPURV II-An unmanned, free-swimming submersible developed for oceanographic research*. in *OCEANS 81*. 1981.

5. Hasvold, O. and Johansen, K.H. *The alkaline aluminium hydrogen peroxide semi-fuel cell for the HUGIN 3000 autonomous underwater vehicle*. in *Autonomous Underwater Vehicles, 2002. Proceedings of the 2002 Workshop on*. 2002.

6. Hegrenses, O., Hallingstad, O., and Jalving, B. *Comparison of mathematical models for the HUGIN 4500 AUV based on experimental data*. in *Underwater Technology and Workshop on Scientific Use of Submarine Cables and Related Technologies, 2007. Symposium on*. 2007.

7. Marthiniussen, R., Vestgard, K., Klepaker, R.A., and Storkersen, N. *HUGIN-AUV concept and operational experiences to date*. in *OCEANS '04. MTTS/IEEE TECHNO-OCEAN '04*. 2004.

8. Purcell, M., Gallo, D., Packard, G., Dennett, M., et al. *Use of REMUS 6000 AUVs in the search for the Air France Flight 447*. in *OCEANS 2011*. 2011.

9. Kukulya, A., Plueddemann, A., Austin, T., Stokey, R., et al. *Under-ice operations with a REMUS-100 AUV in the Arctic*. in *Autonomous Underwater Vehicles (AUV), 2010 IEEE/OES*. 2010.

10. Yeo, R. *Surveying the underside of an Arctic ice ridge using a man-portable GAVIA AUV deployed through the ice*. in *OCEANS 2007*. 2007.

11. Gonzalez, L., *Design, modelling and control of an autonomous underwater vehicle*. 2004, University of Western Australia: Wattke Grove, Australia.

12. Helble, T., Mailey, C., Stenson, R., Gazagnaire, J., et al., *AUVSI/ONR engineering primer document for the autonomous underwater vehicle*

competition. 2007, Association for Unmanned Vehicle Systems International and the Office of Naval Research.

13. Tamura, K., Aoki, T., Nakamura, T., Tsukioka, S., et al. *The development of the AUV-Urashima*. in *OCEANS 2000 MTS/IEEE Conference and Exhibition*. 2000.

14. Des, E., Madhan, R., and Maury, P., *Potential of autonomous underwater vehicles as new generation ocean data platforms*. 2006.

15. Blidberg, D.R., *The development of autonomous underwater vehicles (AUV); a brief summary*, in *International Conference on Robotics and Automation*. 2001.

16. Yuh, J., *Design and control of autonomous underwater robots: a survey.* Auton. Robots, 2000. **8**(1): p. 7-24.

17. Do, K.D. and Pan, J. *Global tracking control of underactuated ships with off-diagonal terms*. in *Decision and Control, 2003. Proceedings. 42nd IEEE Conference on*. 2003.

18. Do, K.D., Jiang, Z.P., and Pan, J., *Universal controllers for stabilization and tracking of underactuated ships.* Systems & Control Letters, 2002. **47**(4): p. 299-317.

19. Lam, W.C. and Ura, T. *Non-linear controller with switched control law for tracking control of non-cruising AUV*. in *Autonomous Underwater Vehicle Technology, 1996. AUV '96., Proceedings of the 1996 Symposium on*. 1996.

20. Aguiar, A.P. and Pascoal, A.M. *Global stabilization of an underactuated autonomous underwater vehicle via logic-based switching*. in *Decision and Control, 2002, Proceedings of the 41st IEEE Conference on*. 2002.

21. Aguiar, A.P. and Hespanha, J.P. *Logic-based switching control for trajectory-tracking and path-following of underactuated autonomous vehicles with parametric modeling uncertainty*. in *American Control Conference, 2004. Proceedings of the 2004*. 2004.

22. Aguiar, A.P., Hespanha, J.P., and Pascoal, A.M. *Stability of switched seesaw systems with application to the stabilization of underactuated vehicles*. in *Decision and Control, 2005 and 2005 European Control Conference. CDC-ECC '05. 44th IEEE Conference on*. 2005.

23. Pettersen, K.Y. and Nijmeijer, H., *Underactuated ship tracking control: theory and experiments.* International Journal of Control, 2001. **74**(14): p. 1435-1446.

24. Pettersen, K.Y., Mazenc, F., and Nijmeijer, H., *Global uniform asymptotic stabilization of an underactuated surface vessel:*

experimental results. Ieee Transactions on Control Systems Technology, 2004. **12**(6): p. 891-903.

25. Mazenc, F., Pettersen, K.Y., and Nijmeijer, H., *Global uniform asymptotic stabilization of an underactuated surface vessel.* Proceedings of the 41st Ieee Conference on Decision and Control, Vols 1-4, 2002: p. 510-515.

26. Yintao, W., Weisheng, Y., Bo, G., and Rongxin, C. *Backstepping-based path following control of an underactuated autonomous underwater vehicle*. in *Information and Automation, 2009. ICIA '09. International Conference on*. 2009.

27. Yuh, J. *Development in underwater robotics*. in *Robotics and Automation, 1995. Proceedings., 1995 IEEE International Conference on*. 1995.

28. Ridao, P., Yuh, J., Batlle, J., and Sugihara, K. *On AUV control architecture*. in *Intelligent Robots and Systems, 2000. (IROS 2000). Proceedings. 2000 IEEE/RSJ International Conference on*. 2000.

29. Valavanis, K.P., Gracanin, D., Matijasevic, M., Kolluru, R., et al., *Control architectures for autonomous underwater vehicles.* Control Systems, IEEE, 1997. **17**(6): p. 48-64.

30. Hasvold, Ø., Størkersen, N.J., Forseth, S., and Lian, T., *Power sources for autonomous underwater vehicles.* Journal of Power Sources, 2006. **162**(2): p. 935-942.

31. Bovio, E., Cecchi, D., and Baralli, F., *Autonomous underwater vehicles for scientific and naval operations.* Annual Reviews in Control, 2006. **30**(2): p. 117-130.

32. *Chapter 10 - Underwater vehicles*, in *The Maritime Engineering Reference Book*, F.M. Anthony, Editor. 2008, Butterworth-Heinemann: Oxford. p. 728-783.

33. Osterloh, C., Pionteck, T., and Maehle, E. *MONSUN II: A small and inexpensive AUV for underwater swarms*. in *Robotics; Proceedings of ROBOTIK 2012; 7th German Conference on*. 2012.

34. Hobson, B., Schulz, B., Janet, J., Kemp, M., et al. *Development of a micro autonomous underwater vehicle for complex 3-D sensing*. in *OCEANS, 2001. MTS/IEEE Conference and Exhibition*. 2001.

35. Zimmer, U.R. and Kottege, N., *Acoustical methods for azimuth, range and heading estimation in underwater swarms.* The Journal of the Acoustical Society of America, 2008. **123**(5): p. 3007.

36. Kottege, N. and Zimmer, U.R. *Acoustical localization in schools of submersibles*. in *OCEANS 2006 - Asia Pacific*. 2006.

37. Schill, F. and Zimmer, U.R. *Effective communication in schools of submersibles*. in *OCEANS 2006 - Asia Pacific*. 2006.

38. Kalantar, S. and Zimmer, U.R. *Contour shaped formation control for autonomous underwater vehicles using canonical shape descriptors and deformable models*. in *OCEANS '04. MTTS/IEEE TECHNO-OCEAN '04*. 2004.

39. Peter, H., Niels, H., and Alf, P., *Application of ultrasonic sensors in the process industry.* Measurement Science and Technology, 2002. **13**(8): p. R73.

40. Henning, B., Daur, P.-C., Prange, S., Dierks, K., et al., *In-line concentration measurement in complex liquids using ultrasonic sensors.* Ultrasonics, 2000. **38**(1–8): p. 799-803.

41. Yuh-Shyan, C. and Yun-Wei, L., *Mobicast routing protocol for underwater sensor networks.* Sensors Journal, IEEE, 2013. **13**(2): p. 737-749.

42. Nawaz, S., Hussain, M., Watson, S., Trigoni, N., et al., *An underwater robotic network for monitoring nuclear waste storage pools*, in *Sensor Systems and Software*, S. Hailes, S. Sicari, and G. Roussos, Editors. 2010, Springer Berlin Heidelberg. p. 236-255.

43. Watson, S.A., Crutchley, D.J.P., and Green, P.N. *The design and technical challenges of a micro autonomous underwater vehicle*. in *Mechatronics and Automation (ICMA), 2011 International Conference on*. 2011.

44. Watson, S.A. and Green, P.N. *A de-coupled vertical controller for micro autonomous underwater vehicles*. in *Mechatronics and Automation (ICMA), 2011 International Conference on*. 2011.

45. Watson, S.A. and Green, P.N. *Propulsion systems for micro autonomous underwater vehicles*. in *Robotics Automation and Mechatronics (RAM), 2010 IEEE Conference on*. 2010.

46. Watson, S.A. and Green, P.N. *Design considerations for micro autonomous underwater vehicles*. in *Robotics Automation and Mechatronics (RAM), 2010 IEEE Conference on*. 2010.

47. Yujia, W., Mingjun, Z., and Hao, S. *Research on the modularization design method for small underwater vehicle*. in *Circuits, Communications and System (PACCS), 2011 Third Pacific-Asia Conference on*. 2011.

48. Cruz, N.A. and Matos, A.C. *The MARES AUV, a modular autonomous robot for environment sampling*. in *OCEANS 2008*. 2008.

49. Sangekar, M., Chitre, M., and Teong Beng, K. *Hardware architecture for a modular autonomous underwater vehicle STARFISH*. in *OCEANS 2008*. 2008.

50. Sibenac, M., Kirkwood, W.J., McEwen, R., Shane, F., et al. *Modular AUV for routine deep water science operations*. in *OCEANS '02 MTS/IEEE*. 2002.

51. Cruz, N.A., Matos, A.C., and Ferreira, B.M. *Modular building blocks for the development of AUVs from MARES to TriMARES*. in *Underwater Technology Symposium (UT), 2013 IEEE International*. 2013.

52. Ulrich, K., *The role of product architecture in the manufacturing firm.* Research Policy, 1995. **24**(3): p. 419-440.

53. Martin, M. and Ishii, K., *Design for variety: developing standardized and modularized product platform architectures.* Research in Engineering Design, 2002. **13**(4): p. 213-235.

54. Hiller, T., Steingrimsson, A., and Melvin, R. *Expanding the small AUV mission envelope; longer, deeper & more accurate*. in *Autonomous Underwater Vehicles (AUV), 2012 IEEE/OES*. 2012.

55. Taylor, M. and Wilby, A. *Design considerations and operational advantages of a modular AUV with synthetic aperture sonar*. in *OCEANS 2011*. 2011.

56. Cruz, N.A., Matos, A.C., Almeida, R.M., Ferreira, B.M., et al. *TriMARES - A hybrid AUV/ROV for dam inspection*. in *OCEANS 2011*. 2011.

57. Brutzman, D.P., Kanayama, Y., and Zyda, M.J. *Integrated simulation for rapid development of autonomous underwater vehicles*. in *Autonomous Underwater Vehicle Technology, 1992. AUV '92., Proceedings of the 1992 Symposium on*. 1992.

58. Nahon, M. *A simplified dynamics model for autonomous underwater vehicles*. in *Autonomous Underwater Vehicle Technology, 1996. AUV '96., Proceedings of the 1996 Symposium on*. 1996.

59. Fossen, T.I. and Fjellstad, O.-E., *Nonlinear modelling of marine vehicles in 6 degrees of freedom.* Mathematical Modelling of Systems, 1995. **1**(1): p. 17 - 27.

60. Goheen, K.R., *Modeling methods for underwater robotic vehicle dynamics.* Journal of Robotic Systems, 1991. **8**(3).

61. Jones, D.A., Clarke, D.B., Brayshaw, I.B., Barillon, J.L., et al., *The calculation of hydrodynamic coefficients for underwater vehicles*, in *DSTO Technical Report*. 2002. p. 31.

62. Jagadeesh, P., Murali, K., and Idichandy, V.G., *Experimental investigation of hydrodynamic force coefficients over AUV hull form.* Ocean Engineering, 2009. **36**(1): p. 113-118.

63. Chao, S., Hong, G.S., Eng, Y.H., and Chitre, M. *Modular modeling of autonomous underwater vehicle*. in *OCEANS 2011*. 2011.

64. Fill Youb, L., Bong Huan, J., Pan Mook, L., and Kihun, K. *Implementation and test of ISiMI100 AUV for a member of AUVs fleet*. in *OCEANS 2008*. 2008.

65. de Barros, E.A., Pascoal, A., and de Sa, E., *Investigation of a method for predicting AUV derivatives.* Ocean Engineering, 2008. **35**(16): p. 1627-1636.

66. Evans, J. and Nahon, M., *Dynamics modeling and performance evaluation of an autonomous underwater vehicle.* Ocean Engineering, 2004. **31**(14–15): p. 1835-1858.

67. Do, K.D. and Pan, J., *Control of ships and underwater vehicles: design for underactuated and nonlinear marine systems*. 2009: Springer.

68. Ferguson, J. and Pope, A. *Explorer-a modular AUV for commercial site survey*. in *Underwater Technology, 2000. UT 00. Proceedings of the 2000 International Symposium on*. 2000.

69. Fossen, T.I., *Guidance and control of ocean vehicles*. 1999, New York: Wiley.

70. Faltinsen, O.M., *Sea loads on ships and offshore structures*. 1990: Cambridge University Press.

71. Brennen, C.E., *A review of added mass and fluid inertial forces*, in *CR 82.010*. 1982, Naval Civil Engineering Laboratory: Port Hueneme, California, USA.

72. Korotkin, A.I., *Added masses of ship structures*. 2009: Springer.

73. Hopkins, J.E., *A semiempirical method for calculating the pitching moment of bodies of revolution at low Mach numbers*, in *NACA-RM-A51C14*. 1951, National Advisory Committee for Aeronautics: Washington.

74. Hoak, D.E., Finck, R.D., Ellison, D.E., and Malthan, L.V., *The USAF stability and control DATCOM*, in *TR-83-3048*. 1978, Air Force Wright Aeronautical Laboratories.

75. Whicker, L.F., Eng, D., and Fehlner, L.F., *Free-stream characteristics of a family of low-aspect-ratio, all-movable control surfaces for application to ship design*, in *Report 933*. 1958, David Taylor Model Basin.

76. Hoerner, S.F., *Fluid dynamic drag: practical information on aerodynamic drag and hydrodynamic resistance*. 1965: Hoerner Fluid Dynamics.

77. Prestero, T. *Development of a six-degree of freedom simulation model for the REMUS autonomous underwater vehicle*. in *OCEANS, 2001. MTS/IEEE Conference and Exhibition*. 2001.

78. Prestero, T., *Verification of a six-degree of freedom simulation model for the REMUS autonomous underwater vehicle*. 2001, Massachusetts Institute of Technology. p. 120.

79. Myring, D.F., *A theoretical study of body drag in subctitical axisymmetric flow.* Aeronautical Quarterly, 1976. **27**(3): p. 186-194.

80. Crowell, J. *Small AUV for hydrographic applications*. in *OCEANS 2006*. 2006.

81. Panish, R. and Taylor, M. *Achieving high navigation accuracy using inertial navigation systems in autonomous underwater vehicles*. in *OCEANS, 2011 IEEE - Spain*. 2011.

82. Hyakudome, T., *Design of autonomous underwater vehicle.* International Journal of Advanced Robotic Systems, 2011. **8**(1): p. 131-139.

83. Rigby, P., Pizarro, O., and Williams, S.B. *Towards geo-referenced AUV navigation through fusion of USBL and DVL measurements*. in *OCEANS 2006*. 2006.

84. Chong-Moo, L., Seok-Won, H., and Woo-Jae, S. *An integrated DVL/IMU system for precise navigation of an autonomous underwater vehicle*. in *OCEANS 2003. Proceedings*. 2003.

85. Grose, B.L. *The application of the correlation sonar to autonomous underwater vehicle navigation*. in *Autonomous Underwater Vehicle Technology, 1992. AUV '92., Proceedings of the 1992 Symposium on*. 1992.

86. Campanella, G. and Holt, W. *Correlation-log-based underwater navigation*. in *Autonomous Underwater Vehicle Technology, 1990. AUV '90., Proceedings of the (1990) Symposium on*. 1990.

87. Boltryk, P., Hill, M., Keary, A., Phillips, B., et al., *An ultrasonic transducer array for velocity measurement in underwater vehicles.* Ultrasonics, 2004. **42**(1–9): p. 473-478.

88. Madgwick, S.O.H., Harrison, A.J.L., and Vaidyanathan, R. *Estimation of IMU and MARG orientation using a gradient descent algorithm*. in *Rehabilitation Robotics (ICORR), 2011 IEEE International Conference on*. 2011.

89. Mahony, R., Hamel, T., and Pflimlin, J.-M., *Nonlinear complementary filters on the special orthogonal group.* Automatic Control, IEEE Transactions on, 2008. **53**(5): p. 1203-1218.

90. Gebre-Egziabher, D., Hayward, R.C., and Powell, J.D., *Design of multi-sensor attitude determination systems.* Aerospace and Electronic Systems, IEEE Transactions on, 2004. **40**(2): p. 627-649.

91. Marins, J.L., Yun, X., Bachmann, E.R., McGhee, R.B., et al. *An extended Kalman filter for quaternion-based orientation estimation using MARG sensors*. in *Intelligent Robots and Systems, 2001. Proceedings. 2001 IEEE/RSJ International Conference on*. 2001.

92. Damus, R., Manley, J., Desset, S., Morash, J., et al. *Design of an inspection class autonomous underwater vehicle*. in *OCEANS '02 MTS/IEEE*. 2002.

93. Yuan, H., Yang, J., Qu, Z., and Kaloust, J. *An optimal real-time motion planner for vehicles with a minimum turning radius*. in *Intelligent Control and Automation, 2006. WCICA 2006. The Sixth World Congress on*. 2006.

94. Shea, D., Riggs, N., Bachmayer, R., and Williams, C. *Prototype development of the SQX-1 autonomous underwater vehicle*. in *OCEANS 2009 - EUROPE*. 2009.

95. Nahon, M. *Determination of undersea vehicle hydrodynamic derivatives using the USAF Datcom*. in *OCEANS '93. Engineering in Harmony with Ocean. Proceedings*. 1993.

96. Yoon, H.K. and Rhee, K.P., *Identification of hydrodynamic coefficients in ship maneuvering equations of motion by Estimation-Before-Modeling technique.* Ocean Engineering, 2003. **30**(18): p. 2379-2404.

97. Zhao, J., Su, Y., Ju, L., and Cao, J. *Hydrodynamic performance calculation and motion simulation of an AUV with appendages*. in *Electronic and Mechanical Engineering and Information Technology (EMEIT), 2011 International Conference on*. 2011.

98. Hong, E.Y., Meng, T.K., and Chitre, M. *Online system identification of the dynamics of an autonomous underwater vehicle*. in *Underwater Technology Symposium (UT), 2013 IEEE International*. 2013.

99. Peyada, N.K., Sen, A., and Ghosh, A.K. *Aerodynamic characterization of HANSA-3 aircraft using equation error, maximum likelihood and filter error methods*. in *International Multiconference of Engineers and Computer Scientists*. 2008. Hong Kong.

100. Jategaonkar, R.V., *Flight vehicle system identification: a time domain methodology*. 2006, Reston: American Institute of Aeronautics and Astronautics.

101. Hong, E.Y., Hong, G.S., and Chitre, M. *Depth control of an autonomous underwater vehicle, STARFISH*. in *OCEANS 2010 IEEE - Sydney*. 2010.

102. Deshpande, P.D., Sangekar, M.N., Kalyan, B., Chitre, M.A., et al., *Design and development of AUVs for cooperative missions*, in *Defence Technology Asia*. 2007: Singapore.

103. Ding, F., Liu, P.X., and Liu, G., *Gradient based and least-squares based iterative identification methods for OE and OEMA systems.* Digital Signal Processing, 2010. **20**(3): p. 664-677.

104. Alessandri, A., Caccia, M., Indiveri, G., and Veruggio, G. *Application of LS and EKF techniques to the identification of underwater vehicles*. in *Control Applications, 1998. Proceedings of the 1998 IEEE International Conference on*. 1998.

105. Martin, S.C. and Whitcomb, L.L. *Preliminary results in experimental identification of 3-DOF coupled dynamical plant for underwater vehicles*. in *OCEANS 2008*. 2008.

106. Fisher, L.R., *Equations and charts for determining the hypersonic stability derivatives of combinations of cons frustums computed by newtonian impact theory*. 1959, NASA.

Publications and Patent of the Author

1. Publications

Shuzhe Chao, Guofeng Guan, Geok-Soon Hong. Combining of empirical and parameter identification methods for estimation of the hydrodynamic coefficients of torpedo shaped AUVs. IEEE/ASME Transactions on Mechatronics, under review

Shuzhe Chao, Geok-Soon Hong. Modular dynamic modeling of micro autonomous underwater vehicle Lancelet. IEEE Journal of Oceanic Engineering, under review

Shuzhe Chao, Geok-Soon Hong, Guofeng Guan. The design and field test of a micro AUV Lancelet with a multi-jet drive propulsion system. Ocean Engineering, under review.

Guofeng Guan, Lidan Wu, Ali Asgar Bhagat, Zirui Li, Peter C. Y. Chen, Shuzhe Chao, Chong Jin Ong, Jongyoon Han. Spiral microchannel with rectangular and trapezoidal cross-sections for size based particle separation. Sci. Rep., 2013. 3.

Chao Shuzhe, Hong Geok Soon, Eng You Hong, Mandar Chitre. Modular modeling of autonomous underwater vehicle. in OCEANS 2011. 2011.

2. Patent

US Provisional Application No.: 61/824,472
Title: Finless Multi-Jet Drive Propulsion System for Torpedo Shaped AUV
ILO Ref: 13242N-US/PRV